

# Leveraging Expert Knowledge to Guide Inverse Optimization: The Case of Nutritional Adherence

Farzin Ahmadi, Fardin Ganjhanloo, Kimia Ghobadi

Department of Civil and Systems Engineering, The Center for Systems Science and Engineering, The Malone Center for Engineering in Healthcare, Johns Hopkins University, Baltimore, MD 21218, fahmadi1@jhu.edu, fganjkh1@jhu.edu, kimia@jhu.edu

Inverse optimization has emerged as a powerful tool for inferring underlying decision-making processes from observed data. However, existing approaches often struggle to balance adherence to observations with satisfaction of problem constraints, especially when observations are noisy or infeasible. This paper introduces the Inverse Learning framework, a novel approach that concurrently learns optimal solutions and underlying cost functions from observed data. We formalize the Observation-Constraint Tradeoff, highlighting the balance between fitting observed data and satisfying problem constraints. To navigate this tradeoff, we develop goal-integrated models that allow incorporating different levels of constraint importance and exploring a spectrum of solutions. Through extensive numerical experiments, we demonstrate that our proposed models outperform benchmark inverse optimization models in terms of solution time and accuracy in recovering correct cost vectors. We apply our framework to the critical problem of personalized diet recommendations, generating flexible diet plans for patients with chronic conditions that balance individual preferences with nutritional guidelines. A prospective feasibility study with a volunteer participant provides initial evidence of our framework's potential impact on dietary interventions and glucose control. We also develop interactive decision support tools, including web-based interfaces, to make our research outcomes accessible for practitioners. This work bridges theoretical advances in inverse optimization with practical applications in healthcare, offering a comprehensive approach to data-driven decision-making under constraints.

*Key words:* Diet recommendation, inverse optimization, linear optimization, data-driven decision-making, utility function, patient adherence

---

## 1. Introduction

Chronic conditions including diabetes and high blood pressure are among the most significant healthcare problems. Lifestyle interventions and guidelines play an important role in the outcomes of patients with chronic conditions. For instance, high blood pressure patients are often prescribed a low-sodium diet as part of their treatment, a typical example of such a diet being the Dietary Approaches to Stop Hypertension (DASH) diet ([Sacks et al. 2001](#), [Liese et al. 2009](#)) which aims to control sodium intake and is shown to lower blood pressure—a known risk factor of diabetes ([Sacks et al. 2001](#)). Studies suggest that adherence to the DASH diet has an inverse relation with type 2 diabetes and can reduce future risk of it by as much as 20% ([Liese et al. 2009](#), [Campbell 2017](#)). Therefore, nutritional interventions are central in chronic care regimens and usually include general guidelines that limit certain food groups and/or provide bounds or requirements on specific nutrients. While inherently essential and useful, many studies point out that patient adherence to these nutritional guidelines remains substantially low, with a harsh mismatch between patient preference and guidelines being a major player. Personalizing nutritional recommendations as a means to improve adherence to nutritional guidelines is, therefore, a natural direction to promote adherence ([Downer et al. 2016](#), [Inelmen et al. 2005](#), [Bazrafkan et al. 2021](#)).

Generally, nutritional interventions occur between the patient and a dietitian (expert). Such interventions can be posed as an optimization problem where the dietitian sets guidelines in the form of nutritional and/or food group requirements (constraints) for the patient, taking into account the nutritional needs of the patient based on their existing conditions. In such cases, the dietitian and the patient might have possibly conflicting goals or objectives. The patient's objectives can be assumed as a combination of maximizing their preference, optimizing costs, and possibly considering the health benefits of the food groups they consume while the dietitian's objectives can be assumed to be around the "healthiest" alternatives among feasible diets. In this setting, the utility function of the patient (while they are aware of the nutritional bounds) is unobservable but their daily nutritional decisions can each account for an observed decision for this optimization problem since the patient can be assumed to be making decisions aware of the feasible set formed by the nutritional constraints. One can also assume that in this setting and post guideline recommendation by the dietitian, the patient's daily nutritional decisions can be influenced by the dietitian's utility function aiming to promote healthiest alternatives.

In this work, we aim to predict the utility function of the patient post-intervention and provide subsequent modifications to their decisions based on their pre-intervention decisions and available expert information on the nature of the interventions. We propose using an inverse optimization-based methodology ([Ahuja and Orlin 2001](#)) to infer the utility function of the patient as the

34 decision maker and adjust their daily nutritional behavior if needed. Inverse optimization recovers  
35 the unknown parameters of a partially known (forward) optimization problem based on given  
36 observed solution(s). Recent studies have shown that inverse optimization models can successfully  
37 recover missing parameters of forward linear optimization problems ranging from linear optimization  
38 problems to integer or convex optimization models with a focus on recovering the unknown cost  
39 function (Beil and Wein 2003, Iyengar and Kang 2005, Bertsimas et al. 2012, Chan et al. 2014, 2019,  
40 Aswani et al. 2018, Shahmoradi and Lee 2022b). We formulate the diet intervention problem as a  
41 linear optimization model with an unknown cost vector representing the conflicting utilities of the  
42 dietitian and patient, and a known feasible set defined by nutritional guidelines. We propose that  
43 nutritional adjustments to existing behaviors can be achieved through alternative loss functions  
44 in the inverse optimization framework that minimize the difference between current and adjusted  
45 behaviors. These adjustments manifest as "nudge" suggestions, recommending modified amounts  
46 of food groups the patient already consumes to bring their overall daily intake within guideline  
47 bounds. The inferred utility function enables dietitians to further personalize recommendations  
48 by potentially adjusting nutritional guidelines to increase adherence or providing alternative meal  
49 plans that closely match existing dietary patterns. This approach balances adherence to nutritional  
50 standards with preservation of patient preferences.

51 While inverse optimization is particularly suitable for the dietary behavior adjustment problem,  
52 existing inverse optimization models are mainly concerned with inferring the unobserved cost  
53 vector of the forward optimization problem prior to intervention. This is while in our application,  
54 nutritional adjustments in the form of projected solutions that satisfy optimality and loss criteria  
55 are desired which contain some notion of the expert input. Balancing between the dietitian and  
56 the patient's objectives motivated this work to modify inverse optimization. We propose a modified  
57 inverse optimization framework, denoted as *Inverse Learning*, that recovers unknown cost functions  
58 of an underlying linear forward optimization problem based on given observation(s), similar to  
59 most inverse optimization models. The modified model, however, is structurally distinct from  
60 inverse optimization paradigms in that it directly learns an optimal solution to the underlying  
61 forward optimization problem in addition to recovering the missing cost function, hence, enabling  
62 preservation of the characteristics of observed solutions while being faster in application (as shown  
63 in our numerical examples). Additionally, this model integrates constraint priority knowledge into  
64 the inverse framework to further guide the optimal solutions' recovery and addressing the expert  
65 knowledge in the model. We additionally develop further models that capture the trade-off in  
66 balancing user and expert's knowledge by providing a range of solutions along with a control  
67 mechanism to balance the inherent tradeoff between optimal solutions that retain observations'  
68 characteristics and those that bind prioritized constraints and goals. We show using simulated

examples that these models are better equipped to learn the cost vector of the user in comparison to benchmark inverse optimization models. We show that even without characterizing constraint priorities, our models are able to better capture correct cost vectors. Our model additionally provides a range of decisions that can be recommended to the user for future behavior.

The distinctive features of the inverse learning framework provide additional flexibility for the diet adjustment problem. Our framework unifies the process of learning forward optimal solutions with the recovery of the underlying cost vector. Simultaneous recovery of both the optimal solutions and the cost vectors enables the inverse framework to better control the characteristics of eventual optimal solutions and cost vectors instead of indirectly impacting the solutions through cost vectors. The additional knowledge of solutions' properties can be embedded into the models, along with any other available information about the cost vector. We show through numerical experiments that in the absence of high volume of data, inverse learning models that concurrently learn the optimal solution and the cost vector perform equally or superior to existing inverse optimization models in terms of correctly estimating cost vectors and minimizing loss to observed behaviors. Another feature of inverse learning is embedding additional constraints' priority knowledge in the learning process, should such information exist. Integration of observations into inverse optimization frameworks has been studied extensively in the literature, especially in the form of a distance function ([Chan et al. 2021, 2014](#), [Keshavarz et al. 2011](#), [Aswani et al. 2018](#), [Ghobadi et al. 2018](#)). However, little attention has been paid to the information conveyed by constraints beyond identifying the feasible region. In particular, those constraints that are active at optimality play vital roles in determining the missing cost vectors and the optimal solution of the forward problem. They may also carry significance in practical settings. For instance, in resource allocation problems, meeting all demands or utilizing the minimum amount of certain resources may be desirable, or in diet problems, maximizing protein or minimizing saturated fat may be meaningful goals for the dieter. This additional information and goals can be provided by end-users, domain experts, or derived from data. The inverse learning framework can incorporate such goals by binding preferred constraints and considering different tiers of constraints in the models. If no additional information exists, the inverse learning model operates as conventional models and treats all constraints equally. The final feature of inverse learning lies in its ability to control tradeoffs between observation-driven and goal-driven information and provide a decision-support system based on user's preferences or by progressively adding goals. The framework aims to balance between the two main inputs to inverse models: observations – as a measure of past behavior or decisions – and constraints – as a measure of rules, restrictions, or goals. The ability to provide a spectrum of solutions enables tailoring the solutions to the needs and preferences of the users.

103 The focus on the learning process in inverse frameworks is motivated by practical settings where  
104 examples of historical solutions or observations are abundant but may not be optimal or even  
105 feasible for the underlying forward problem. For instance, expert decisions in healthcare planning or  
106 treatments, customer decisions in service industries, or patients' nutritional decisions, among others.  
107 These solutions highlight the behavior and decisions of the user or the status of the system. In these  
108 settings, finding optimal solutions that represent observations may be paramount as they represent  
109 underlying patterns or preferences that may not be captured in the model otherwise. Incorporating  
110 inputs from observations and constraint priorities directly into the models guides finding optimal  
111 solutions that are relevant and appropriate for the problem. The additional flexibility and control  
112 also empower users to tailor the solutions or obtain a set of solutions that gradually improves goals,  
113 and indirectly, improve cost vector stability and sensitivity to outliers.

114 We demonstrate the applicability of the inverse learning framework using a subset of the NHANES  
115 ([CDC 2020b](#)) dataset including a population of 2,090 patients with a self-reported hypertension  
116 and/or diabetes or pre-diabetes diagnosis. Precision nutrition is increasingly used as part of medical  
117 treatments to prevent or control symptoms in prediabetic, hypertension, or kidney failure patients.  
118 Observations of patients' past food intake can provide insights into their preferences, while the DASH  
119 diet constraints provide nutritional goals and constraints. A spectrum of diet recommendations that  
120 traverse from preserving patients' behavior to diets that increasingly improve nutritional goals (e.g.,  
121 minimizing sodium, maximizing fiber, minimizing sugar, etc.) can provide patients with a range  
122 of choices. Starting with diets closer to patients' current behaviors and gradually introducing new  
123 goals may provide a more personalized diet recommendation that can improve patients' adherence  
124 as opposed to a one-size-fits-all approach.

125 We pose a forward optimization problem based on the DASH diet nutritional constraints with  
126 an unknown cost vector of patients' preferences and palate. We then use inverse learning models to  
127 recommend diets for patient classes. We demonstrate how inverse learning models can be used to  
128 directly recommend a set of diets with clear interpretations for the patients and the dietitians and  
129 recover the underlying cost function. The recommendations provide a control mechanism to balance  
130 the trade-off between past food intake and nutritional goals. The added flexibility in recommending  
131 decisions advocates algorithm usability through algorithm aversion ([Dietvorst et al. 2015](#), [Grand-](#)  
[Clément and Pauphilet 2022](#)) as it provides means for decision-makers and users to gain control  
133 over decisions resulting from the algorithms ([Dietvorst et al. 2018](#)). The outcomes demonstrate a  
134 nutrition path for the patients to initially maintain their habits as much as possible while adhering  
135 to the prescribed diet. Gradually, the recommended diets can bind more nutritional constraints and  
136 move towards meeting more nutritional goals and the ideal nutrition plan for the patients.

The rest of this section includes a review of the most relevant literature and discussion of the contributions. We then introduce the forward and inverse learning models in Section 2 and extend to goal-integrated inverse learning models to control the observation-goal tradeoff in Section 3. Detailed numerical examples and simulations are provided in Section 4, and finally, we apply our full framework to the diet recommendation problem and showcase web-based decision-support tools for the diet recommendation problem that enables exploring various diets based on the user's preferences and goals in Section 5. Concluding remarks are provided in Section 6 and proofs are outlined in an electronic companion.

145 **1.1. Literature Review**

146 **1.1.1. Inverse Optimization** Early investigations of inverse problems can be traced back to the works of Burton and Toint (1992) who considered the inverse shortest path problem and discussed inverse combinatorial optimization problems. Inverse settings of combinatorial and general linear optimization problems gained more traction in time (Yang and Zhang 1999, Zhang and Liu 1996, 1999, Zhang and Ma 1999). Heuberger (2004) provided a survey on inverse combinatorial problems and the existing methods for approaching such problems. However, Ahuja and Orlin (2001) was the first to use the term “Inverse Optimization” and pose it as a general problem of recovering cost vectors of linear programming problems. Since then, a common setting in inverse optimization has been to recover the cost function and implicit preferences of a decision-maker in a constrained environment in the form of a (forward) optimization problem (Chan et al. 2014, Aswani et al. 2018, Esfahani et al. 2018, Shahmoradi and Lee 2022b) and solve the recovered problem with known methods to find optimal solutions. While the majority of the literature considers the given observation(s) as a single optimal (Ahuja and Orlin 2001, Iyengar and Kang 2005) or near-optimal point (Ghate 2015, Chan et al. 2019, Zhang and Xu 2010, Schaefer 2009, Wang 2009, Ghate 2020, Lasserre 2013, Naghavi et al. 2019, Roland et al. 2013), in practice, often a collection of past solutions can be observed from the forward problem (Keshavarz et al. 2011, Shahmoradi and Lee 2022b, Babier et al. 2021) or from similar but differently constrained problems (Černý and Hladík 2016). In such cases, existing methods rely on minimizing optimality gap measures in terms of primal-dual objective values to recover unknown parameters. However, it has been argued in the literature that such methods result in inconsistent estimations in data-driven settings (Aswani et al. 2018).

166 Multi-observation settings in inverse optimization have increasingly gained traction due to their real-world applicability. Recent studies have considered various methods to recover linear problems in the presence of multiple observations for cost vectors (Babier et al. 2021, Esfahani et al. 2018, Aswani et al. 2018, Tan et al. 2019, Hewitt and Frejinger 2020, Moghaddass and Terekhov 2021) or for constraint parameters (Ghobadi and Mahmoudzadeh 2021, Chan and Kaw 2020, Schede et al.

171 2019). Others have considered online settings, considering the cases in which a stream of observations  
172 is given, as opposed to an existing batch of observations (Dong et al. 2018) or generalized models for  
173 both settings (Besbes et al. 2023). Statistical approaches in noisy settings (Aswani 2019, Shahmoradi  
174 and Lee 2022b,a) and deep learning models in data-driven settings are also explored (Tan et al.  
175 2019).

176 Many applications of inverse optimization methodologies have also been studied including finance  
177 (Bertsimas et al. 2012), network and telecommunication (Faragó et al. 2003), supply chain planning  
178 (Pibernik et al. 2011), transportation problems (Chow and Recker 2012), facility location problems  
179 (Crönert et al. 2024), control systems (Akhtar et al. 2021), and auction mechanisms (Beil and  
180 Wein 2003). Bärmann et al. (2018) consider a setting where the decision-maker decides on the  
181 variables in different domains and provides an online-learning framework for inverse optimization.  
182 Konstantakopoulos et al. (2017) combine inverse optimization and game theory methods to learn  
183 the utility of agents in a non-cooperative game. Other studies consider healthcare applications to  
184 employ inverse optimization's unique ability to recover unknown parameters in multi-objective and  
185 highly-constrained settings (Chan and Lee 2018, Gorissen et al. 2013), including cancer treatment  
186 (Corletto et al. 2003, Chan et al. 2014, 2022b, Ajayi et al. 2022), patient care delivery systems  
187 (Chan et al. 2022a), and the diet recommendation problem (Ghobadi et al. 2018, Shahmoradi and  
188 Lee 2022b, Aswani et al. 2019). The diet recommendation problem is further discussed in Section  
189 5. For a recent survey on inverse optimization theory and applications, we refer the readers to the  
190 study by Chan et al. (2021).

191 The inverse learning framework is most closely related to the works of Chan et al. (2019) and  
192 Shahmoradi and Lee (2022b) in the literature. The work by Chan et al. (2019) discusses inverse  
193 linear optimization models with noisy data. They employ the recover-then-optimize approach to  
194 find the forward optimal solutions which provides little guarantee about compatibility of the final  
195 optimal solutions with the given observations, especially when the optimal decision space contains  
196 infinitely many points. Shahmoradi and Lee (2022b), alternatively, focus on finding extreme-point  
197 optimal solutions to address the instability of optimal forward solutions in the recover-then-optimize  
198 approach while controlling for outliers. This approach is computationally more expensive and relies  
199 on user-given parameters to find the solutions. Additionally, extreme points may bind a high number  
200 of constraints which can make the model more goal-driven in the observation-goal tradeoff we  
201 demonstrate through a two dimensional example that neither of these models are sufficient for  
202 correctly estimating cost vectors.

203 **1.1.2. Diet Recommendation** The diet recommendation problem is among the most well-  
204 studied problems in operations research (Stigler 1945, Bassi 1976, Dantzig 1965, Gazan et al. 2018).

205 The goal of the classical diet recommendation problem, as first introduced by Stigler (1945), is to find  
206 the optimal food intake of a patient or a set of patients based on some given cost function subject to  
207 a given set of constraints (Stigler 1945, Garille and Gass 2001). Many studies have focused on finding  
208 optimal diets for individuals and communities based on existing behaviors (Stigler 1945, Sacks et al.  
209 2001, Bas 2014). The more recent literature has focused on providing more realistic constraints and  
210 relaxing previous simplifying assumptions of the original diet recommendation problem, such as the  
211 linear relationship between the nutrients and foods and the varying effects of different combinations  
212 of foods (Bas 2014).

213 In the inverse optimization literature, the diet recommendation problem has been studied to  
214 recover missing cost functions (Ghobadi et al. 2018, Shahmoradi and Lee 2022b) or constraint  
215 parameters (Ghobadi and Mahmoudzadeh 2021) based on a given set of observed nutritional  
216 decisions. However, no previous work has considered the role of the dietitian in adjusting the patients  
217 behaviors after diagnosis. In our case study, we concentrate on recommending diets and recovering  
218 a corresponding cost function based on a given set of observed daily nutritional decisions. Similar  
219 to Ghobadi et al. (2018), in the definition of the diet recommendation problem, we assume that the  
220 cost function is inversely associated with the preferences of the individual, meaning that the more  
221 palatable a particular food item for an individual, the smaller its cost.

222 In this work, we consider the food intake behaviors of individuals who self-reported hypertension  
223 and the risk of developing type II diabetes. Roughly one out of every two adults in the United States  
224 experiences some level of hypertension or high blood pressure (CDC 2020a). For such patients,  
225 many clinicians recommend the Dietary Approaches to Stop Hypertension (DASH) eating plan that  
226 aims to decrease sodium intake and control blood pressure (Challa et al. 2021). The DASH diet has  
227 been shown to lower both systolic and diastolic blood pressures in individuals (Sacks et al. 2001,  
228 Challa et al. 2021). However, maintaining a long-term and realistic diet is a persistent challenge  
229 for many patients. Diets with clear options that resemble the existing nutritional behaviors of the  
230 patients and have increased palatability are more likely to be adhered to by the patient for long-  
231 term commitments (Bentley et al. 2005). Many of the existing methods in the literature rely on  
232 defining specific constraints in hopes of achieving more palatable diets (Ferguson et al. 2006, Xu  
233 et al. 2018). Here, we consider a forward optimization model based on the DASH diet nutritional  
234 constraints and the palatability objective. We then utilize the inverse learning models using given  
235 nutritional behavior data of patients to recommend diets ranging from diets similar to the decisions  
236 of the patients while adhering to DASH guidelines to quality diets that are richer in many nutrients.

## 237 1.2. Contributions

238 This paper makes several significant contributions to the fields of inverse optimization and data-  
239 driven decision-making, with particular applications in healthcare and personalized interventions:

- 240 1. We introduce the Inverse Learning (IL) framework, a novel approach that extends inverse  
241 optimization to concurrently learn optimal solutions and underlying cost functions from  
242 observed data. This framework provides a more flexible and robust method for recovering  
243 unknown parameters in partially known optimization problems, addressing key limitations  
244 in existing inverse optimization approaches with regard to robustness to noisy data,  
245 enhanced interpretability, computational efficiency, and flexibility in handling additional  
246 expert knowledge information. We additionally extend our framework to convex parametric  
247 optimization problems, suggesting a modified approach for a specific type of inverse  
248 optimization problem in the general convex setting, showing how the IL model can be used to  
249 model the inverse optimization problem in a simpler way and broadening its applicability to a  
250 wider class of optimization problems.
- 251 2. We conceptualize and formalize the Observation-Constraint Tradeoff, highlighting the balance  
252 between fitting observed data and satisfying problem constraints in recovering cost functions  
253 for linear problems. This new perspective on inverse optimization problems enables more  
254 nuanced solutions and provides a theoretical foundation for understanding the interplay  
255 between data and model constraints. We develop the Goal-Integrated Inverse Learning (GIL)  
256 model, which allows for incorporating different levels of constraint importance. This model  
257 enables decision-makers to prioritize certain constraints and explore a spectrum of solutions,  
258 significantly enhancing the practical relevance and flexibility of inverse optimization in real-  
259 world applications. We also propose the MGIL model for sequential constraint binding,  
260 providing a structured approach to navigating the optimal solution set by incrementally  
261 binding more constraints. This model offers a systematic method for balancing user preferences  
262 with expert guidelines, a critical consideration in many decision-making contexts, and shows  
263 significant improvements in the ability to recover the correct cost vectors.
- 264 3. Through extensive numerical experiments, we demonstrate that our proposed models  
265 outperform benchmark inverse optimization models in terms of solution time and accuracy  
266 in recovering correct cost vectors. These results provide strong evidence for the practical  
267 superiority of our approach in a wide range of problem settings.
- 268 4. We apply our framework to the critical problem of personalized diet recommendations,  
269 demonstrating its practical utility in generating personalized and gradually improving diet  
270 plans for patients with chronic conditions. This application showcases the potential of our  
271 approach to address important healthcare challenges. We also conduct a prospective feasibility  
272 study with a volunteer participant, providing initial evidence of our framework's potential  
273 impact on dietary interventions and glucose control. We develop interactive decision support  
274 tools, including web-based interfaces for exploring diet recommendations. These tools bridge

275 the gap between theory and practice, making our research outcomes accessible and usable for  
276 practitioners in healthcare and nutrition.

## 277 2. Including Expert Knowledge in Inverse Optimization

278 In this section, we consider inverse linear optimization models to enable learning for the settings  
279 where multiple instances of an optimal solution with noise or bounded rationality exist. This  
280 unknown optimal solution, for instance, can represent the best recommendation that the dietitian  
281 and the patient can settle on which promotes the necessary dietary requirements as well as patient  
282 preference as much as possible. We assume that for our setting, the parameters constituting the  
283 feasible set of the linear optimization problem are known but the cost vector (as a representative of  
284 preferences for example) is unknown. We propose the inverse learning framework which focuses on  
285 recovering the optimal solution and the underlying cost vector to a partially known linear forward  
286 optimization based on a given set of (feasible or infeasible) observations and an optional given set  
287 of active constraint priorities (goals).

288 Our approach fundamentally differs from existing inverse optimization models in its underlying  
289 assumptions. While traditional models assume observed decisions stem from the same cost vector,  
290 we posit that these decisions are noisy realizations of a single optimal solution. This assumption shift  
291 tremendously makes modeling easier, as cases where the true cost vector provides unique optimal  
292 solutions will be similar across our models and traditional inverse optimization while our assumption  
293 set handles cases with non-unique optimal solutions organically. As such, our goal is twofold: to learn  
294 the optimal solution and to recover the missing cost vector of the forward optimization problem  
295 (FO). Through extensive examples, we demonstrate that this modification not only preserves the  
296 ability to correctly estimate the true cost vector but also enhances the model's robustness to  
297 noise and outliers. Furthermore, we introduce a novel framework to accommodate different tiers of  
298 constraints based on their importance in the decision-making process. This hierarchical approach to  
299 constraints can be generalized to any number of tiers without loss of generality, offering a flexible  
300 and nuanced method for capturing complex decision environments. As we proceed to detail our  
301 inverse linear optimization model for unknown cost vectors, it is crucial to keep these foundational  
302 assumptions and objectives in mind, as they underpin the subsequent methodological developments  
303 and results. To set up the framework, we first detail the forward optimization problem. We then  
304 introduce our inverse linear optimization model and the inverse learning model and discuss its desired  
305 characteristics. We present the observation-goal tradeoff and the corresponding goal-integrated  
306 inverse learning to Section 3, which is capable of incorporating both the objectives of the nutritionist  
307 and the patient.

308 **2.1. Preliminaries: Inverse Linear Optimization of Unknown Cost Vectors**

For a given cost vector  $\mathbf{c} \in \mathbb{R}^n$  and a non-empty feasible set  $\Omega = \{\mathbf{x} \in \mathbb{R}^n | \mathbf{Ax} \geq \mathbf{b}\}$ , a linear (forward) optimization is modeled as  $\arg \min_{\mathbf{x}} \{\mathbf{c}'\mathbf{x} | \mathbf{x} \in \Omega\}$ . In the inverse optimization setting, the goal is to recover the cost vector  $\mathbf{c} \in \mathbb{R}^n$  based on a given set of observation(s),  $\mathcal{X} = \{\mathbf{x}^k \in \mathbb{R}^n : k \in \mathcal{K}\}$ ,  $\mathcal{K} = \{1, \dots, K\}$  which may be noised by error or bounded rationality and not necessarily optimal for FO. If  $\mathbf{y} \in \mathbb{R}_{\geq 0}^m$  is the corresponding dual variables for the constraints forming  $\Omega$ , the classic inverse linear optimization model (Aswani et al. 2018, Chan et al. 2019, Shahmoradi and Lee 2022b) for linear optimization problems is provided as follows:

$$\text{IO}(\mathcal{X}, \Omega) : \underset{\mathbf{c}, \mathbf{y}, \mathbf{z}^k}{\text{minimize}} \quad \sum_{k \in \mathcal{K}} \|\mathbf{x}^k - \mathbf{z}^k\|_l \quad (1a)$$

$$\text{subject to} \quad \mathbf{z}^k \in \Omega, \quad \forall k \in \mathcal{K} \quad (1b)$$

$$\mathbf{c}'\mathbf{z}^k = \mathbf{b}'\mathbf{y}, \quad \forall k \in \mathcal{K} \quad (1c)$$

$$\mathbf{A}'\mathbf{y} = \mathbf{c}, \quad (1d)$$

$$\|\mathbf{c}\|_p = 1, \quad (1e)$$

$$\mathbf{c} \in \mathbb{R}^n, \quad \mathbf{z}^k \in \mathbb{R}^n, \quad \mathbf{y} \in \mathbb{R}_{\geq 0}^{|\mathcal{R}|}. \quad (1f)$$

309 In the above model, constraint (1b) enforces primal feasibility for the perturbed optimal solutions  
 310  $\mathbf{z}^k$ , constraints (1d) and (1f) are dual feasibility and constraint (1c) is the strong duality constraint  
 311 so that the recovered  $\mathbf{c}$  optimizes the perturbed points  $\mathbf{z}^k$ . Finally, constraint (1e) ensures that the  
 312 trivial solution  $\mathbf{c} = 0$  is removed from the feasible set of IO by regularizing the norm of the vector  
 313 by some norm  $p$ . Note that IO has  $n + m + (n \times K)$  variables and  $2K + 2$  constraints,  $K + 1$  of  
 314 which are non-convex. Specifically, we note that both the number of variables and the number of  
 315 constraints grow with the number of observations  $K$ . Previous work has extensively studied this  
 316 problem (for instance, see Aswani et al. (2018), Chan et al. (2019)). The inverse model recovers the  
 317 cost vector that minimizes an optimality criterion.

318 **2.2. Learning Optimal Solutions of Partially Known Linear Optimization Problems with  
 319 Constraints Priorities**

The inverse optimization model IO outlined in the previous section is useful in recovering the unknown cost vector of a linear FO, however, this model is too complex and does not scale well to larger instances, due mainly to non-convex constraints in the order of observations and dimensionality issues arising from addition of new perturbed points for each observation. However, a natural observation dictates that if the optimal solution of FO is obtained using the noisy observations and the known parameters of FO, then the true cost vector can become readily available

(Tavashioğlu et al. 2018). This observation leads to an alternative model of the inverse optimization problem, where a new metric of optimality is minimized so that the closest possible optimal solution of FO to the observations is achieved with respect to a predefined metric. As such, in this section, we detail the models for solving the inverse optimization problem by learning the optimal solution of FO. We define the FO model as follows:

$$\text{FO}(\mathbf{c}, \Omega) : \underset{\mathbf{x}}{\text{minimize}} \quad \mathbf{c}'\mathbf{x} \quad (2a)$$

$$\text{subject to} \quad \mathbf{Ax} \geq \mathbf{b}, \quad (2b)$$

$$\mathbf{A}_T \mathbf{x} \geq \mathbf{b}_T, \quad (2c)$$

$$\mathbf{x} \in \mathbb{R}^n. \quad (2d)$$

Without loss of generality, we categorize the constraints shaping  $\Omega$  based on their importance in the problem context. We introduce three constraint types: (i,) *relevant constraints* ( $\mathcal{R} \neq \emptyset$ ): Important constraints considered by the decision-maker, analogous to conventional constraints in optimization frameworks. (ii,) *preferred constraints* ( $\mathcal{P} \subseteq \mathcal{R}$ ): A subset of relevant constraints that the decision-maker prefers to have active at optimality. (iii,) *trivial constraints* ( $\mathcal{T}$ ): Constraints necessary for problem well-definedness but not of primary interest to the decision-maker. For example, in a diet recommendation problem, nutritional requirements could be relevant constraints, specific nutritional goals (e.g., maximizing protein intake) could be preferred constraints, and non-negativity constraints on food servings could be trivial constraints. For simplicity, we treat all preferred constraints as equally important, though the methodology can accommodate different preference levels. The distinction between preferred and relevant constraints is explored in Sections 4 and 5 to illustrate meaningfully different optimal solutions. This section focuses primarily on relevant and trivial constraints. If all constraints are equally important or their significance is unknown, we set  $\mathcal{P} = \mathcal{T} = \emptyset$ , with all constraints included in  $\mathcal{R}$ .

For the FO model,  $\mathbf{c}$  is the cost function (2a) and is assumed to be unknown and the feasible set  $\Omega$  is known and characterized as  $\Omega = \{\mathbf{x} \in \mathbb{R}^n | \mathbf{Ax} \geq \mathbf{b}, \mathbf{A}_T \mathbf{x} \geq \mathbf{b}_T\}$ , where  $\mathbf{A} \in \mathbb{R}^{|\mathcal{R}| \times n}$ ,  $\mathbf{b} \in \mathbb{R}^{|\mathcal{R}|}$  represent the relevant (conventional) constraints ( $|\mathcal{R}| \geq 1$ ), and  $\mathbf{A}_T \in \mathbb{R}^{|\mathcal{T}| \times n}$ ,  $\mathbf{b}_T \in \mathbb{R}^{|\mathcal{T}|}$  the trivial constraints ( $\mathcal{T}$ ). Since  $\mathcal{P} \subseteq \mathcal{R}$ , if  $\mathcal{P} \neq \emptyset$ , we can write  $\mathbf{A} = [\mathbf{A}_{\mathcal{P}}; \mathbf{A}_{\mathcal{R} \setminus \mathcal{P}}]$  and  $\mathbf{b} = [\mathbf{b}_{\mathcal{P}}; \mathbf{b}_{\mathcal{R} \setminus \mathcal{P}}]$ , where  $\mathbf{A}_{\mathcal{P}}$  and  $\mathbf{b}_{\mathcal{P}}$  correspond to the preferred constraints and  $\mathbf{A}_{\mathcal{R} \setminus \mathcal{P}}$  and  $\mathbf{b}_{\mathcal{R} \setminus \mathcal{P}}$  are the not-preferred relevant constraints. For ease of notation, we define  $\mathcal{J}$  and  $\mathcal{J}_T$  to be the set of indices of constraints in  $\mathcal{R}$  and  $\mathcal{T}$ , respectively. We denote  $\Omega^{opt}(\mathbf{c})$  as the set of optimal solutions to  $\text{FO}(\mathbf{c}, \Omega)$ , and define  $\Omega^{opt} = \bigcup_{c \neq 0} \Omega^{opt}(\mathbf{c})$ . Additionally, we also define  $\Omega_{\mathcal{R}}^{opt} = \{\mathbf{x} \in \Omega^{opt} | \mathbf{a}_j \mathbf{x} = b_j, \exists j \in \mathcal{J}\}$  and  $\Omega_{\mathcal{T}}^{opt} = \{\mathbf{x} \in \Omega^{opt} | \mathbf{a}_j \mathbf{x} = b_j, \exists j \in \mathcal{J}_T\}$  and observe that  $\Omega^{opt} = \Omega_{\mathcal{R}}^{opt} \cup \Omega_{\mathcal{T}}^{opt}$ . For a linear optimization problem,  $\Omega^{opt}$  represents the boundary of the closed polyhedral feasible set  $\Omega$  and  $\Omega_{\mathcal{R}}^{opt}$  represents a subset

<sup>344</sup> of the boundary that has an intersection with one facet defining inequality from the relevant  
<sup>345</sup> constraints.

Our assumption diverges from the mainstream inverse optimization literature. We posit that all observations are perturbations of a single, unknown optimal decision, rather than noisy realizations of potentially different optimal solutions. This distinction is crucial when the FO problem has a multi-valued solution set. While existing IO models are suitable when FO has a single-valued solution set (Aswani et al. 2018), many practical settings involve non-unique optimal solutions for a fixed cost vector  $\mathbf{c}$ . In such cases, our approach modifies IO to find  $\mathbf{c}$  such that  $\mathbf{x} \in \Omega^{opt}$  is contained in  $\Omega^{opt}(\mathbf{c})$  and minimizes the sum of distances to observations  $\mathcal{X}$ . This generalization is crucial for non-unique optimal solution set, providing a more robust framework for inverse optimization, while drastically reducing the problem size. Then, our goal is to learn the optimal solution  $\mathbf{z} \in \Omega^{opt}$  and the cost vector  $\mathbf{c} \in \mathbb{R}^n$  of FO based on a given set of observation(s),  $\mathcal{X}$  which may be noised by error or bounded rationality and not necessarily optimal or feasible for FO. Let  $\mathbf{y} \in \mathbb{R}_{\geq 0}^{|\mathcal{R}|}$  and  $\bar{\mathbf{y}} \in \mathbb{R}_{\geq 0}^{|\mathcal{T}|}$  be the corresponding dual variables for the relevant constraints  $\mathcal{R}$  (2b) and the trivial constraints  $\mathcal{T}$  (2c), respectively. A solution  $\mathbf{z} \in \Omega$  to  $\text{FO}(\mathbf{c}, \Omega)$  is contained in  $\Omega^{opt}$  if and only if a primal-dual feasible pair  $(\mathbf{z}, (\mathbf{y}, \bar{\mathbf{y}}))$  exists such that  $\mathbf{c}'\mathbf{z} = \mathbf{y}'\mathbf{b} + \bar{\mathbf{y}}'\mathbf{b}_T$  and  $\mathbf{c} \neq \mathbf{0}$ . We formulate our *Inverse Learning* model (IL).

$$\text{IL}(\mathcal{X}, \Omega) : \underset{\mathbf{c}, \mathbf{y}, \bar{\mathbf{y}}, \mathbf{z}}{\text{minimize}} \quad \sum_{k \in \mathcal{K}} \|\mathbf{x}^k - \mathbf{z}\|_l \quad (3a)$$

$$\text{subject to} \quad \mathbf{A}\mathbf{z} \geq \mathbf{b}, \quad (3b)$$

$$\mathbf{A}_T \mathbf{z} \geq \mathbf{b}_T, \quad (3c)$$

$$\mathbf{c}'\mathbf{z} = \mathbf{b}'\mathbf{y}, \quad (3d)$$

$$\mathbf{A}'\mathbf{y} = \mathbf{c}, \quad (3e)$$

$$\bar{\mathbf{y}} = \mathbf{0}, \quad (3f)$$

$$\mathbf{1}'_{|\mathcal{R}| \times 1} \mathbf{y} = 1, \quad (3g)$$

$$\mathbf{c}, \mathbf{z} \in \mathbb{R}^n, \quad \mathbf{y} \in \mathbb{R}_{\geq 0}^{|\mathcal{R}|}, \quad \bar{\mathbf{y}} \in \mathbb{R}_{\geq 0}^{|\mathcal{T}|}. \quad (3h)$$

<sup>346</sup> Constraints (3b) and (3c) enforce primal feasibility for the learned solution  $\mathbf{z}$ . Constraints (3e)–(3f)  
<sup>347</sup> and (3h) are dual feasibility for relevant and trivial constraints. The dual variables corresponding  
<sup>348</sup> to relevant constraints ( $y_{j \in \mathcal{J}}$ ) can assume non-zero values to minimize any influence of the trivial  
<sup>349</sup> constraints  $\mathcal{T}$  (if any) on the recovered cost vector. Constraint (3d) is the strong duality constraint  
<sup>350</sup> for relevant constraints so that the recovered  $\mathbf{c}$  is not influenced by trivial constraints; therefore the  
<sup>351</sup> zero term  $\bar{\mathbf{y}}'\mathbf{b}_T$  is dropped based on constraint (3f). Finally, the convex constraint (3g) ensures that  
<sup>352</sup> the trivial solution  $\mathbf{c} = \mathbf{0}$  is excluded from the model. We show in proposition (2) that the focus

353 to learn one optimal solution of FO allows for replacing the non-convex constraint (1e) with the  
 354 convex constraint (3g). Next we show that IL is feasible for any set of observations, as Proposition  
 355 1 shows by constructing a feasible solution.

356 PROPOSITION 1. *IL is feasible for any given  $\mathcal{X} \in \mathbb{R}^{n \times K}$ . In particular, the solution  $(\mathbf{a}'_j, \mathbf{e}_j, \mathbf{0}, \mathbf{z}_0)$  is*  
 357 *feasible for  $IL(\mathcal{X}, \Omega)$ , where  $\mathbf{a}_j$  is the  $j^{\text{th}}$  row of  $\mathbf{A}$ , and  $j \in \mathcal{J}$  corresponds to a constraint in  $\mathcal{R}$  for*  
 358 *which  $\mathbf{a}_j \mathbf{z}_0 = b_j$ .*

359 One difference between IL and the existing models lies in the distinction between relevant and  
 360 trivial constraints, where trivial constraints are not of interest to be active at optimality (constraint  
 361 (3f)). Note that this constraint does not mean that trivial constraints will not be binding at all  
 362 for  $\mathbf{z}$ , and instead, ensures that the cost vector can be written as a conic combination of only the  
 363 rows of the relevant matrix,  $\mathbf{A}$ . Another notable difference is that a linear constraint, (3g), is used  
 364 to normalize  $\mathbf{c}$  and avoids trivial solutions for the cost vector replacing the non-convex constraint  
 365 (1e) in IO. Proposition 2 shows that in IL the linear constraint (3g) is sufficient to rule out trivial  
 366 solutions such as  $\mathbf{c} = \mathbf{0}$  and thus results in reduced complexity of the inverse model.

367 PROPOSITION 2. *For any feasible solution  $(\hat{\mathbf{c}}, \hat{\mathbf{y}}, \hat{\bar{\mathbf{y}}}, \hat{\mathbf{z}})$  for IL, we have  $\hat{\mathbf{c}} \neq \mathbf{0}$ .*

368 Proposition 2 is shown by proving that any solution with  $\mathbf{c} = \mathbf{0}$  results in an implicit inequality  
 369 for  $\Omega$  which contradicts  $\Omega$  being full dimensional. We note that a desirable characteristic of IL is  
 370 that for a feasible solution  $(\mathbf{c}, \mathbf{y}, \bar{\mathbf{y}}, \mathbf{z})$  for IL, the learned solution  $\mathbf{z}$  is optimal for  $FO(\mathbf{c}, \Omega)$ . This is  
 371 important since if IL is learning the true FO optimal solution (in probability), then the true cost  
 372 vector (or a set containing the true cost vector) is readily available (Tavashoglu et al. 2018). We  
 373 show first in Theorem 1 that the inverse learning approach learns an optimal solution to the original  
 374 FO using the observed solutions  $\mathcal{X}$  directly. We then show in Theorem 2 that IL indeed finds the  
 375 true FO optimal solution in probability and therefore is an alternative model to solve the inverse  
 376 optimization problem. We also note that this is all achieved while IL has less number of variables  
 377 ( $n + m + n$ ) and constraints (5) in comparison to IO. Additionally, the number of constraints and  
 378 variables of IL do not increase with the number of observations and only depend on the dimensions  
 379 and the number of constraints of FO

380 THEOREM 1. *For each feasible solution  $(\hat{\mathbf{c}}, \hat{\mathbf{y}}, \hat{\bar{\mathbf{y}}}, \hat{\mathbf{z}})$  for IL,  $\hat{\mathbf{z}} \in \Omega_{\mathcal{R}}^{\text{opt}}$ . For an optimal solution*  
 381  *$(\mathbf{c}^*, \mathbf{y}^*, \bar{\mathbf{y}}^*, \mathbf{z}^*)$  for IL,  $\|\mathbf{x}^k - \mathbf{z}^*\|_l \leq \|\mathbf{x}^k - \mathbf{z}\|_l \quad \forall \mathbf{z} \in \Omega_{\mathcal{R}}^{\text{opt}}$*

382 Theorem 1 illustrates that the learned solution through the inverse model is optimal for the  
 383 forward model given the recovered cost vector through the model and removes the need to solve the  
 384 forward model afterwards. This distinction is important since solving  $FO(\mathbf{c}^*, \Omega)$  does not necessarily  
 385 find the closest optimal solution to  $\mathcal{X}$  if  $\dim(\Omega^{\text{opt}}(\mathbf{c}^*)) \geq 1$ , as highlighted as an issue of instability in

386 Shahmoradi and Lee (2022b). Additionally, since IL distinguishes between relevant  $\mathcal{R}$  and trivial  $\mathcal{T}$   
 387 constraints, the solution  $\mathbf{z}$  prioritizes the relevant constraints to bind at optimality with a recovered  
 388  $\mathbf{c}$  that is a conic combination of them, hence, improving the cost vector recovery capabilities in the  
 389 existence of such information.

390 THEOREM 2. *Let  $(\mathbf{c}^{opt}, \mathbf{x}^{opt})$  be the true cost vector and optimal solution of FO and let  $(\mathbf{c}^*, \mathbf{y}^*, \bar{\mathbf{y}}^*, \mathbf{z}^*)$   
 391 be an optimal solution for  $IL(\mathcal{X}, \Omega)$ . If all observations in  $\mathcal{X}$  are noised realizations of  $\mathbf{x}^{opt}$ , then  
 392  $\mathbb{E}(\mathbf{z}^*) = \mathbf{x}^{opt}$ .*

393 Theorem 2 recognizes that IL is suited to learn the true optimal solution given noised realizations  
 394 of the optimal solution for a partially known linear optimization problem. Moreover, if the true cost  
 395 vector is normalized to specific values, the cost vector found by IL also reaches the true cost vector  
 396 in expectation, as stated without proof in Corollary 1.

397 COROLLARY 1. *Let  $(\mathbf{c}^*, \mathbf{y}^*, \bar{\mathbf{y}}^*, \mathbf{z}^*)$  be an optimal solution for  $IL(\mathcal{X}, \Omega)$ . If all observations in  $\mathcal{X}$   
 398 are noisy realizations of the true optimal solution  $\mathbf{x}^{opt}$  of the forward problem  $FO(\mathbf{c}^{opt}, \Omega)$ , then  
 399  $\mathbb{E}(\mathbf{c}^*) = \mathbf{c}^{opt}$ .*

400 Figure 1 illustrates behavior of the IL model. This schematic figure showcases a given feasible  
 401 region with two observations (gray dots). Employing a 2-norm distance metric, we recover the  
 402 underlying FO solution and cost vector using classical inverse optimization (black ink) and the  
 403 IL model (green ink) for two cases. In the first case (Figure 1(a)), we assume all constraints are  
 404 conventional, or using our terminology they are all relevant (dashed gray lines), and no expert  
 405 information or additional knowledge was conveyed about any of the constraints. Solving this problem  
 406 with both classical inverse optimization and IL results in the same cost vector. In this example,  
 407 the main difference between the models is that IL finds an optimal solution ( $\mathbf{x}_1^*$ ) that is as close  
 408 as possible to the observations. The classical inverse optimization returns an extreme point as the  
 409 optimal solution ( $\bar{\mathbf{x}}$ ), which is situated further from the observations. In the second case (Figure  
 410 1(b)), we assume additional knowledge is available that two of the constraints are indeed trivial  
 411 (dotted red lines), meaning that they are not important to the user to bind at optimality. For  
 412 instance, these constraints may be in place to keep the problem well-defined or represent resources  
 413 that the user has a surplus of and is not concerned with binding them at optimality. The solution  
 414 found by the classical inverse optimization will not change. The IL, however, can use this additional  
 415 information to find an optimal solution ( $\mathbf{x}_2^*$ ) that binds at least one of the relevant constraints.  
 416 In this example, the corresponding cost vector ( $\mathbf{c}_2^*$ ) also changes to remain in the cone of relevant  
 417 constraints instead of being defined solely by trivial constraints. We note that these differences stem  
 418 from the inclusion of different tiers of constraints as well as the differentiating assumption in our

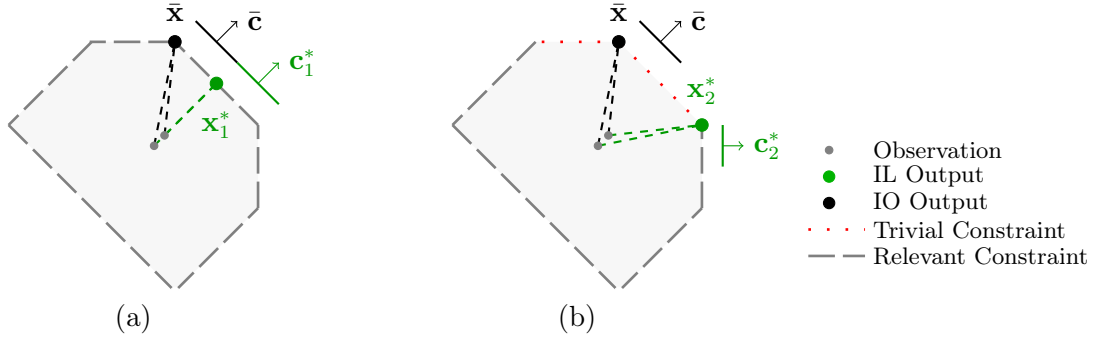


**Figure 1** The figures show a given feasible region (shaded gray) and two observations (gray dots). Using a 2-norm distance metric, classical inverse optimization recovers  $\bar{c}$  and  $\bar{x}$  as the cost vector and optimal solution of FO. The inverse learning approach (green ink), however, finds a closer optimal solution ( $x_1^*$ ) in Figure (a), even though the cost vector  $c_1^*$  remains similar to that recovered by inverse optimization. In Figure (b), additional information is provided that two of the constraints are trivial (red dotted lines). In this case, the inverse learning approach adjusts and recovers the closest point that binds at least one relevant constraint (dashed gray).

model that observations are noised realizations of the same optimal solution, rather than noised optimal solutions of the same cost vector.

The Inverse Learning model offers several compelling advantages over traditional Inverse Optimization approaches. Most important is its superior scalability with respect to the number of observations. While IO models grow linearly in complexity with each additional data point, IL maintains a constant structure, significantly enhancing its applicability to large-scale problems. This scalability is further augmented by IL's reduced number of non-convex constraints—only one compared to IO's  $K + 1$ —leading to more tractable and reliable solution methods. The streamlined formulation of IL not only improves computational efficiency but also potentially increases robustness to outliers, as it doesn't introduce separate variables for each observation. Furthermore, IL's ability to handle infeasible observations more naturally broadens its applicability to real-world scenarios where data may not always conform to model constraints. By learning a single optimal solution rather than fitting each observation individually, IL may better capture the underlying problem structure, potentially improving generalization to unseen data. In addition to having  $K$  primal feasibility conditions for the perturbations, IO includes  $K + 1$  non-convex constraints while IL only has one non-convex strong duality constraint and one primal feasibility constraint (for each tier of constraints) for the learned optimal solution. This reduction significantly improves solution times of IL in comparison to IO (as shown in the numerical example 2). These comparisons are summarized in Table 1.

Considering that constraint (3d) is bilinear and non-convex in IL, we can break down IL to simpler models to improve solution time. Analogous to other inverse linear optimization models in

**Table 1** Comparison of constraint and variable counts in IO and IL models

Model	Variables	Total Constraints	Non-convex Constraints	Change with Observations ( $K$ )	Change with FO Constraints ( $m$ )
IO	$n + m + (n \times K)$	$(m \times K) + K + 2$	$K + 1$	+2n vars, +2 constraints per observation	+1 var per constraint
IL	$n + m + n$	$m + 4$	1	No change	+1 per constraint

$n$ : dimension of decision variables,  $m$ : number of constraints in FO,  $K$ : number of observations

the literature, a similar approach to Chan et al. (2019) can be adapted for the IL framework by solving a series of  $|\mathcal{R}|$  linearly constrained problems. For any feasible solution  $(\mathbf{c}, \mathbf{y}, \bar{\mathbf{y}}, \mathbf{z})$  there exists  $j \in \mathcal{J}$  such that  $\mathbf{a}_j \mathbf{z} = b_j$ , where  $\mathbf{a}_j$  is the  $j^{th}$  row of the matrix  $\mathbf{A}$ . Therefore,  $\mathbf{z} \in \Omega_{\mathcal{R}}^{opt}(\mathbf{a}_j)$ ,  $\forall j \in J$ . Considering solutions that bind at least one relevant constraint allows for removing duality and complementary slackness constraints from IL. As such, there exists an optimal solution  $(\mathbf{c}, \mathbf{y}, \bar{\mathbf{y}}, \mathbf{z})$  for IL where  $\mathbf{c}$  is orthogonal to at least one of the relevant constraints of FO, as formalized in Proposition 3.

PROPOSITION 3. Let  $\mathbf{c} = \mathbf{a}'_j$  and  $\mathbf{y} = e_j$ . Formulation (4) finds  $\mathbf{z}^j \in \Omega_{\mathcal{R}}^{opt}$  which binds the  $j^{th}$  constraint in  $\mathcal{R}$  and minimizes the same objective function as IL. Let  $j_{min} = argmin_{j \in \mathcal{J}} \left\{ \sum_{k \in \mathcal{K}} \|\mathbf{x}^k - \mathbf{z}^j\|_l \right\}$  and  $\mathbf{z}^*$  be the optimal solution of  $IL_{j_{min}}$ , then if the optimal objective value of IL is  $\mathcal{D}^*$ , we have  $\mathcal{D}_{min} = \mathcal{D}^*$  and  $(\mathbf{a}'_{j_{min}}, e_{j_{min}}, \mathbf{0}, \mathbf{z}^*)$  is optimal for IL.

$$IL_j(\mathcal{X}, \Omega) : \underset{\mathbf{z}}{\text{minimize}} \quad \sum_{k \in \mathcal{K}} \|\mathbf{x}^k - \mathbf{z}^j\|_l \quad (4a)$$

$$\text{subject to} \quad \mathbf{a}_j \mathbf{z}^j = b_j, \quad (4b)$$

$$\mathbf{A} \mathbf{z}^j \geq \mathbf{b}, \quad (4c)$$

$$\mathbf{A}_{\mathcal{T}} \mathbf{z}^j \geq \mathbf{b}_{\mathcal{T}}, \quad (4d)$$

$$\mathbf{z}^j \in \mathbb{R}^n. \quad (4e)$$

Proposition 3 demonstrates that since all learned solutions from IL bind at least one relevant constraint, it suffices to solve convex linearly constrained optimization models that find FO solutions that bind specified relevant constraint while minimizing the distance objective. As such, an optimal solution for FO (which is a part of an optimal solution of IL) can be achieved by solving such optimization problems for all relevant constraints and choosing the solution corresponding to the minimum distance among all obtained solutions. We also note that for the special case where  $\mathcal{X} \cap \Omega = \emptyset$ , one can simplify solving IL even further by leveraging the structure of  $\mathcal{X}$  to solving one optimization problem, as outlined in the following:

PROPOSITION 4. Let  $\mathbf{z}^*$  be an optimal solution to formulation 5. If  $\mathcal{X} \cap \Omega = \emptyset$ , then  $\mathbf{z}^* \in \Omega^{opt}$  and  $(\mathbf{a}'_j, e_j, \mathbf{0}, \mathbf{z}^*)$  is optimal for IL where  $j \in \mathcal{J}$  designates a relevant constraint where  $\mathbf{a}_j \mathbf{z}^* = b_j$  and  $e_j$  is the  $j^{th}$  unit vector.

$$\underset{\mathbf{z}}{\text{minimize}} \quad \sum_{k \in \mathcal{K}} \|\mathbf{x}^k - \mathbf{z}\|_l \quad (5a)$$

$$\text{subject to} \quad \mathbf{A}\mathbf{z} \geq \mathbf{b}, \quad (5b)$$

$$\mathbf{A}_{\mathcal{T}}\mathbf{z} \geq \mathbf{b}_{\mathcal{T}}, \quad (5c)$$

$$\mathbf{z} \in \mathbb{R}^n \quad (5d)$$

455 Based on Proposition 4, for the case where  $\mathcal{X} \cap \Omega = \emptyset$ , an optimal solution to  $\text{IL}(\mathcal{X}, \Omega)$  is efficiently  
 456 found. We additionally note for the case where  $|\mathcal{X}| = 1$ , IL is equal to IO, for which previous works  
 457 have developed closed form solutions (Chan et al. 2019). The inverse learning models described  
 458 in the previous section aim to tackle three main known issues with inverse optimization models,  
 459 namely, controlling the distance of the forward optimal solution to the set of given observations,  
 460 the issue of non-uniqueness of forward optimal solutions and reduced complexity for inverse linear  
 461 optimization. We next outline how the IL models can be interpreted for the convex parametric case  
 462 where pairs of observations and parameters are observed.

### 463 2.3. Extension of Inverse learning to Convex Parametric Optimization

We extend the inverse learning models to the setting of convex optimization with both known and unknown parameters, where for each known parameter, we have a set of noisy observations of an optimal solution. Consider a convex forward optimization problem  $\text{FO}(f(\mathbf{x}, \mathbf{u}, \theta), \Omega(\mathbf{u}, \theta))$  where the objective function  $f : \mathbb{R}^n \times \mathbb{R}^q \times \mathbb{R}^p \rightarrow \mathbb{R}$  is convex in  $\mathbf{x}$  for fixed  $(\mathbf{u}, \theta)$  and strictly monotone, and the feasible set  $\Omega(\mathbf{u}, \theta) = \{\mathbf{x} \in \mathbb{R}^n | g_i(\mathbf{x}, \mathbf{u}, \theta) \leq 0, i = 1, \dots, m\}$  is characterized by convex constraint functions  $g_i$  that depend on decision variables  $\mathbf{x}$ , known parameters  $\mathbf{u} \in \mathbb{R}^q$ , and unknown parameters  $\theta \in \mathbb{R}^p$ . We are given  $K$  distinct parameter values  $\mathbf{u}^k \in U, k = 1, \dots, K$ , and for each  $\mathbf{u}^k$ , we have a set of observations  $\{\mathbf{x}^{k,j} \in \mathbb{R}^n : j \in J_k\}$  that are noisy realizations of one optimal solution  $\mathbf{x}_{opt}^k \in S(\mathbf{u}, \theta)$ , where  $S(\mathbf{u}, \theta)$  is the solution set of  $\text{FO}(f(\mathbf{x}, \mathbf{u}, \theta), \Omega(\mathbf{u}, \theta))$  for given  $\mathbf{u}$  and  $\theta$ . Each  $\mathbf{x}^{k,j}$  is a noisy measurement of some  $\mathbf{x}_{opt}^k \in S(\mathbf{u}^k, \theta_0)$ , with  $\theta_0$  being the true unknown parameter. The goal is to learn the optimal solutions  $\mathbf{x}_{opt}^k$  and estimate the unknown parameters  $\theta$ . The Convex Inverse Learning (CIL) model is a generalization of the inverse learning framework for convex optimization problems with both known and unknown parameters. The model aims to learn the optimal solutions  $\mathbf{x}_{opt}^k$  for each known parameter set  $\mathbf{u}^k$  and estimate the unknown parameters  $\theta$  using the noisy observations  $\{\mathbf{x}^{k,j} : j \in J_k\}$  of the optimal solutions. CIL can be formulated as:

$$\text{CIL}(\{\mathbf{x}^{k,j} : j \in J_k\}, \mathbf{u}^k) : \underset{\mathbf{x}_{opt}^k, \theta, \lambda_i^k}{\text{minimize}} \quad \sum_{k=1}^K \sum_{j \in J_k} \|\mathbf{x}^{k,j} - \mathbf{x}_{opt}^k\|_\ell \quad (6a)$$

$$\text{subject to } g_i(\mathbf{x}_{opt}^k, \mathbf{u}^k, \theta) \leq 0, \quad i = 1, \dots, m, \quad \forall k \quad (6b)$$

$$\nabla_{\mathbf{x}} f(\mathbf{x}_{opt}^k, \mathbf{u}^k, \theta) + \sum_{i=1}^m \lambda_i^k \nabla_{\mathbf{x}} g_i(\mathbf{x}_{opt}^k, \mathbf{u}^k, \theta) = 0, \quad \forall k \quad (6c)$$

$$\lambda_i^k g_i(\mathbf{x}_{opt}^k, \mathbf{u}^k, \theta) = 0, \quad i = 1, \dots, m, \quad \forall k \quad (6d)$$

$$\lambda_i^k \geq 0, \quad i = 1, \dots, m, \quad \forall k \quad (6e)$$

$$\mathbf{1}'_{|\mathcal{R}| \times 1} \sum_{i=1}^m \lambda_i^k = 1, \quad \forall k \quad (6f)$$

where  $\{\mathbf{x}^{k,j} : j \in J_k\}$  are decision variables representing the noisy observations of the optimal solutions for each known parameter set  $\mathbf{u}^k$ , and  $\lambda_i^k$  are dual variables associated with the  $i$ -th constraint for the  $k$ -th known parameter set. The objective function minimizes the sum of the  $\ell$ -norm distances between the learned optimal solutions  $\mathbf{x}_{opt}^k$  and the corresponding noisy observations  $\mathbf{x}^{k,j}$  across all known parameter sets  $\mathbf{u}^k$  and their respective observations. Constraint (6b) ensures primal feasibility of the learned optimal solutions  $\mathbf{x}_{opt}^k$  with respect to the convex constraints  $g_i(\mathbf{x}, \mathbf{u}^k, \theta) \leq 0$  for each known parameter set  $\mathbf{u}^k$ . Constraint (6c) represents the stationarity condition of the KKT optimality conditions, which requires that the gradient of the Lagrangian function with respect to  $\mathbf{x}$  is zero at the optimal solution  $\mathbf{x}_{opt}^k$  for each known parameter set  $\mathbf{u}^k$ . Constraint (6d) represents the complementary slackness condition of the KKT optimality conditions, which ensures that either the constraint  $g_i(\mathbf{x}_{opt}^k, \mathbf{u}^k, \theta)$  is active (i.e., equal to zero) or the corresponding dual variable  $\lambda_i^k$  is zero for each constraint  $i$  and known parameter set  $\mathbf{u}^k$ . Constraint (6e) ensures the non-negativity of the dual variables  $\lambda_i^k$  for each constraint  $i$  and known parameter set  $\mathbf{u}^k$ . Finally, constraint (6f) is a normalization constraint that prevents trivial solutions (e.g., all dual variables being zero) and ensures that the dual variables sum up to one for each known parameter set  $\mathbf{u}^k$ . This constraint is similar to the one used in the inverse learning model to avoid trivial solutions. The CIL model has several important properties that make it suitable for learning optimal solutions and estimating unknown parameters in convex optimization problems:

**PROPOSITION 5.** *CIL is feasible if the forward optimization problem  $FO(f(\mathbf{x}, \mathbf{u}, \theta), \Omega(\mathbf{u}, \theta))$  is feasible for all known parameter sets  $\mathbf{u}^k$  and the true unknown parameters  $\theta_0$ .*

The feasibility of the CIL model, as established in Proposition 5, lays the foundation for further analysis of its properties. With the assurance that the model admits a solution under mild conditions, we can now shift our focus to the optimality of the obtained solutions. Proposition 6 builds on the feasibility result and provides a crucial characterization of the solutions returned by the CIL model. It establishes a connection between the optimality of the learned solutions and the underlying forward optimization problem, demonstrating the effectiveness of the CIL model in recovering meaningful and consistent solutions. This optimality result is a key stepping stone towards understanding the broader capabilities and performance guarantees of the CIL model.

492 PROPOSITION 6. If  $(\mathbf{x}_{opt}^{k*}, \theta^*, \lambda_i^{k*})$  is an optimal solution to CIL, then  $\mathbf{x}_{opt}^{k*}$  is an optimal solution to  
 493 the forward problem  $FO(f(\mathbf{x}, \mathbf{u}^k, \theta^*), \Omega(\mathbf{u}^k, \theta^*))$  for each known parameter set  $\mathbf{u}^k$ .

494 The optimality of the solutions obtained from the CIL model, as established in Proposition 6, is a  
 495 significant result that highlights the model's ability to learn solutions that align with the underlying  
 496 optimization problem. However, to fully understand the performance of the CIL model, it is crucial  
 497 to investigate how well these learned solutions approximate the true optimal solutions, especially  
 498 in the presence of noisy observations. Theorem 3 takes the analysis a step further by providing  
 499 a rigorous convergence guarantee for the CIL model. It quantifies the relationship between the  
 500 learned solutions and the true optimal solutions, establishing bounds on their expected distance as  
 501 a function of the number of observations and the noise level. This convergence result demonstrates  
 502 the reliability of the CIL model and its ability to accurately learn optimal solutions.

503 THEOREM 3. Let  $(\mathbf{x}_{opt}^{k*}, \theta^*, \lambda_i^{k*})$  be an optimal solution to the CIL model. If the noisy  
 504 observations  $\mathbf{x}^{k,j}$  are generated as  $\mathbf{x}^{k,j} = \mathbf{x}_{true}^k + \epsilon^{k,j}$ , where  $\mathbf{x}_{true}^k$  is an optimal solution to  
 505  $FO(f(\mathbf{x}, \mathbf{u}^k, \theta_0), \Omega(\mathbf{u}^k, \theta_0))$  and  $\epsilon^{k,j}$  are independent random noises with  $\mathbb{E}[\epsilon^{k,j}] = 0$  and  $\mathbb{E}[||\epsilon^{k,j}||_\ell^2] \leq$   
 506  $\sigma^2$  for all  $k$  and  $j$ , then

$$\mathbb{E}[||\mathbf{x}_{opt}^{k*} - \mathbf{x}_{true}^k||_\ell] \leq \frac{2\sigma}{\sqrt{J_k}}, \quad \forall k, \quad (7)$$

507 where  $J_k$  is the number of observations for the  $k$ -th known parameter set.

508 We note that the convergence rate provided in Theorem 3 is not particularly fast, however, this  
 509 result holds for a general case of convex parametric inverse optimization. Faster convergence rates  
 510 can be explored for specific problem structures, but this is beyond the scope of this paper and is  
 511 deferred to future work. The CIL model can be seen as a generalization of the inverse learning  
 512 (IL) model presented in the paper. The IL model considers a linear forward optimization problem  
 513 with an unknown cost vector and a known feasible set, and aims to learn the optimal solution and  
 514 the cost vector using a set of noisy observations. The CIL model extends the IL model in several  
 515 aspects: 1. The forward problem in the CIL model is a general convex optimization problem with  
 516 both known and unknown parameters, while the IL model considers a linear optimization problem  
 517 with an unknown cost vector. 2. The CIL model learns the optimal solutions for multiple known  
 518 parameter sets, while the IL model learns a single optimal solution. 3. The CIL model estimates the  
 519 unknown parameters of the forward problem, while the IL model focuses on learning the unknown  
 520 cost vector. 4. The CIL model uses the KKT optimality conditions to ensure the optimality of the  
 521 learned solutions, while the IL model relies on the strong duality condition and the complementary  
 522 slackness condition. Despite these differences, the core idea of learning optimal solutions from noisy  
 523 observations remains the same in both models. The CIL model can be seen as a more general and  
 524 flexible framework that can handle a wider range of optimization problems and incorporate more  
 525 complex parameter structures.

526 THEOREM 4. Let  $(\mathbf{x}_{opt}^{k*}, \theta^*, \lambda_i^{k*})$  be an optimal solution to the CIL model. Suppose the following  
 527 conditions hold:

- 528 1. The noisy observations  $\mathbf{x}^{k,j}$  are generated as  $\mathbf{x}^{k,j} = \mathbf{x}_{true}^k(\theta_0) + \epsilon^{k,j}$ , where  $\mathbf{x}_{true}^k(\theta_0)$  is an optimal  
 529 solution to  $FO(f(\mathbf{x}, \mathbf{u}^k, \theta_0), \Omega(\mathbf{u}^k, \theta_0))$  and  $\epsilon^{k,j}$  are independent and identically distributed  
 530 random noises with  $\mathbb{E}[\epsilon^{k,j}] = 0$  and  $\mathbb{E}[||\epsilon^{k,j}||_\ell^2] \leq \sigma^2$  for all  $k$  and  $j$ .
- 531 2. The feasible set mapping  $\Omega(\mathbf{u}, \theta)$  is continuous in  $\theta$  for all  $\mathbf{u} \in U$ .
- 532 3. The objective function  $f(\mathbf{x}, \mathbf{u}, \theta)$  is strictly monotone in  $\theta$  and the constraints  $g_i(\mathbf{x}, \mathbf{u}, \theta)$  are  
 533 strictly monotone in  $\theta$  for all  $i = 1, \dots, m$ , for all  $\mathbf{x} \in \mathbb{R}^n$ , and for all  $\mathbf{u} \in U$ .

534 Then, as the number of observations  $J_k$  goes to infinity for all  $k$ , the estimated parameters  $\theta^*$   
 535 converge in probability to the true parameters  $\theta_0$ , i.e.,  $\theta^* \xrightarrow{P} \theta_0$ .

536 Theorem 4 establishes the consistency of the parameter estimation in the CIL model. Under the  
 537 assumptions of unbiased and bounded noisy observations, continuity of the feasible set mapping,  
 538 and strict monotonicity of the objective function and constraints with respect to the unknown  
 539 parameters, the estimated parameters  $\theta^*$  converge in probability to the true parameters  $\theta_0$  as the  
 540 number of observations increases. This result ensures that the CIL model can accurately recover the  
 541 true parameters asymptotically.

### 542 3. Balancing User Preferences with Expert Interventions

543 In this section, we consider a setting where there is discrepancies between decision maker preferences  
 544 and expert recommendations. This discrepancy can manifest in the noised observations (decision  
 545 maker preference indicator) and the feasible set boundary (expert recommendation indicator). For  
 546 instance, historical dietary behaviors of a user provide a notion of the user preference and dietary  
 547 guidelines provided to the user by an expert bear a notion of expert recommendation. In this setting,  
 548 merely using IO to recover the cost vector will result in FO optimal solutions that are always corner  
 549 points, and hence might not be representative of the user preferences even for the same feasible  
 550 sets. This is while solving IL and minimizing distance functions translates to binding only a few  
 551 constraints for the optimal solution. However, other boundary solutions exist that are farther from  
 552 the observations but bind more constraints, yet are not corner points. As such, we observe a trade-off  
 553 in inverse problems with regards to binding more constraints (trusting the known parameters and  
 554 expert recommendations) and mimicking the observed solutions (trusting the observations and user  
 555 behavior).

556 In this section, we explore the implications of the observation-goal tradeoff in two settings.  
 557 First, we analyze the inverse problem with the goal of formulating models that are aware to the  
 558 observation-goal tradeoff. We propose models that can learn solutions contained in  $\Omega_{\mathcal{R}}^{opt}$  with specific  
 559 characteristics around the number of binding relevant constraints (Section 3.1). We argue that these

models lead to an organic decomposition of the inverse optimization problem that significantly reduces problem size even with the addition of some binary variables. Next, we propose a similar model that aims to navigate  $\Omega^{opt}(\mathbf{c})$  in search of solutions that bind more preferred constraints, giving the decision maker more flexibility in making decisions for any recovered  $\mathbf{c}$  from any inverse optimization model(Section 3.2).

### 3.1. Decomposition of the Inverse Problem and the Observation-Goal Tradeoff

With the aim of controlling the observation-goal tradeoff, we develop the GIL model that finds the closest boundary solution to the observations that binds a given number of relevant constraints. We introduce a set of binary variables,  $v_j$  for all  $j \in \mathcal{J}$ , and an input parameter  $1 \leq r \leq n$  that controls the number of binding relevant constraints. In this case, let  $\mathbf{P} \subseteq \mathcal{J}$  be the set of indices of preferred relevant constraints,  $\mathbf{v}$  the vector of binary variables  $v_j$ ,  $j \in \mathcal{J}$ . The GIL model can be written as follows.

$$\text{GIL}(\mathcal{X}, \Omega, r, \mathbf{P}) : \underset{\mathbf{v}, \mathbf{z}}{\text{minimize}} \quad \omega \sum_{k \in \mathcal{K}} \|\mathbf{x}^k - \mathbf{z}\|_l - (1 - \omega) \sum_{s \in \mathbf{P}} v_s \quad (8a)$$

$$\text{subject to} \quad v_j \mathbf{a}_j \mathbf{z} = v_j b_j, \quad \forall j \in \mathcal{J} \quad (8b)$$

$$\mathbf{A} \mathbf{z} \geq \mathbf{b}, \quad (8c)$$

$$\mathbf{A}_{\mathcal{T}} \mathbf{z} \geq \mathbf{b}_{\mathcal{T}}, \quad (8d)$$

$$\sum_{j \in \mathcal{J}} v_j = r, \quad (8e)$$

$$\mathbf{z} \in \mathbb{R}^n, \quad \mathbf{v} \in \{0, 1\}^{|\mathcal{J}|}. \quad (8f)$$

Constraints (8b) and (8e) ensure that exactly  $r$  relevant constraints are binding for  $\mathbf{z}$ . Note that constraint (8b) is bilinear but can be replaced by linear constraints using the big-M method ( $\mathbf{A} \mathbf{z} \leq \mathbf{b} + M(1 - \mathbf{v})$ ). If no knowledge of the exact value for  $r$  is available, we can either assume  $r = 1$  or convert constraint (8e) to a Lagrangian multiplier to maximize the number of binding relevant constraints. The objective function of GIL forces the learned solution  $\mathbf{z}$  to minimize  $\mathcal{D}$  while binding as many preferred constraints as possible. The parameter  $\omega$  is a user-defined weight that adjusts the observation-goal tradeoff to the desirable balance between the distance to the observations and binding additional preferred constraints. Figure 2 illustrates the observation-goal tradeoff in a schematic two-dimensional example with a single observation (gray dot). The trivial constraints are shown in red dots, relevant constraints in dashed gray, and the preferred constraint in the solid black line in the figures, and a 2-norm metric is used as the distance function. The preferred constraint is not highlighted for binding (i.e.,  $\omega = 1$ ) in Figure 2(a). Instead, the model is solved to bind one and then two relevant constraints,  $\mathbf{z}|_{r=1}$  and  $\mathbf{z}|_{r=2}$ , respectively. As the figure shows, as the value

579 of  $r$  increases, the distance between observations and the learned solution may also increase as the  
 580 solutions rely more on constraints information as opposed to the observations. Figure 2(b) depicts  
 581 the same model but when the preferred constraint is engaged. The model aims to bind the preferred  
 582 constraint when possible. This preference may increase the distance from observations depending  
 583 on the location of the preferred constraints. Note that feasibility of the GIL model may depend on  
 584 the input parameter  $r$ .

585 PROPOSITION 7. *We have the following for GIL:*

- 586 (a)  $GIL(\mathcal{X}, \Omega, r, \mathbf{P})$  is feasible for  $r = 1$ .
- 587 (b)  $GIL(\mathcal{X}, \Omega, r, \mathbf{P})$  is feasible for any  $\forall r \in \{1, \dots, n\}$  when  $\mathcal{T} = \emptyset$ .
- 588 (c) If  $\mathcal{T} = \emptyset$  and  $1 \leq r_1 \leq r_2 \leq n$ , then  $\mathcal{D}_{r_1}^* \leq \mathcal{D}_{r_2}^*$ , where  $\mathcal{D}_{r_1}^*$  and  $\mathcal{D}_{r_2}^*$  are the optimal distance  
 589 objective terms in  $GIL(\mathcal{X}, \Omega, r_1, \mathbf{P})$  and  $GIL(\mathcal{X}, \Omega, r_2, \mathbf{P})$ , respectively.
- 590 (d)  $GIL(\mathcal{X}, \Omega, r, \mathbf{P})$  is feasible for  $r \in \{1, \dots, r_0\}$  if  $\Omega$  has at least one face  $\mathcal{F}$  with  $r_0$  binding relevant  
 591 constraints. In particular, GIL is feasible for all  $r \in \{1, \dots, n\}$  if  $\Omega$  has at least one extreme  
 592 point with  $n$  binding relevant constraints.

593 As Proposition 7 shows, the GIL model is always feasible for  $r = 1$ . In general, the feasibility of  
 594 GIL is contingent on the existence of a face of  $\Omega$  with  $r$  relevant binding constraints. Although  
 595 showing that such faces exist for different values of  $r$  is non-trivial (Civril and Magdon-Ismail 2009),  
 596 Proposition 7(b) asserts that in the absence of trivial constraints where all constraints are assumed  
 597 to be relevant and conventional, GIL is always feasible. Proposition 7(c) summarizes the tradeoff  
 598 between distance to the observations and binding more constraints at optimality for distance-based  
 599 metrics. The observation-goal tradeoff is controlled by the input parameter  $r$ , and as the value of  $r$   
 600 increases, so does the value of  $\mathcal{D}$  at optimality.

601 Proposition 7(d) outlines the condition with which GIL becomes feasible for all  $r \in \{1, \dots, n\}$ . We  
 602 note that this condition is not guaranteed to be satisfied in the general case where  $\mathcal{T} \neq \emptyset$ . In this  
 603 case, feasibility of GIL is equivalent to solving the maximum feasible subset problem (maxFS) for  
 604 the system  $\{\mathbf{x} \in \mathbb{R}^n | \mathbf{Ax} = \mathbf{b}, \mathbf{A}_{\mathcal{T}}\mathbf{z} \geq \mathbf{b}_{\mathcal{T}}\}$ . As such, proposition (8) provides a way to find the range  
 605 of  $r$  values for which GIL is feasible.

PROPOSITION 8. *Let  $(\mathbf{v}^*, \mathbf{z}^*)$  be an optimal solution to the following maximum feasible subset  
 problem:*

$$\underset{\mathbf{v}, \mathbf{z}}{\text{maximize}} \quad \sum_{j \in \mathcal{J}} v_j \quad (9a)$$

$$\text{subject to} \quad v_j \mathbf{a}_j \mathbf{z} = v_j b_j, \quad \forall j \in \mathcal{J} \quad (9b)$$

$$\mathbf{A}_{\mathcal{T}} \mathbf{z} \geq \mathbf{b}_{\mathcal{T}}, \quad (9c)$$

$$v_j \in \{0, 1\}, \quad \forall j \in \mathcal{J}. \quad (9d)$$

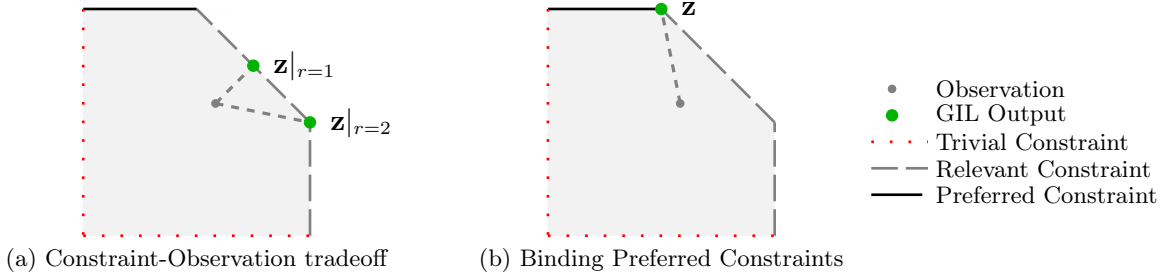


**Figure 2** A schematic figure to illustrate the observation-goal tradeoff in GIL. Figure (a) shows the results for  $r = 1, 2$  when the preferred constraint is not activated ( $\omega = 1$ ). The learned solution  $\mathbf{z}|_{r=1}$  binds one relevant constraint (dashed gray lines) and  $\mathbf{z}|_{r=2}$  binds two, although the distance to observations increases. Figure (b) illustrates the model with an activated preferred constraint ( $\omega \neq 1$ ). The learned solution prioritizes binding the preferred constraint (solid black lines) when possible.

606 Then, GIL is feasible for  $1 \leq r \leq \sum_{j \in \mathcal{J}} v_j^*$  and  $(\mathbf{v}^*, \mathbf{z}^*)$  is a feasible solution for  
 607 GIL( $\mathcal{X}, \Omega, \sum_{j \in \mathcal{J}} v_j^*, \mathbf{P}$ ).

608 Based on Proposition (8), feasibility of GIL for different values of  $r$  can be established by solving  
 609 one instance of the maximum feasible subset problem, which is NP-hard in general. As such, one  
 610 can additionally show that solving GIL is at least as hard as solving the maximum feasible subset  
 611 problem. Hence, the following corollary is provided without proof.

612 COROLLARY 2. GIL is NP-hard.

613 We note that GIL does not explicitly recover a cost vector. Instead, since one can recover the  
 614 binding constraints of any  $\mathbf{z} \in \Omega^{opt}$ , we can readily find a cost vector  $\mathbf{c}$  such that  $\mathbf{z}$  is optimal for  
 615 FO( $\mathbf{c}, \Omega$ ) using previous results (Tavashioğlu et al. 2018). Theorem 5 characterizes the set of all such  
 616 cost vectors. We use the notation  $\mathcal{J}_z \subseteq \mathcal{J}$  to characterize the set of all indices of relevant constraints  
 617 that are binding for  $\mathbf{z}$ . We note that this translates to a natural decomposition of the inverse learning  
 618 problem to finding the optimal solution and then recovering the cost vectors.

619 THEOREM 5. Let  $(\mathbf{v}^*, \mathbf{z}^*)$  be optimal for GIL( $\mathcal{X}, \Omega, r_0, \mathbf{P}$ ). Then,  $\mathbf{z}^*$  is optimal for FO( $\mathbf{c}, \Omega$ ) for any  
 620  $\mathbf{c} \in \text{cone}(\mathbf{a}_t : t \in \mathcal{J}_{z^*})$ .

621 Theorem 5 illustrates two important properties of the goal-integrated inverse learning model.  
 622 First, GIL indeed learns an optimal solution to FO( $\mathbf{c}, \Omega$ ), where  $\mathbf{c}$  is contained in the recovered cone.  
 623 This result asserts that GIL is capable of solving the inverse problem for recovering the missing  
 624 parameters and learning an optimal solution. Second, Theorem 5 shows that learning the optimal  
 625 solution for FO is sufficient to characterize a set of inverse optimal cost vectors. The user can then  
 626 choose their desired cost vector to recover FO, using their method of choice. If no such method

exists, we propose the following method to select a single  $\mathbf{c}$  from the recovered cone. Let  $\mathbf{z}^* \in \Omega^{opt}$  be the learned solution from  $GIL(\mathcal{X}, \Omega, r, \mathbf{P})$ , then the set of non-trivial  $\mathbf{c}$  which makes  $\mathbf{z}^*$  optimal for  $FO(\mathbf{c}, \Omega)$  is characterized by Theorem 5 as

$$\mathcal{Q}(\mathbf{z}^*) = \left\{ \mathbf{c} \in \mathbb{R}^n \mid \mathbf{c} \in \text{cone}(\mathbf{a}_t : t \in \mathcal{J}_{z^*}), \|\mathbf{c}\|_L = 1 \right\}, \quad (10)$$

where a normalization  $\|\cdot\|_L$  is added so that each direction of  $\mathbf{c}$  is represented exactly once in  $\mathcal{Q}$ . To characterize a specific  $\mathbf{c} \in \mathcal{Q}$ , for instance, the objective value of the observations ( $\sum_{k=1}^K \mathbf{c}' \mathbf{x}^k$ ) can be maximized by the following model.

$$\underset{\mathbf{c}}{\text{maximize}} \quad \sum_{k=1}^K \mathbf{c}' \mathbf{x}^k \quad (11a)$$

$$\text{subject to} \quad \mathbf{c} \in \mathcal{Q}(\mathbf{z}^*). \quad (11b)$$

We keep the general definition of  $\mathcal{Q}$  for GIL as a generalization of IL. IL is a reduced version of GIL when  $\mathbf{P} = \emptyset$ , i.e., no preferred constraints are indicated either due to a lack of knowledge or the choice of the user to assume no preferred constraint. Theorem 6 summarizes this result.

**THEOREM 6.** *A solution  $(\mathbf{v}_{GIL}, \mathbf{z}_{GIL})$  is optimal for  $GIL(\mathcal{X}, \Omega, r = 1, \mathbf{P} = \emptyset)$  if and only if there exists  $(\mathbf{c}_{IL}, \mathbf{y}_{IL}, \bar{\mathbf{y}}_{IL}, \mathbf{z}_{IL})$  optimal for  $IL(\mathcal{X}, \Omega)$  such that  $\mathbf{z}_{IL} = \mathbf{z}_{GIL}$ .*

Theorem 6 shows that GIL generalizes IL for learning  $\mathbf{z} \in \Omega^{opt}$ . Since IL learns a solution that minimizes the metric  $\mathcal{D}$ , Theorem 6 shows that  $GIL(\mathcal{X}, \Omega, r = 1, \mathbf{P} = \emptyset)$  also finds a solution  $\mathbf{z} \in \Omega^{opt}$  that minimizes  $\mathcal{D}$  when  $r = 1$  for the given  $\mathcal{X}$ , hence the two models become equivalent in solving  $\mathbf{z}$  as Corollary 3 shows.

**COROLLARY 3.** *Let  $(\mathbf{v}^*, \mathbf{z}^*)$  be optimal for  $GIL(\mathcal{X}, \Omega, r = 1, \mathbf{P} = \emptyset)$ , then  $\forall \hat{\mathbf{c}} \in \text{cone}(\mathbf{a}_t : t \in \mathcal{J}_{z^*})$  where  $\hat{\mathbf{c}} \neq \mathbf{0}$ , we have  $\hat{\mathbf{c}} = \mathbf{A}' \hat{\mathbf{y}}$  where  $\hat{\mathbf{y}} \in \mathbb{R}_{\geq 0}^{|\mathcal{R}|}$  such that  $\hat{y}_j = 0, \forall j \notin \mathcal{J}_{z^*}$  and  $(\hat{\mathbf{c}}, \hat{\mathbf{y}}, \mathbf{0}, \mathbf{z}^*)$  is optimal for  $IL(\mathcal{X}, \Omega)$ .*

Using the expression of Corollary 3, we observe that the learned solution  $\mathbf{z}$  applying GIL to a given set of observations  $\mathcal{X}$  does in fact satisfy strong duality conditions, and consequently, the complementary slackness constraints for  $FO(\mathbf{c}, \Omega)$  for any non-zero  $\mathbf{c} \in \text{cone}(\mathbf{a}_t : t \in \mathcal{J}_{z^*})$ . For the remainder of this section, we turn our attention to the interplay between the behavior of GIL and different choices for  $\mathbf{P}$ . Remark 1 shows that GIL learns a solution  $\mathbf{z} \in \Omega^{opt}$  that returns a larger value of the metric  $\mathcal{D}$  when there are preferred constraints. In other words, when  $\mathbf{P} \neq \emptyset$ , then the solution of GIL is no better than when  $\mathbf{P} = \emptyset$  because inclusion of preferred constraints results in learning solutions with increased values of the distance metric  $\mathcal{D}$  at optimality.

Figure 3 shows an example of how learned solutions of GIL compare against each other for the case of a 2-norm distance metric. Three learned solutions are demonstrated in Figure 3, where

( $\mathbf{v}_1, \mathbf{z}|_{r=1}^{\mathbf{P}=\emptyset}$ ) and ( $\mathbf{v}_2, \mathbf{z}|_{r=2}^{\mathbf{P}=\emptyset}$ ) are optimal solutions to  $\text{GIL}(\mathcal{X}, \Omega, r=1, \mathbf{P}=\emptyset)$  and  $\text{GIL}(\mathcal{X}, \Omega, r=2, \mathbf{P}=\emptyset)$ , respectively, and ( $\mathbf{v}_3, \mathbf{z}|_r^{\mathbf{P}\neq\emptyset}$ ) is an optimal solution to  $\text{GIL}(\mathcal{X}, \Omega, r, \mathbf{P}\neq\emptyset)$ . A feasible region with trivial (red dots) and relevant (dashed gray) constraints is considered. For cases where  $\mathbf{P}\neq\emptyset$ , the preferred constraint is shown with a solid line. The figure demonstrates the observation-goal tradeoff with distance to observations increasing as the number of relevant binding constraints or preferred constraints increases, as also highlighted in Remark 1.

REMARK 1. Let  $(\mathbf{v}_1^1, \mathbf{z}_1^1)$  and  $(\mathbf{v}_2^2, \mathbf{z}_2^2)$  be optimal for  $\text{GIL}_1(\mathcal{X}, \Omega, r, \mathbf{P}_1 = \emptyset)$  and  $\text{GIL}_2(\mathcal{X}, \Omega, r, \mathbf{P}_2 \neq \emptyset)$  respectively. Then,  $\sum_{k \in \mathcal{K}} \|\mathbf{x}^k - \mathbf{z}_1^1\|_l \leq \sum_{k \in \mathcal{K}} \|\mathbf{x}^k - \mathbf{z}_2^2\|_l$ .

We illustrated that GIL generalizes the inverse optimization problem, however, in the presence of a high number of relevant constraints, different faces of  $\Omega$  may bind for different values of  $r$ . While this effect is in accordance with the observation-goal tradeoff, it makes comparisons and interpretations of the learned solutions in terms of their binding constraints and slack values more challenging. In the next section, we further study GIL derivatives that enhance user's ability to compare the learned solutions for different values of  $r$ . The adaptive model provides a platform to successively increase  $r$  to include more goals while navigating the tradeoff of each additional goal.

### 3.2. Navigating the Forward Optimal Solution Set: Balancing User Preferences with Expert Guidelines

The GIL model learns optimal solutions of the forward optimization problem when the user provides one set of relevant ( $\mathcal{R}$ ), trivial ( $\mathcal{T}$ ), and preferred constraints ( $\mathcal{P} \subseteq \mathcal{R}$ ). In settings where additional solutions are desired or those in which the optimal solution includes a high number of relevant constraints that draws it away from the observations, it is paramount to have a model that can

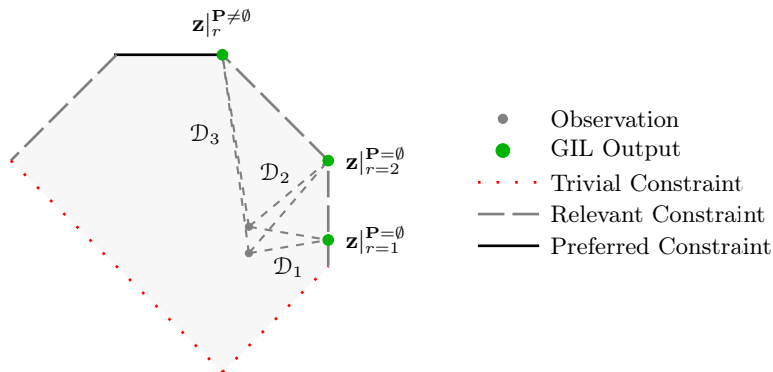


**Figure 3** The learned optimal solutions  $\mathbf{z}_1$  and  $\mathbf{z}_2$  bind one and two relevant constraints, respectively, and  $\mathbf{z}_3$  binds two relevant constraints with one of them being the sole preferred constraint. Although, the distance to observation increases with  $\mathcal{D}_3 > \mathcal{D}_2 > \mathcal{D}_1$  where  $\mathcal{D}_1 = \sum_{k \in \mathcal{K}} \|\mathbf{x}^k - \mathbf{z}|_{r=1}^{\mathbf{P}=\emptyset}\|_l$ ,  $\mathcal{D}_2 = \sum_{k \in \mathcal{K}} \|\mathbf{x}^k - \mathbf{z}|_{r=2}^{\mathbf{P}=\emptyset}\|_l$ , and  $\mathcal{D}_3 = \sum_{k \in \mathcal{K}} \|\mathbf{x}^k - \mathbf{z}|_r^{\mathbf{P}\neq\emptyset}\|_l$ .

balance the observation-goal tradeoff in a structured manner. In particular, for any  $\mathbf{c}$  recovered by an inverse model, a model that can adapt prior solutions to bind more relevant constraints without losing the already binding constraints can better contrast the tradeoff and accommodate a more informed comparison between these solutions, by keeping them contained in a single face of  $\Omega$ . The increased control also enables obtaining a sequence of solutions that spans the observation-goal tradeoff space. In more detail, assuming that an inverse model such as IL or IO has recovered a  $\mathbf{c}$ , we aim to provide a model that can navigate the optimal solution set of  $\text{FO}(\mathbf{c}, \Omega)$  to find solutions that bind a specific number of relevant constraints. Naturally, binding more relevant comes at the cost of increasing  $\mathcal{D}(\mathcal{X}, \mathbf{z})$ .

The application of the diet recommendation problem is a prime example of a case where comparability of solutions for different values of  $r$  is essential. For instance, if a learned solution from  $\text{GIL}(\mathcal{X}, \Omega, 1, \mathbf{P})$  only binds the maximum protein limit constraint and the learned solution from  $\text{GIL}(\mathcal{X}, \Omega, 2, \mathbf{P})$  binds the nutritional constraints for minimum sodium and maximum iron levels, the process of deciding between the two solutions is non-intuitive unless the user has quantified preferences over these nutritional constraints. However, if the learned solution from  $\text{GIL}(\mathcal{X}, \Omega, 2, \mathbf{P})$  also binds the maximum protein constraint, the user can directly assess the cost of binding additional constraints in terms of the metric  $\mathcal{D}$ . In addition to enabling comparison between different solutions, adapting the GIL to keep the previous binding constraints provides a base for the users to traverse the space between observation-driven to goal-driven solutions. The obtained sequence of solutions as  $r$  increases provides a path for the users to start as close as possible to the observations and their habits and gradually bind more constraints to reach a more conventional (goal-driven) optimal solution.

In more detail, let  $\mathbf{z}_0$  be a known solution to  $\text{FO}(\mathbf{c}, \Omega)$  for  $\mathbf{c} \in \text{cone}(\mathbf{a}_t : t \in \mathcal{J}_{z_0})$  such that  $\mathcal{J}_{z_0} \neq \emptyset$ . Such a solution  $\mathbf{z}_0$  might be available to the user from prior knowledge or might be the result of solving  $\text{GIL}(\mathcal{X}, \Omega, r_0, \mathbf{P})$  for a known set of observations. We next propose the MGIL model that takes the previous solution,  $\mathbf{z}_r$ , as an input and finds a new solution such that at least one additional relevant constraint is appended to the set of previously binding constraints. For given  $\mathbf{z}_r$ , a new solution  $\mathbf{z}_{r+1}$  is found by shifting  $\mathbf{z}_r$  in a direction that binds at least one more relevant constraint with minimal perturbation from  $\mathcal{X}$ , if such a shift is possible, while maintaining all previously binding relevant constraints. The MGIL model can be formulated as follows.

$$\text{MGIL}(\mathcal{X}, \Omega, \mathbf{z}_r, \mathbf{P}) : \underset{\mathbf{v}, \mathbf{z}_{r+1}}{\text{minimize}} \quad \omega \sum_{k \in \mathcal{K}} \|\mathbf{x}^k - \mathbf{z}_{r+1}\|_l - (1 - \omega) \sum_{s \in \mathbf{P}} v_s \quad (12a)$$

$$\text{subject to} \quad v_j \mathbf{a}_j \mathbf{z}_{r+1} = v_j b_j, \quad \forall j \in \mathcal{J} \quad (12b)$$

$$\mathbf{A} \mathbf{z}_{r+1} \geq \mathbf{b}, \quad (12c)$$

$$\mathbf{A}_\mathcal{T} \mathbf{z}_{r+1} \geq \mathbf{b}_\mathcal{T}, \quad (12d)$$

$$\sum_{j \in \mathcal{J}} v_j \geq |\mathcal{J}_{z_i}| + 1, \quad (12e)$$

$$\mathcal{J}_{z_r} = \{j \in \mathcal{J} \mid \mathbf{a}_j \mathbf{z}_r = b_j\}, \quad (12f)$$

$$v_j = 1, \quad \forall j \in \mathcal{J}_{z_r}, \quad \mathbf{v} \in \{0, 1\}^{|\mathcal{J}|}. \quad (12g)$$

695 Formulation (12) inputs a known solution  $\mathbf{z}_r$  that is optimal for  $\text{FO}(\mathbf{c}, \Omega)$  and learns a solution  
 696  $\mathbf{z}_{r+1}$  that binds more relevant constraints. Given an initial solution  $\mathbf{z}_r$ , a sequence of solutions  $\{\mathbf{z}_l\}$   
 697 can be achieved where for each  $r \leq l \leq L$ ,  $|\mathcal{J}_{z_{l+1}}| \geq |\mathcal{J}_{z_l}| + 1$  and we have  $|\mathcal{J}_{z_L}| \leq n$ . Remark 2 shows  
 698 the tradeoff in observation distance as  $r$  increases in MGIL leading to more binding constraints.

699 REMARK 2. Let  $(\mathbf{v}_{r+1}, \mathbf{z}_{r+1})$  be optimal for  $\text{MGIL}(\mathcal{X}, \Omega, \mathbf{z}_r, \mathbf{P} = \emptyset)$ ,  $\forall r \in \{1, \dots, L\}$ , then  
 700  $\sum_{k \in \mathcal{K}} \|\mathbf{x}^k - \mathbf{z}_1\|_l \leq \sum_{k \in \mathcal{K}} \|\mathbf{x}^k - \mathbf{z}_2\|_l \leq \dots \leq \sum_{k \in \mathcal{K}} \|\mathbf{x}^k - \mathbf{z}_L\|_l$ .

701 Despite the increase in the distance to observations at optimality as the number of binding  
 702 relevant constraints grows, comparison between the solutions is easier since the sequence of solutions  
 703  $\mathbf{z}_1, \mathbf{z}_2, \dots, \mathbf{z}_L$  are all contained in one face of  $\Omega$ .

704 REMARK 3. Let  $(\mathbf{v}_{r+1}, \mathbf{z}_{r+1})$  be optimal for  $\text{MGIL}(\mathcal{X}, \Omega, \mathbf{z}_r, \mathbf{P})$ ,  $\forall r \in \{1, \dots, L\}$ , then  $\mathbf{z}_r \in \mathcal{F} =$   
 705  $\{\mathbf{z} \in \Omega \mid \mathbf{a}_j \mathbf{z} = b_j \forall j \in \mathcal{J}_{z_1}\}, \forall r \in \{1, \dots, L\}$ .

706 Remark 3 shows that for a sequence of solutions from MGIL, all are contained in a face of  $\Omega$   
 707 by noting that Constraint (12f) ensures prior binding constraints will be tight at optimality. A  
 708 subsequent result is that all the solutions in the sequence are optimal for any cost vector that makes  
 709 the previous solutions optimal, as shown in Theorem 7.

710 THEOREM 7. Let  $\mathbf{z}_1, \mathbf{z}_2, \dots, \mathbf{z}_L$  be a sequence of learned solutions from successively solving MGIL.  
 711 Then,  $\forall r \in \{1, \dots, L\}$ ,  $\mathbf{z}_r$  is optimal for  $\text{FO}(\bar{\mathbf{c}}_l, \Omega)$  where  $\bar{\mathbf{c}}_l \in \text{cone}(\mathbf{a}_t : t \in \mathcal{J}_{z_l})$ ,  $\forall l \in \{1, \dots, r\}$  and  
 712  $\bar{\mathbf{c}}_l \neq \mathbf{0}$ .

713 Using the results of Theorem 7, we observe that by adaptively increasing the number of binding  
 714 constraints in solutions using MGIL, we achieve new solutions that are still optimal for the  
 715 previously achieved cost vectors but bind additional relevant constraints. This trait and the shared  
 716 binding relevant constraints among the solutions in a sequence provide easier comparison across the  
 717 candidate learned solutions for the user. In other words, the user can assess the “cost” of binding  
 718 more relevant or preferred constraints.

719 The inverse learning methodology detailed in Sections 2 and 3 is capable of incorporating existing  
 720 knowledge of a linear optimization problem and known observations to learn optimal solutions, as  
 721 well as recovering the missing parameters of the problem. The IL model incorporates information

722 on constraints, if available, to learn optimal solutions that bind relevant constraints. The goal-  
 723 integrated model, GIL, generalizes IL to control the observation-goal tradeoff through adjusting the  
 724 number and the type of binding constraints. Finally, the MGIL models adapt a prior solution that is  
 725 desirable to an improved new solution by preserving the previously binding constraints while adding  
 726 to them. Iteratively solving MGIL leads to a sequence of solutions that gradually increases achieved  
 727 goals, hence, empowering users to balance and navigate the inherent tradeoff.

728 Finally, we note that while both GIL and MGIL models presented are mixed-integer bilinear  
 729 programs, a class of optimization problems known for their computational complexity, their  
 730 moderate number of constraints and variables and the independence of the size of the problem from  
 731 the number of observations makes these models relatively suitable for even large-scale applications.  
 732 To assess the practical scalability of these models, we conducted computational experiments on  
 733 instances of varying sizes, with results and comparisons with benchmark IO models shown later  
 734 in Section 4. In Section 5, we apply the MGIL model to the diet recommendation problem and  
 735 demonstrate how comparable diet options can be derived for users. We show that by employing  
 736 MGIL and creating a sequence of solutions starting with the solution that minimizes  $\mathcal{D}$ , we can  
 737 provide diverse diet recommendations with different yet desirable and measurable characteristics  
 738 for the patients.

## 739 4. Numerical Experiments

740 In this section, we consider two illustrative two-dimensional examples to visually demonstrate the  
 741 results of the inverse learning and the inverse optimization approaches. In the first example, We  
 742 consider a linear forward optimization problem with an unknown cost vector and seven known  
 743 constraints, as outlined below, and a set of 20 feasible and infeasible observations (blue dots), as  
 744 depicted in Figure 4. In the second example. we consider 100 randomly generated two dimensional  
 745 feasible sets and compare the results of the models against true cost vectors and optimal solutions.

### 746 4.1. Numerical Example 1

747 Consider a given  $FO(\mathbf{c}, \Omega) = \max_{\mathbf{x} \in \mathbb{R}^2} \{\mathbf{c}'\mathbf{x} \mid \Gamma_1 : -x_1 + x_2 \leq 10, \quad \Gamma_2 : -0.5x_1 + x_2 \leq 11,$   
 748  $\Gamma_3 : 0.5x_1 + x_2 \leq 16, \quad \Gamma_4 : x_1 + x_2 \leq 20, \quad \Gamma_5 : x_1 \leq 10, \quad \Gamma_6 : x_1 \geq 0, \quad \Gamma_7 : x_2 \geq 0\}$ , where the cost  
 749 vector  $\mathbf{c}$  is not known but the feasible set  $\Omega$  is characterized by seven constraints  $\Gamma_1$  to  $\Gamma_7$ . We assume  
 750 constraints  $\Gamma_1$ – $\Gamma_5$  are relevant with  $\Gamma_3$  being a preferred constraint and note that the example is  
 751 designed in such a way that knowledge of relevant constraints does not change the results of the  
 752 benchmark literature model IO to facilitate a fair comparison. The preferred constraint is only added  
 753 to showcase the goal-integrated inverse learning model (GIL) performance. For GIL, we consider  
 754 three cases: binding one or two relevant constraints (i.e.,  $r = 1, 2$ ) with and without prioritizing the

755 preferred constraint, i.e.,  $\mathbf{P} = \{3\}$  and  $\mathbf{P} = \emptyset$ , respectively. As an example of how GIL compares with  
 756 the benchmark inverse optimization model IO, we solve the recovered FO( $\mathbf{c}, \Omega$ ) using the Simplex  
 757 method to find an optimal solution for the case of the recovered cost vector from IO. For all models  
 758 and whenever appropriate, we used the 2-norm distance metric to learn FO optimal solutions and  
 759 to recover the best cost vector.

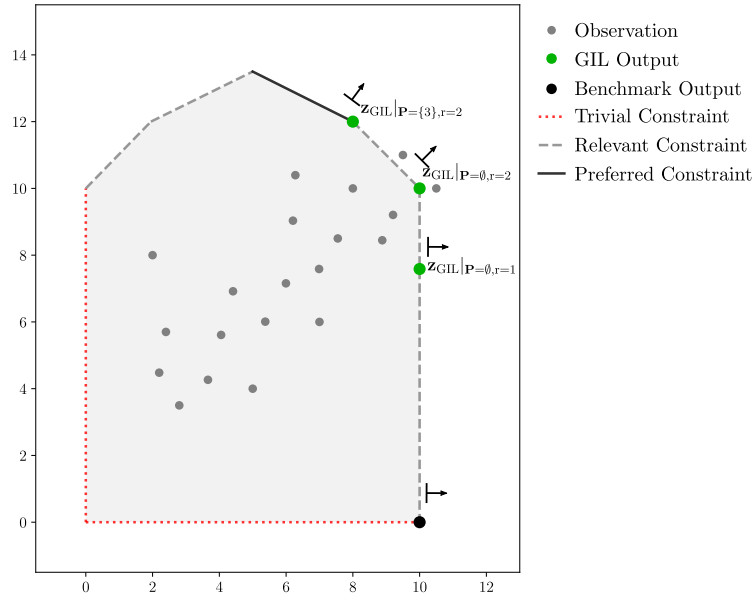


**Figure 4** An illustrative 2D example with 20 observations. The recovered optimal solutions and cost vectors of FO are shown for the benchmark model IO and the goal-integrated inverse learning model (GIL). The observations demonstrate a trait of recurring closer to the top-right constraint bounds. GIL captures this trend while the benchmark solution can be far from the observations. If additional constraint knowledge is included, GIL can incorporate them to adjust the learned solution and cost vector accordingly.

**Table 2** Results from applying the inverse learning model and the benchmark model. The solutions learned from inverse learning models exhibit reduced distances to the observations and recover similar cost vectors.

Model	Avg. Distance to Observations	Set of FO Cost Vectors	FO Cost Vector	FO Optimal Solution	Avg. Objective Value*
<b>Inverse Learning Models</b>					
GIL( $r = 1, \mathbf{P} = \emptyset$ )	6.0	$C^{**}((1,0))$	(1,0)	(10, 7.58)	5.9
GIL( $r = 2, \mathbf{P} = \emptyset$ )	7.0	$C((1,0),(1,1))$	(0.7,0.7)	(10, 10)	9.2
GIL( $r = 2, \mathbf{P} = \{3\}$ )	7.4	$C((1,1),(0.5,1))$	(0.63,0.78)	(8, 12)	9.4
<b>Benchmark Inverse Optimization Model</b>					
IO	11.4	(1,0)	(1,0)	(10, 0)	5.9

\*Average forward objective values for all the observations using the recovered cost vector in the forward problem.

\*\*Represents the cone of vectors.

760 Assume a set of 20 observations for a decision making problem are given as shown in Figure 4.  
 761 As Figure 4 illustrates, the forward optimal solution from IO may be far from the observations  
 762 depending on the method that FO is solved with, highlighting the fact that only recovering the  
 763 cost vector will blind the forward models to the information available with the current decisions.  
 764 The learned solutions of GIL, however, can resemble the observations' trends since the loss function  
 765 in inverse learning models minimizes the distance between the optimal solution and the observed  
 766 decisions. The optimal solution returned by  $GIL(\mathcal{X}, \Omega, r = 1, \mathbf{P} = \emptyset)$  (which is equivalent to the  
 767 IL model) is the closest to the observations. The location of the learned solution can be further  
 768 controlled by requiring two relevant constraints to be active, as shown in  $GIL(\mathcal{X}, \Omega, r = 2, \mathbf{P} = \emptyset)$   
 769 which returns the closest extreme point to the observations. We can further tailor the solution by  
 770 prioritizing constraint  $\Gamma_3$  to bind as our preferred constraint by setting  $GIL(\mathcal{X}, \Omega, r, \mathbf{P} = \{3\})$  which  
 771 returns the closest feasible point on  $\Gamma_3$  but at a potential cost of moving away from the observations.  
 772 While it is possible to characterize the set of all inverse optimal cost vectors using GIL models (as  
 773 demonstrated in Theorem 5), using formulation (11) allows GIL models to find cost vectors that do  
 774 not solely depend on  $\Omega$ , and that are informed of the observations as well.

775 Table 2 summarizes the results shown in Figure 4. The set of returned optimal cost vectors and the  
 776 selected cost vector from said cones, and the optimal solutions are provided. The average distance  
 777 to the observations is the smallest in  $IL^\emptyset$  although it can increase as the solutions are tailored to  
 778 specific constraint goals. The last column of Table 2 indicates how using formulation (11) results  
 779 in maximizing the average objective value of the observations for FO. We note that this example is  
 780 designed to illustrate the behavior of different models in a numerical setting. In the next numerical  
 781 experiment, we consider randomly generated two dimensional feasible sets and compare inverse  
 782 learning and inverse optimization models against true cost vectors and optimal solutions.

#### 783 4.2. Numerical Example 2

784 In our second numerical experiment, we consider randomly generated feasible sets where the true  
 785 cost vector and true optimal solution are known and we compare the results of IL, GIL, MGIL,  
 786 and IO against the true values. For this numerical experiment, we run a procedure that generates  
 787 a non-empty feasible set  $\Omega$  for a pre-determined  $n$  dimensional space. Considering that classic  
 788 inverse optimization and inverse learning assumptions differ, we consider both assumptions and run  
 789 the analysis separately for each. In our first analysis, we capture inverse learning assumptions by  
 790 generating a random true optimal solution  $(\mathbf{x}^*)$  on  $\Omega^{opt}$  along with a true cost vector  $(\mathbf{c}^*)$  that  
 791 would render  $\mathbf{x}^*$  optimal for  $FO(\mathbf{c}^*, \Omega)$ . We designate the pair  $(\mathbf{x}^*, \mathbf{c}^*)$  as the true cost vector and  
 792 true optimal solution. We generate random perturbations of  $\mathbf{x}^*$  (between 2 and 8 points) to form  
 793 a set of observations  $\mathcal{X}$ . In our second analysis, we capture inverse optimization assumptions by

generating a random cost vector as the true cost vector  $\mathbf{c}^*$ . We then find 2 to 8 optimal solutions for  $\mathbf{c}^*$  and generate a random perturbation for each (if multiple optimal solutions exist, otherwise, we noise the unique optimal solution multiple times). Note that we allow the noised observations to be either feasible or infeasible for  $\Omega$ . Figure 5 shows examples of these settings for the two assumption sets. We then solve the models IL, IO, GIL, and MGIL and compare the results against the true values  $(\mathbf{x}^*, \mathbf{c}^*)$ . Since GIL and MGIL do not explicitly return cost vectors, we use formulation 10 to find all cost vectors that render the solution found by GIL, and MGIL as optimal and check to see whether the true cost vector is contained in these sets. For fair benchmarking, we consider a similar condition for IO and IL where the returned cost vector is evaluated as being contained in the cone of all cost vectors that render an optimal solution of the recovered cost vector optimal. For each assumption set, we compare models across problems in two to 10 dimensions and consider 100 randomly generated instances for each dimension. At each iterations, a new feasible set and true value combinations are generated. For each instance, all decision variables are limited to the interval of -10 to 10.

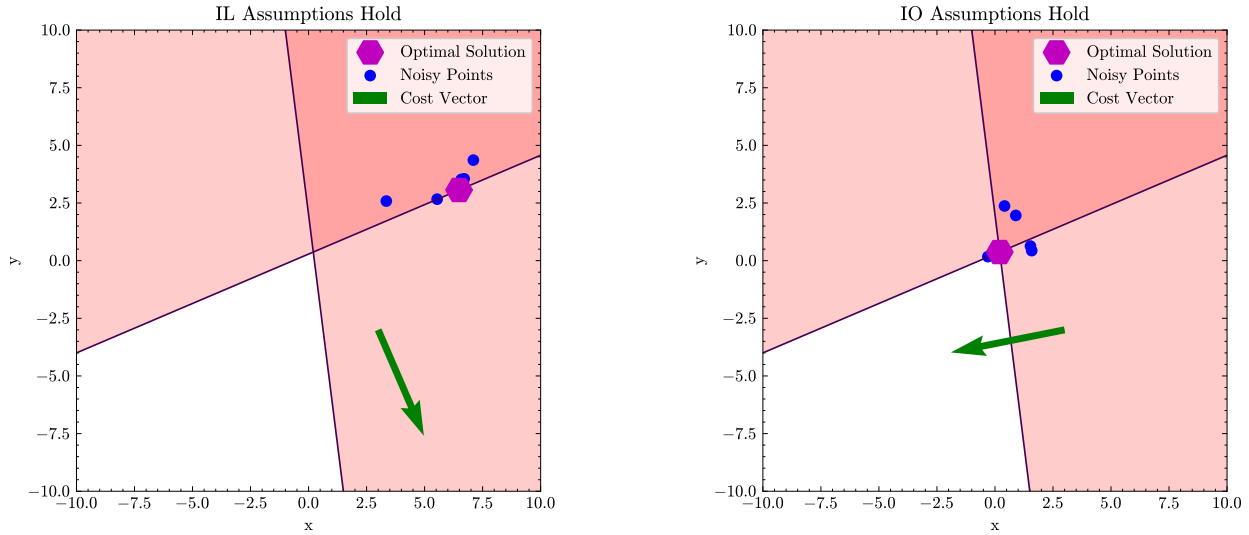


**Figure 5** Examples of the two assumption sets in developing the second numerical example. Feasible portions of each hyperplane is shown in color. (Left) IL Assumptions are shown where a random point on the border of the feasible set is assumed to be the true optimal solution. Then, a cost vector rendering this solution optimal for FO is deemed as the true cost vector and the optimal solution is noised to create the observation set. (Right) IO Assumptions are shown where a random two dimensional array is assumed to be the true cost vector. Optimal solutions for FO assuming this cost vector are achieved and noised to create the observation set.

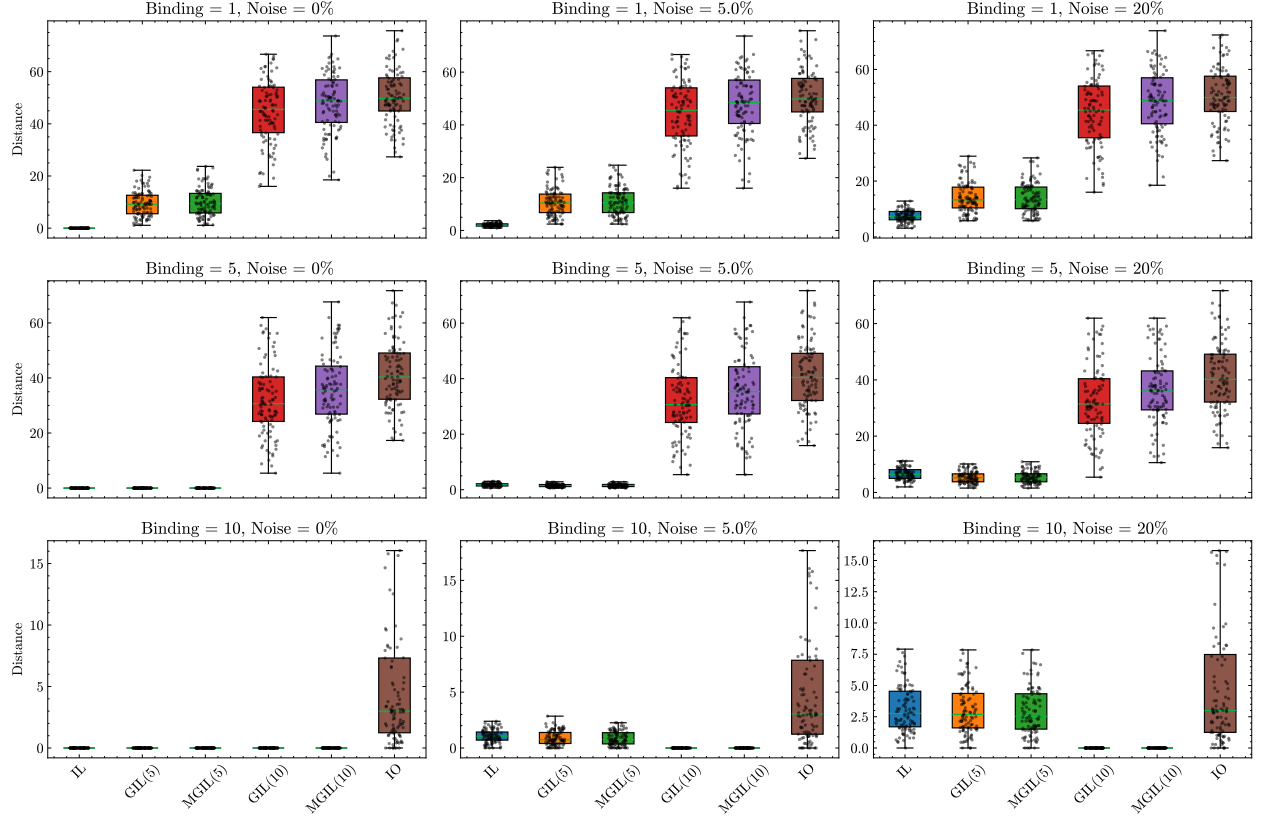


**Figure 6** Comparison of model distances across knowledge and noise levels for the **IL Assumption** case. The boxplots show the distribution of distances between the learned solutions and the observations for various models (IL, GIL, MGIL, and IO) under different settings of the number of binding constraints for the true optimal solution (1, 5, and 10) and noise levels for observations (0%, 5%, and 20%) in 10 dimensions. The scatter points represent the individual distances, with jittered positions for visibility. As the number of binding constraint increases for the learned solution, the distances to the true optimal solution generally increase, indicating the trade-off between fitting the observations and satisfying the binding constraints. The GIL and MGIL models with higher numbers of binding constraints tend to have larger distances compared to the IL and IO models, especially at lower noise levels. The results highlight the impact of incorporating expert knowledge through constraint binding on the learned solutions in the inverse learning framework.

Figure 6 provides a comparison between distances from the learned optimal solution of each model and the true optimal solution(s) across all the iterations, for the IL assumption. As expected, considering the inverse learning models explicitly aim to minimize this distance, IL, GIL, and MGIL in general learn solutions that are closer to the true optimal solution than the solution returned by solving FO for the cost vector that IO recovers. The results demonstrate that the inverse learning models, particularly MGIL and GIL, are able to effectively learn solutions that align closely with the true optimal solutions, even under varying levels of knowledge binding and

noise. The incorporation of expert knowledge through constraint binding helps guide the learning process towards more accurate solutions. Notably, the performance of the inverse learning models remains robust across different problem dimensions and assumptions, showcasing their versatility and reliability in recovering optimal solutions.

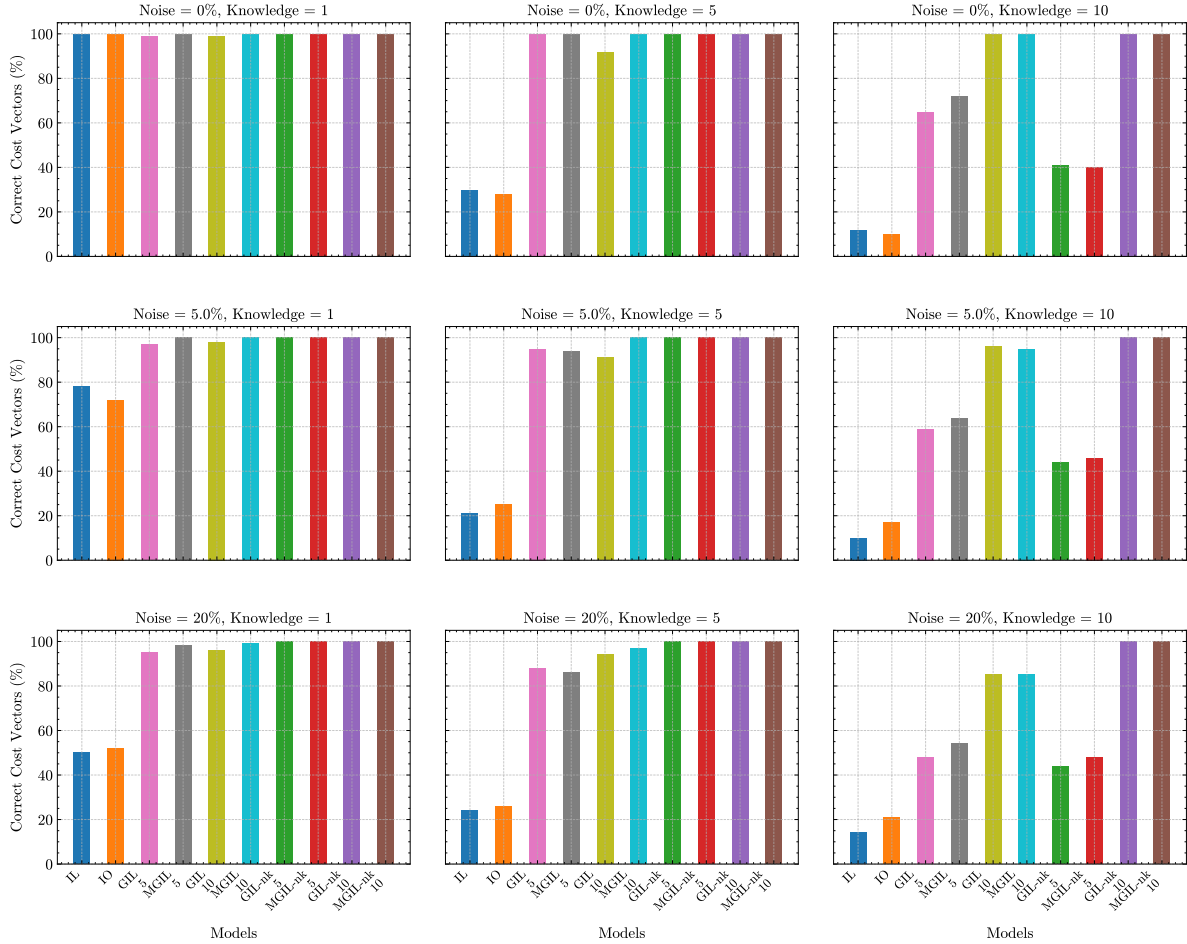


**Figure 7** Comparison of correct cost vector recovery across models under varying number of binding constraints and noise levels for the **IL Assumption** case. The bar charts display the percentage of correctly recovered cost vectors for different inverse optimization models (IL, GIL, MGIL, and IO). Each subplot corresponds to a specific combination of the number of binding constraints for the true optimal solution (1, 5, or 10) and the noise level (0%, 5%, or 20%). The models are categorized based on their incorporation of binding constraints and the use of preferred constraints (denoted by "-nk" for no knowledge and "5" or "10" for the number of binding constraints of the true optimal solution provided to the models). The results demonstrate that models incorporating knowledge binding, such as GIL and MGIL, generally achieve higher percentages of correct cost vector recovery compared to the IL and IO models, particularly at lower noise levels. As the noise level increases, the performance gap between the models narrows. The subplots also highlight the impact of increasing knowledge binding, with higher binding levels leading to improved cost vector recovery in most cases.

819 In addition to comparing distances to the true optimal solutions, we also compare the models  
820 in terms of the percentage of times they correctly return the true cost vector. Figure 7 provides  
821 comparisons for the percentage of correctly recovered cost vectors for all models. For both  
822 analyses, MGIL and GIL consistently outperform the other models in recovering the true cost  
823 vector across different knowledge binding levels and noise scenarios. The performance gap is  
824 particularly pronounced when the assumptions of the inverse learning models hold, highlighting  
825 their effectiveness in leveraging available information to estimate the true cost vectors accurately.  
826 The results showcase the value of incorporating expert knowledge and preferred constraints into  
827 the inverse optimization framework, as demonstrated by the superior performance of the MGIL  
828 and GIL models. Interestingly, IL and IO exhibit similar performance in terms of cost vector  
829 recovery, indicating that the traditional inverse optimization approaches may have limitations in  
830 fully exploiting the available data and knowledge. Overall, the comparative analysis underscores the  
831 advantages of the inverse learning models in recovering the true cost vectors under various settings.

832 Similar to Figures 6 and 7, Figures 8 and 9 provide similar results for the case where the  
833 IO assumptions hold. Similar simulation is conducted and the models are compared across 100  
834 instances. These figures provide a comprehensive comparison of the performance of various inverse  
835 optimization models in distances to true solutions and correctly recovering cost vectors under  
836 different scenarios. Notably, models incorporating knowledge binding, such as GIL and MGIL,  
837 generally achieve higher percentages of correct cost vector recovery compared to the IL and  
838 IO models, particularly at lower noise levels. As the noise level increases, the performance gap  
839 between the models narrows, however, the knowledge binding models with and without preferred  
840 constraints achieve superior performance compared to the benchmark IO model, even for the  
841 case where traditional IO assumptions hold. The figures also highlight the impact of increasing  
842 knowledge binding, with higher binding levels often leading to improved cost vector recovery. These  
843 results demonstrate the advantages of the inverse learning framework in accurately estimating cost  
844 vectors under various conditions, especially when incorporating expert knowledge through constraint  
845 binding.

846 Finally, Table 3 provides a comprehensive comparison of solution times across different inverse  
847 models under the distinct assumption sets in the second numerical example. The results, showcase  
848 the average time required to solve 100 instances for different noise levels and is reported in seconds.  
849 These results reveal significant variations in computational efficiency among the models. Under  
850 both IL and IO assumptions, the MGIL model demonstrates superior performance, with the fastest  
851 average solution times of 3.58 and 3.21 seconds, respectively. The GIL model follows closely, with  
852 solution times approximately twice as fast as those of IL. Notably, the IO model exhibits the  
853 longest solution times in both scenarios, taking about 47 seconds on average. This stark contrast

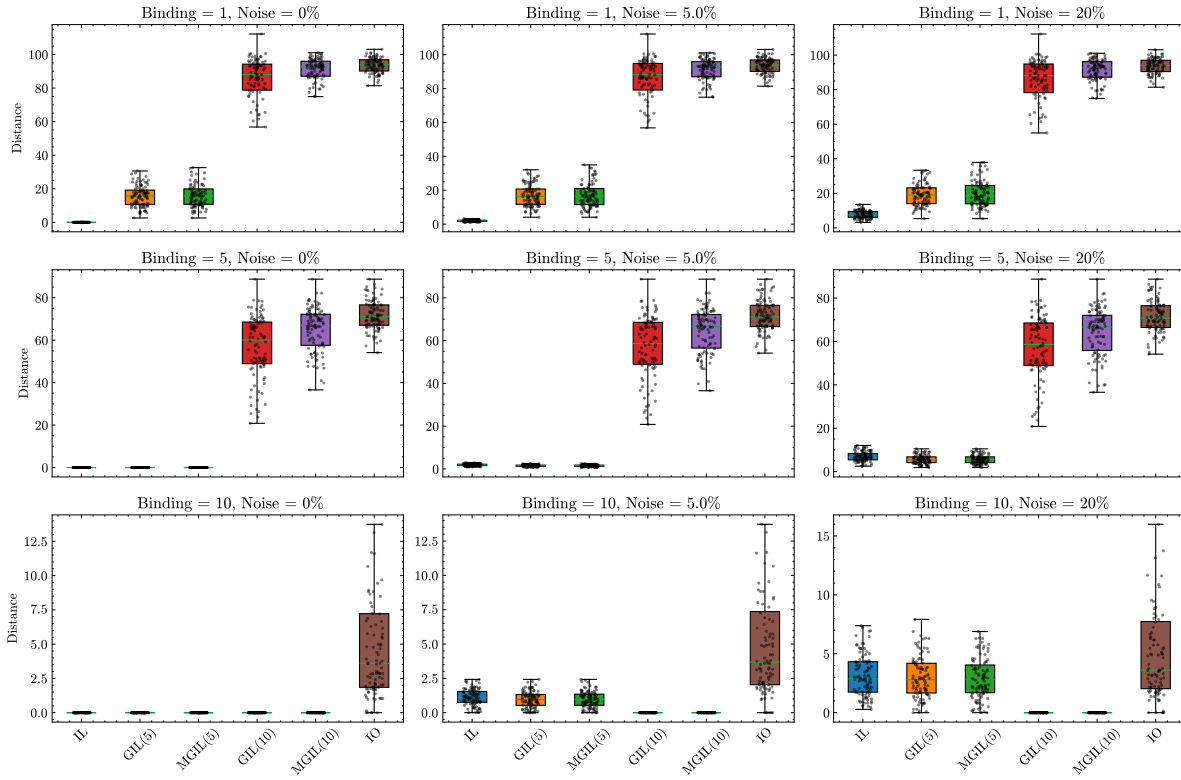


**Figure 8** Comparison of correct cost vector recovery across models under varying number of binding constraints and noise levels for the **IO Assumption** case.

in performance highlights the computational advantages of the newer MGIL and GIL models over traditional approaches. The consistency of this trend across both assumption sets underscores the robustness of these performance differences, suggesting that the enhanced efficiency of MGIL and GIL is not dependent on the underlying assumptions of the problem.

**Table 3** Comparisons of solution times across models and assumption sets for numerical example 2. The numbers indicate the average solution time of 100 instances in seconds. No major difference across binding levels are observed for GIL and MGIL, therefore, only the highest run times are provided.

Assumption Set	IO	IL	GIL	MGIL
IL Assumptions	46.85	14.75	6.23	3.58
IO Assumptions	47.40	15.48	4.67	3.21

## 5. Application to Personalized Diet Recommendations

In this section, we simulate optimal diet recommendations using the models developed in this work. We employ a set of publicly available nutrition data explained in Section 5.1. From the available data, we specifically consider users that have self-reported chronic conditions including

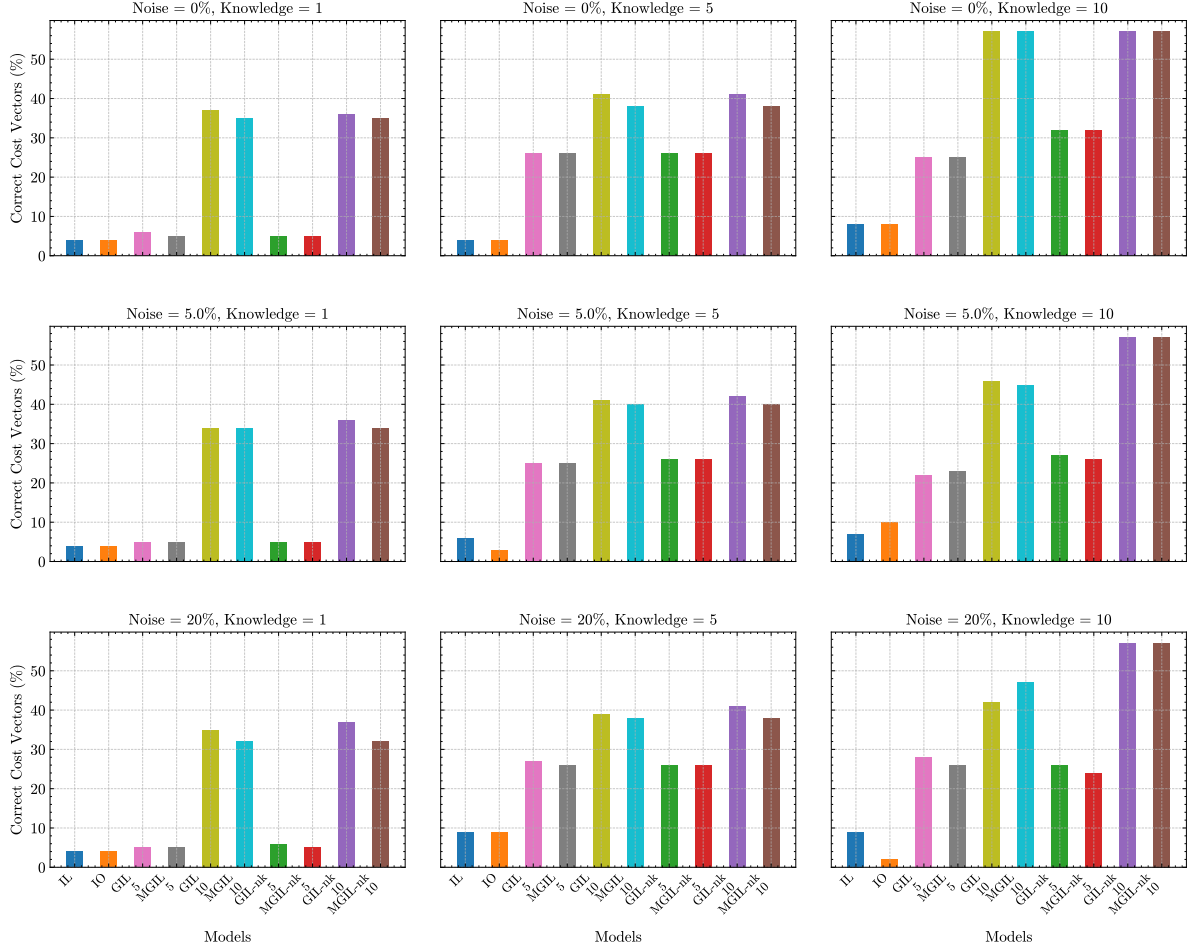


**Figure 9** Comparison of correct cost vector recovery across models under varying number of binding constraints and noise levels for the **IO Assumption** case.

hypertension and assume that they aim to adhere to the DASH diet. We consider observations from the 2,090 hypertension patients and additionally introduce a web-based decision-support tool for exploring the data and the results and providing the users with personalized recommendations. The recommendations present themselves in the form of minimal changes to existing behaviors that would allow the user to adhere to the pre-selected diet. We showcase the results of applying inverse learning for the purpose of recommending improvements/corrections in Section 5.2. Finally, we detail the web-based online tool in Section 5.4 that can be used to provide and compare inverse learning recommendations for user inputs of daily intakes. The tool additionally showcases results for different groups of patients in our dataset.

### 871 5.1. Data

872 The input to the inverse models includes observation(s) and constraint(s) that form the known  
 873 feasible set  $\Omega$ . We use data from the National Health and Nutrition Examination Survey (NHANES)  
 874 ([CDC 2020b](#)) and the United States Department of Agriculture (USDA) database ([USDA 2019](#))  
 875 to generate the observations and the feasible set of the forward optimization problem, respectively.  
 876 NHANES database includes self-reported information on the daily food intakes of 9,544 individuals,  
 877 along with their demographics, for two days. From this population, 2,090 individuals self-reported  
 878 a diagnosis of hypertension totaling to 4,024 observations of daily food intake for patients who did  
 879 report their daily food intakes for two days. We consider the DASH diet as the expert driven diet for  
 880 our FO problem and build lower-bound and upper-bound nutritional constraints based on this diet  
 881 recommendation for patient clusters based on their age and gender ([Liese et al. 2009](#), [Sacks et al.](#)  
 882 [2001](#)). To calculate the nutrients per serving of each food group and construct the feasibility set, we  
 883 employ information from the USDA databases. The USDA datasets are detailed with approximately  
 884 5,000 food types listed. For simplicity and tractability in our models, we group the food types into  
 885 38 food groups as shown in Table [EC.1](#) in the electronic companion. We additionally consider 22  
 886 nutritional constraints and 76 box constraints on food types and limit the intake amount for each  
 887 food item to a maximum of eight servings per day. The main focus for the DASH diet is getting the  
 888 sodium intakes under control.

**Table 4** DASH nutrient bounds for women of 51+ age group. The nutritional coefficients per serving of foods  
 for a sample of food groups are also provided.

Nutrients	DASH Nutritional Bounds		Nutrient Per Serving for Select Food Types			
	Lower bound	Upper bound	Milk (244g)	Stew (140g)	Bread (25g)	Tropical Fruits** (182g)
Carbohydrates (g)	225*	325	18.8	21.3	12.3	27.8
Protein (g)	50	150*	7.2	16.8	2.5	1.4
Total Fat (g)	45*	80	6.3	14.3	1.5	1.9
Total Sugars (g)	0*	100	18.0	4.5	1.7	19.0
Dietary Fiber (g)	25	40*	0.2	1.5	0.9	4.1
Sat. Fat (mg)	10*	22	3.3	4.6	0.4	0.31
Cholesterol (mg)	0*	150	14.0	53.9	1.2	0.0
Sodium (mg)	1000*	2300	108.3	639.4	119.0	10.7

\* Indicates relevant constraint.

\*\* Includes apples, apricots, avocados, bananas, cantaloupes, cherries, grapes, mangoes, and pineapples.

889 The complete dataset of the self-reported dietary decisions of patients in NHANES is highly  
 890 heterogeneous and the DASH diet recommends different target calories based on age and gender.  
 891 As a result, we consider a demographic clustering based on the age and gender of the participants.

**Table 5** Description of the nutritional facts of the observations for patients alongside minimum and maximum value of each nutrient among observations with 25, 50, 75<sup>th</sup> percentiles.

Nutrient	Avg.	Std	Min	25%	50%	75%	Max
Food Energy (kcal)	1,889.8	787.1	400.5	1,329.3	1,780.9	2,323.6	4,969.5
Carbohydrate (gm)	242.5	105.3	48.1	167.7	231.6	299.2	647.9
Protein (gm)	69.6	34.1	10.6	46.4	64.1	85.3	233.9
Total Fat (gm)	74.6	36.8	6.4	48.7	69.3	93.2	239.4
Sugars (gm)	104.9	54.8	16.3	65.0	96.9	131.9	446.6
Dietary Fiber (gm)	15.6	8.8	1.5	9.7	13.6	19.8	54.9
Saturated Fat (gm)	23.0	11.5	1.6	14.6	21.2	29.9	72.5
Cholesterol (mg)	250.2	192.9	5.5	124.8	196.9	331.7	1,262.0
Iron (mg)	13.6	7.7	2.3	8.3	12.1	16.5	52.9
Sodium (mg)	3,413.4	1,643.2	324.7	2,205.5	3,106.6	4,288.4	9,942.8
Caffeine (mg)	138.3	119.1	0.0	54.9	114.3	190.4	1,021.3

892 For illustrative purposes, we focus on the subset of patients who identify as women and are 51+  
 893 years old, who have self-reported both hypertension and pre-diabetes. These restrictions reduces  
 894 our sample population to 230 patients and 460 observations (two days of nutritional intake data  
 895 for each patient). Other demographic groups can be explored in our web-based tool described in  
 896 Section 5.4.

897 Table 4 presents the DASH diet bounds on nutrients for our representative demographic group.  
 898 The table also indicates the relevant constraints and demonstrates the coefficients for a sample  
 899 of food items. All nutrients include at least one desirable bound which is considered a relevant  
 900 constraint. For the cases where we do not assume any preference for the nutrient, both bounds are  
 901 considered as relevant constraints. Table 5 summarizes the nutritional values of the 460 observed  
 902 dietary decisions corresponding to our representative patient group (since each patient reports two  
 903 days of food intake). A quick comparison with Table 4 shows that a large number of observations are  
 904 infeasible, especially for the sodium constraint which the DASH diet aims to restrict. For instance,  
 905 in the representative group of 51+ year-old women, roughly 80% of observations are infeasible with  
 906 sodium causing the most number of infeasibilities (70%). These infeasible observations still contain  
 907 information about patient preferences, and hence, we include them in our inverse learning models.  
 908 For further information about the constraints, food types, observed dietary decisions, and other  
 909 relevant information, please see Section EC.2 in the electronic companion.

## 910 5.2. Retrospective Diet Recommendation and Preference Elicitation

911 In this section, we demonstrate how the inverse learning models translate to the diet recommendation  
 912 setting. Considering the assumptions of the inverse learning framework, the developed models can  
 913 be applied to a setting where the patient is aware (or is made aware by an expert) of their goal

914 diet and is making dietary decisions with these goals in mind. Then these decisions can be input  
915 to the inverse learning models in conjunction with the dietary goals set by the expert (in the form  
916 of nutritional constraints) to provide the patient with “nudged” intake values that represent the  
917 intended optimal behavior that best resembles their noisy behavior. The decision-maker (either the  
918 expert or the patient) can additionally inform the models of their preferred nutritional constraints,  
919 if any, and inform the inverse model of any explicit preference that the decisions fail to demonstrate.  
920 This allows learning recommended diets that balance between distance to prior observed dietary  
921 decisions and binding preferred constraints.

922 In this setting, the general inverse learning model MGIL can provide multiple levels of solutions  
923 to the diet recommendation problem with different values of  $r$ . As demonstrated experimentally  
924 in Section 4, inverse learning models can be used to estimate both the optimal solution and the  
925 cost vector of a partially known linear optimization problem. In the diet recommendation setting,  
926 this translates to providing the user with the optimal decision they are trying to make when  
927 the observations are realized. As such, Figure 10 showcases the results of applying IL to each  
928 patient’s noised observations from the dataset described in Section 5.1. In order to demonstrate the  
929 multi-observation capabilities of the inverse learning models, 20 randomly noised observations are  
930 generated around each observed daily dietary intake values. These noised values can represent 20  
931 repeated days of intake where the patient is trying to eat a specific diet (for instance, their preset diet  
932 for only Mondays) and the goal of the inverse learning model is to nudge their behaviors minimally  
933 to make the food combinations optimal for the recommended diet. This comparison between the  
934 observed behavior and the optimal behavior outlines how a nudging recommendation systems might  
935 be able to guide patients towards the optimal diet intakes suited to their preferences.

936 In addition to IL, the MGIL model was shown in the numerical examples to be capable of providing  
937 better estimates for the true cost vector. MGIL can provide a range of recommended diets that  
938 conform to the observation-goal tradeoff by differentiating the parameter  $r$ . As such, Figure 11  
939 showcases how different values of  $r$  provide different optimal diets resulting from the MGIL model  
940 on the same set of randomized observations for each patient and each intake day.

### 941 5.3. Prospective Dietary Interventions

942 To further demonstrate the practical applicability of our inverse learning framework, we additionally  
943 conducted a prospective feasibility study with a single volunteer participant to observe the  
944 potential usefulness of the Inverse Learning framework in providing relevant dietary intervention  
945 recommendations to the volunteer. This study aimed to illustrate how the theoretical concepts  
946 developed in this paper translate to real-world dietary interventions, particularly in the context of  
947 personalized nutrition and the observation-goal tradeoff.

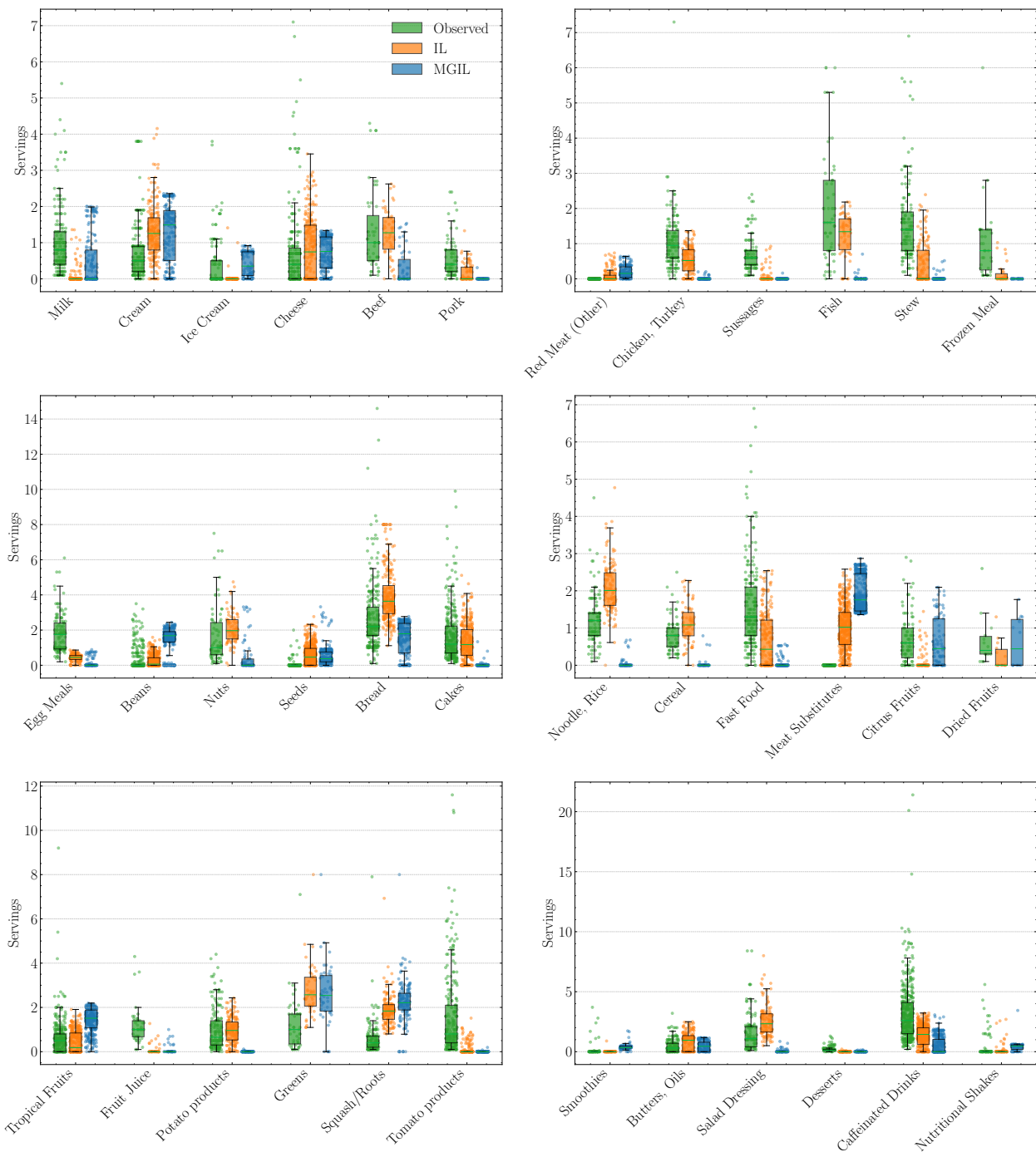


**Figure 10** Recommended optimal nudged diets for randomized observations of 230 patients. one day intake of a patient is randomized 20 times and input to the IL model. the resulting optimal solution from IL is shown for each food item in a box plot in the right while the original non-randomized values are shown for all patients and for each food item in a box plot in the left. Food item values that are equal to zero for all the observations and the recommended diet are excluded from the figure.

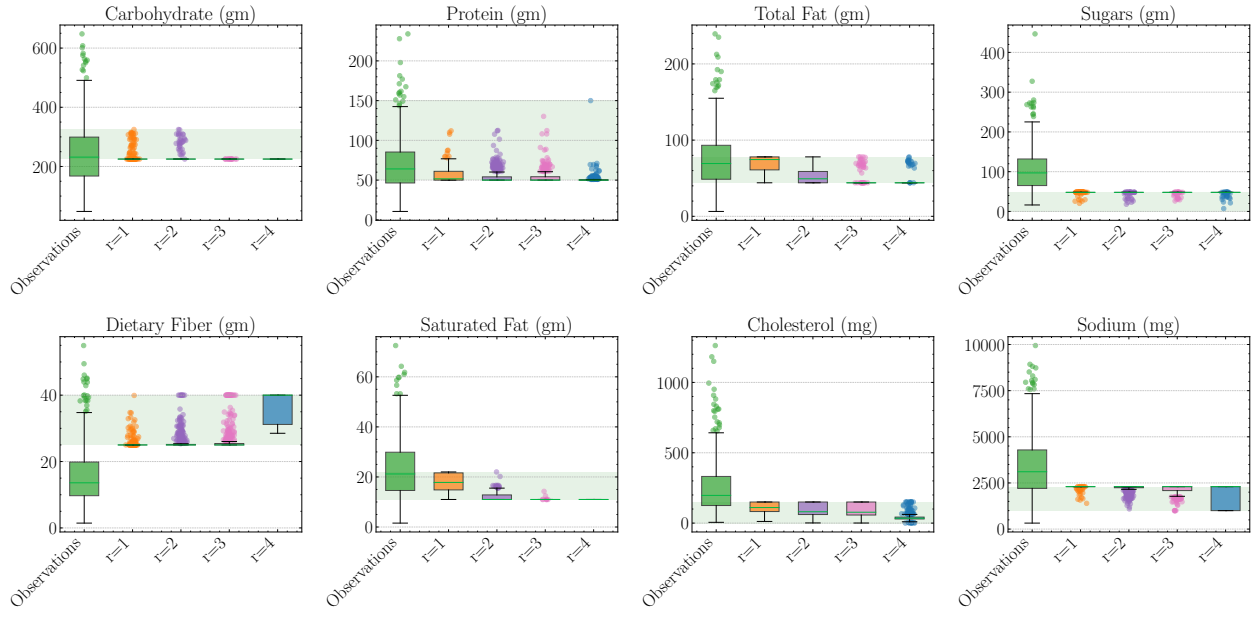


**Figure 11** Different diet recommendations using MGIL for varying values of the parameter  $r$  controlling the number of binding relevant constraints. As shown, while all recommended diets are feasible for the provided guidelines, as  $r$  increases, the diets become more stringent in their nutritional value distributions.

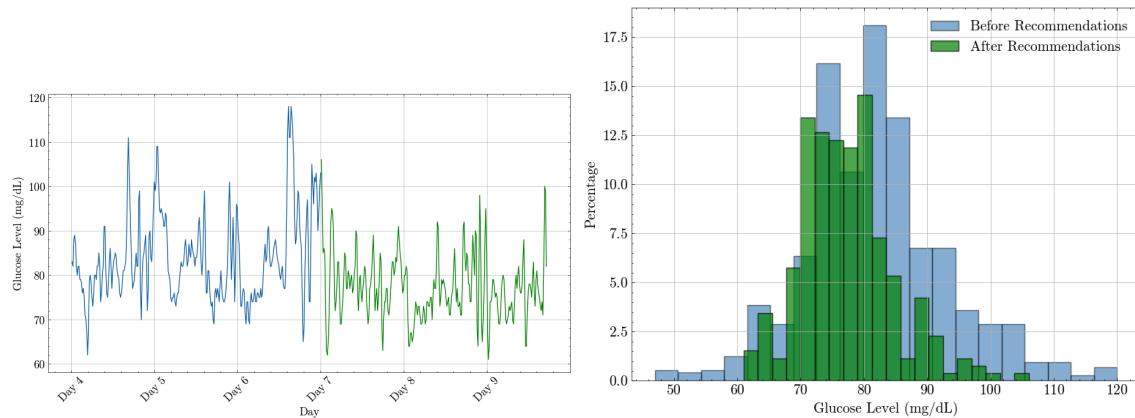
We conducted a two-week prospective feasibility study with a healthy volunteer interested in following a low-carbohydrate diet with a 2,000-calorie daily target, aiming to optimize blood glucose levels. The study employed continuous glucose monitoring (CGM) throughout. In the first week, the participant maintained their usual dietary habits, logging food intake via a nutrition tracking app. For the second week, we provided dietary recommendations generated by our inverse learning model, based on Week 1 observations and tailored to meet low-carbohydrate and calorie goals. This design allowed us to observe how the inverse learning model balanced the participant's revealed preferences with the desired nutritional goals, exemplifying the observation-goal tradeoff discussed in Section 3. Crucially, the participant maintained complete autonomy over their dietary choices throughout the study, receiving no incentives to follow the recommendations. This approach mirrors real-world scenarios where individuals have access to dietary advice but retain decision-making freedom. Due to CGM accuracy limitations at the beginning and end of its usage period, we focused our analysis on data from the latter half of Week 1 and the first half of Week 2. We applied the MGIL model to the participant's Week 1 dietary data, emphasizing sugar reduction. The feasible region  $\Omega$  was defined by low-sugar diet nutritional constraints and the 2,000-calorie target. We set  $r = 3$  to ensure binding of key nutritional constraints while maintaining similarity to observed behaviors. This concise design allowed us to evaluate the practical applicability of our inverse learning framework in a real-world dietary intervention setting, balancing personalization with nutritional goals.

Figure 12 illustrates the impact of the inverse learning-based dietary recommendations on the participant's blood glucose levels. The graph reveals a notable reduction in both the average glucose level and its variability following the recommendations. Specifically, the mean glucose level decreased from 81.90 mg/dL to 77.17 mg/dL. This improvement is further evidenced by the decrease in the percentage of readings above 100 mg/dL, dropping from 6.63% to 0.38%, and an increase in the percentage of readings within the optimal 60-100 mg/dL range, rising from 91.30% to 99.62%. These changes suggest that the personalized diet recommendations not only lowered overall glucose levels but also contributed to more stable glucose control, demonstrating the potential of the inverse learning approach to generate dietary advice that effectively balances individual food preferences with health objectives. A summary of statistical measures' comparison before and after the recommendations is provided in Table 6.

**Table 6** Summary Statistics of Continuous Glucose Monitoring Data Before and After Dietary Recommendations

Statistic	Before Recommendations	After Recommendations
Mean (mg/dL)	81.90	77.17
Median (mg/dL)	81.00	76.00
Minimum (mg/dL)	47.00	61.00
Maximum (mg/dL)	120.00	106.00
Standard Deviation (mg/dL)	11.30	7.29
% Readings >100 mg/dL	6.63%	0.38%
% Readings 60-100 mg/dL	91.30%	99.62%

Tables 7 and 8 provide detailed insights into the participant's dietary changes resulting from the inverse learning-based recommendations. Table 7 shows day-to-day nutritional intake, allowing



**Figure 12** Continuous glucose monitoring (CGM) data before and after dietary recommendations over time for the periods before (blue) and after (green) implementing the inverse learning-based dietary recommendations.

for a granular view of dietary patterns, while Table 8 summarizes these changes by comparing average intakes between the baseline and intervention weeks. Notable shifts include a substantial reduction in average daily calorie intake from 2,445 to 2,084 kcal, representing a 14.8% decrease. Carbohydrate consumption saw a marked 30.4% reduction from 250g to 174g per day, aligning with the low-sugar goal. Importantly, sugar intake was nearly halved, dropping from 71g to 40g daily, indicating a significant improvement in diet quality. These changes demonstrate the model's ability to generate recommendations that substantially alter dietary composition while still maintaining similarity to the participant's original eating patterns, as evidenced by the relatively stable fiber intake. This nuanced approach to dietary modification exemplifies the inverse learning model's capacity to balance health goals with individual dietary preferences, potentially enhancing long-term adherence to nutritional interventions.

**Table 7** Daily nutritional intake over a two week period

Date	Calories	Carbs (g)	Fat (g)	Protein (g)	Cholest (mg)	Sodium (mg)	Sugar (g)	Fiber (g)
Day 1	2,646	206	94	175	320	2,916	63	38
Day 2	2,420	217	118	135	705	2,366	66	28
Day 3	2,416	223	85	136	278	2,732	77	31
Day 4	2,515	254	98	183	513	2,709	82	22
Day 5	2,535	252	71	196	114	813	75	22
Day 6	2,324	274	87	82	511	2,492	84	13
Day 7	2,256	325	74	163	184	2,318	47	35
Day 8	2,102	227	83	119	150	1,560	48	22
Day 9	2,200	222	104	111	528	3,181	31	13
Day 10	2,289	141	132	143	595	3,497	30	28
Day 11	1,898	149	77	131	347	2,223	40	35
Day 12	1,930	160	87	126	491	2,805	28	17
Day 13	2,085	146	109	140	656	2,184	54	20

**Table 8** Comparison of Average Daily Nutrient Intake before and after recommendations (for the two weeks period).

Nutrient/Item	Before Recommendations	After Recommendations
Calories	2,445	2,084
Carbohydrates (g)	250	174
Fat (g)	90	98
Protein (g)	153	132
Sugar (g)	71	40
Fiber (g)	27	24

Figure 13 illustrates the effectiveness of our inverse learning-based dietary recommendations and the subsequent behavioral changes observed in the volunteer participant. The graph compares the

original dietary behavior (blue), the recommendations (green), and the actual post-recommendation behavior (orange) across various food groups, with values normalized relative to the original behavior. Several key observations emerge: First, the algorithm successfully identified areas for significant dietary adjustments, as evidenced by the variations between original behavior and recommendations for food groups such as avocado and meats. Second, the participant's actual behavior demonstrates a degree of adherence to the recommendations, particularly in reducing dessert items' intake and increasing consumption of avocados. However, discrepancies between recommended and actual behavior in some categories highlight the inherent challenges in fully adopting dietary changes. Interestingly, in some cases, the participant exceeded the recommended adjustments, suggesting potential areas of over-compensation or preference. These results show the algorithm's capacity to generate personalized, actionable dietary recommendations while also revealing the complex nature of dietary behavior change, where individual preferences and habits continue to play a significant role in actual food choices.

Figure 14 provides a comprehensive visualization of the changes in nutrient intake resulting from the inverse learning-based dietary recommendations, emphasizing the results from Tables 7 and 8. While overall calories intake is decreased slightly, total sugars exhibit significant contrast before and after recommendations. This is while fat consumption remains relatively stable, suggesting the model's ability to maintain certain aspects of the participant's original diet while adjusting others. Protein intake shows a slight decrease but remains within a healthy range. These nuanced changes

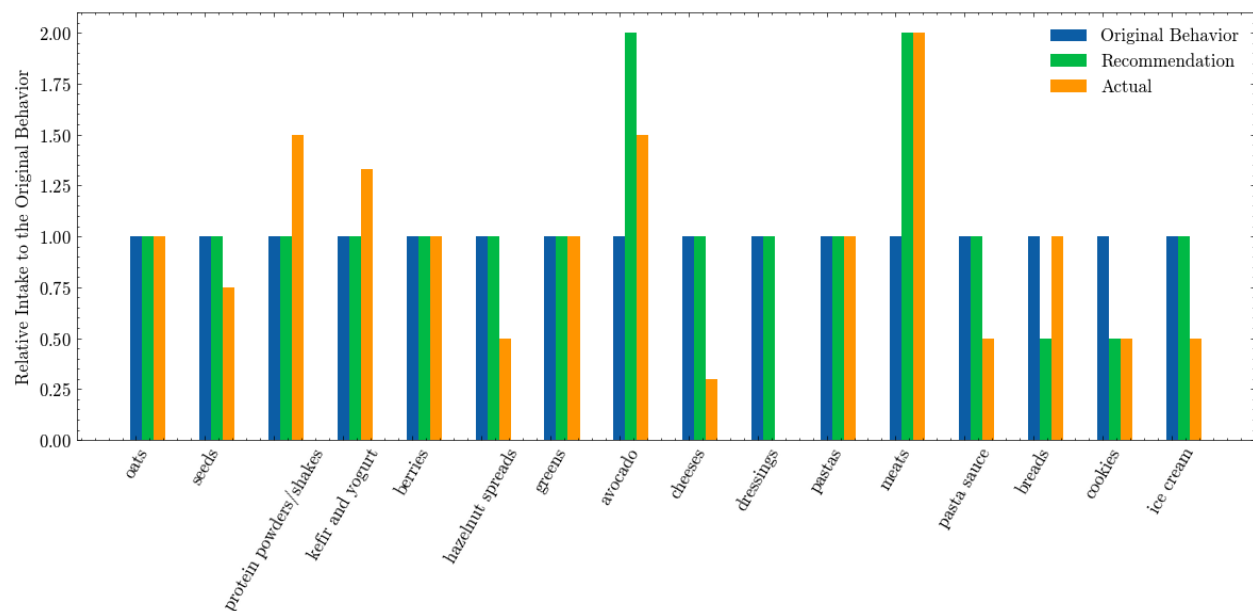


**Figure 13** Comparison of original dietary behavior, recommended adjustments, and actual post-recommendation behavior across food groups. Values are normalized relative to original behavior (1.0).

1011 demonstrate the inverse learning model's capacity to generate recommendations that significantly  
1012 alter diet composition in alignment with health goals while still respecting individual dietary  
1013 patterns. This may contribute to improved adherence and sustainable dietary changes, addressing  
1014 a key challenge in nutritional interventions.

1015 The prospective dietary intervention experiment provides evidence for the efficacy of our inverse  
1016 learning framework in generating personalized, actionable dietary recommendations. The continuous  
1017 glucose monitoring data revealed a significant improvement in glycemic control, with reducing the  
1018 mean glucose level from 81.90 mg/dL to 77.17 mg/dL. The intervention successfully met the primary  
1019 objectives of reducing calorie intake and sugar consumption. Caloric intake decreased by 14.8%  
1020 (from 2,445 to 2,084 kcal/day), while sugar intake reduced by 40.4% (from 71g to 40g/day), aligning  
1021 closely with the low-sugar goal. The model demonstrated an ability to make targeted changes while  
1022 preserving certain aspects of the participant's original diet. For instance, while significantly reducing  
1023 sugar intake, it maintained relatively stable levels of fat and fiber intake. This nuanced approach  
1024 suggests the model's capacity to balance health goals with individual dietary preferences.

1025 By generating recommendations that significantly altered diet composition while still resembling  
1026 the participant's original eating patterns, the model showcases potential for enhancing long-term  
1027 adherence to nutritional interventions. The study demonstrated that the inverse learning framework  
1028 can be successfully translated from theoretical models to practical, real-world dietary interventions,  
1029 providing actionable recommendations that resulted in measurable physiological improvements.

1030 Despite these promising results, several limitations of this experiment should be acknowledged.  
1031 Naturally, with a single-participant study, the generalizability of these results is limited at best.  
1032 Future research should involve larger, more diverse cohorts to validate the model's efficacy  
1033 across different populations and dietary preferences. The two-week timeframe, while sufficient to  
1034 demonstrate short-term impacts, does not allow for assessment of long-term adherence or sustained  
1035 health benefits. Longitudinal studies are needed to evaluate the long-term effectiveness of this  
1036 approach. Additionally, our study involved a healthy volunteer interested in optimizing their diet.  
1037 Results may differ for individuals with existing health conditions or less motivation to change their  
1038 dietary habits. The absence of a control group limits our ability to definitively attribute the observed  
1039 changes solely to the inverse learning-based recommendations. The participant's awareness of being  
1040 monitored may have influenced their behavior, potentially leading to better adherence than might  
1041 be expected in a non-study setting. Finally, while glucose monitoring provided valuable quantitative  
1042 insights, a more comprehensive set of health markers (e.g., lipid profiles, blood pressure) would offer  
1043 a more complete picture of the intervention's health impacts.

1044 These limitations notwithstanding, this prospective experiment provides a promising proof-of-  
1045 concept for the application of inverse learning in personalized nutrition. It demonstrates the potential

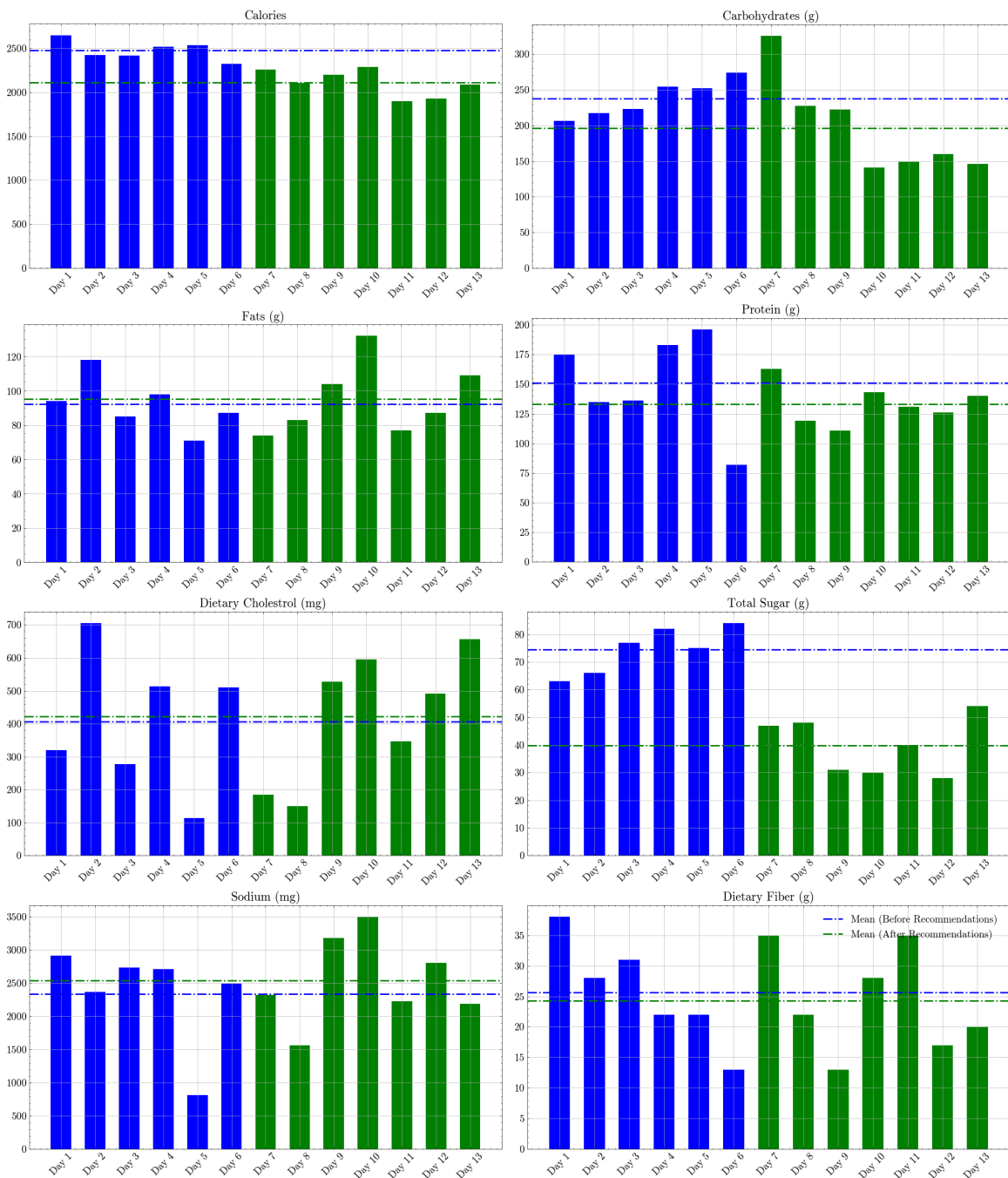


**Figure 14** Comparison of daily nutrient intake before and after implementation of inverse learning-based dietary recommendations for the days that reliable glucose readings are available. Blue bars represent intake during the baseline period (before recommendations), while green bars show intake during the intervention period (after recommendations). Dashed lines indicate the mean intake for each nutrient before (blue) and after (green) the recommendations.

1046 of this approach to bridge the gap between theoretical optimization models and practical dietary  
1047 interventions, opening avenues for further research and development in the field of precision nutrition  
1048 and lifestyle medicine.

1049 **5.4. Diet Recommendation Decision-support Tools**

1050 The inverse learning framework enables the integration of additional knowledge (provided by  
1051 domain experts or derived from data) in providing recommendations and solving inverse problems.  
1052 Considering the inherent observation-goal tradeoff, exploring a set of results allows the user to select  
1053 the best solution or a sequence of solutions that best fit their needs. Given this flexibility, we develop  
1054 two interactive and user-friendly decision-support tools as proof of concepts to how inverse learning  
1055 can recommend decisions in the nutrition domain and empower users further.

1056 We have developed a proof of concept diet recommendation modality based on the models  
1057 developed in this work. Users can input a set of food intakes for a day and ask the tool to  
1058 provide recommendations based on specific dietary regiments (e.g. DASH, low-carbohydrates, etc.),  
1059 assuming that the specific dietary regiments alongside with preferred constraints are resulting from  
1060 expert opinions and knowledge. In this setting, recommendations using inverse learning translate  
1061 to minimal changes to the daily intakes so as to ensure adherence to the guidelines set forth by  
1062 the expert. Considering the MGIL model and the inherent observation-goal tradeoff, this results in  
1063 a step-wise recommendation system that in each step, the recommendations assume more weight  
1064 on the expert guidelines than the observed behavior. As the number of binding constraints (or  
1065 nutritional bounds in this setting) increases, the recommendations become less personalized but of  
1066 higher quality (from the perceived value system of the expert). Considering that finding the optimal  
1067 balance in the observation-goal tradeoff requires post intervention data, our attempt to capture a  
1068 range of recommendation is a remedy to the unknown post intervention setting. This tool is publicly  
1069 available at <https://optimal-lab.com/nutrition-recommender/>. Figure 15 provides a screenshot of  
1070 the user input portion of the tool, where the user can provide daily intakes of the 38 food groups and  
1071 Figure 16 showcases results of recommendations to modify intake of the food groups with minimal  
1072 additions and restrictions to adhere to the pre-selected dietary regimen. Figure 17 showcases the  
1073 visual representation of the comparison of nutrient values across recommendations and the user  
1074 input.

1075 The interactive decision-support tool enables users to access a range of recommended diets and  
1076 explore different settings and preferences. They will be able to examine the impact of binding more  
1077 goals (achieving more nutritional goals) in a step-by-step manner and evaluate the gains and the  
1078 price, in the form of moving away from their habits and prior selections. The online tool contrasts

Food Item:	Milk (244 g)	Servings:	1	<input type="button" value="X"/>
Food Item:	Chicken, Turkey (110 g)	Servings:	2	<input type="button" value="X"/>
Food Item:	Bread (25 g)	Servings:	2	<input type="button" value="X"/>
Food Item:	Citrus Fruits (236 g)	Servings:	2	<input type="button" value="X"/>
Food Item:	Greens (38 g)	Servings:	2	<input type="button" value="X"/>
Dietary Regimen:	DASH			

DASH: Carbs: 50-60% Fats: 25-30% Protein: 15-20% Sodium: 1000-1600 mg

[Preference to maximize/minimize nutrients?](#)

Lower Bounds	Upper Bounds
<input type="checkbox"/> Calories	<input type="checkbox"/> Calories
<input type="checkbox"/> Carbs	<input type="checkbox"/> Carbs
<input type="checkbox"/> Protein	<input checked="" type="checkbox"/> Protein
<input type="checkbox"/> Fats	<input type="checkbox"/> Fats
<input type="checkbox"/> Total Sugars	<input type="checkbox"/> Total Sugars
<input type="checkbox"/> Dietary Fiber	<input checked="" type="checkbox"/> Dietary Fiber
<input type="checkbox"/> Saturated Fat	<input type="checkbox"/> Saturated Fat
<input type="checkbox"/> Cholesterol	<input type="checkbox"/> Cholesterol
<input checked="" type="checkbox"/> Sodium	<input type="checkbox"/> Sodium

[Add Entry](#) [Submit Diary](#)

**Figure 15** First snapshot of the interactive diet recommendation tool. The upper section includes modalities for the user to input their intended daily food intake values followed by a dietary regimen selection panel which also shows how the feasible set for the selected regimen is created. In addition to selecting a regimen modality, users can also select specific preferences in terms of binding lower- or upper-bounds on select nutrients in different steps.

1079 with one-size-fits-all dietary approaches. It expands diet recommendations from a single fixed diet  
 1080 to a flexible range of diets that are informed by the user, which may improve adherence.

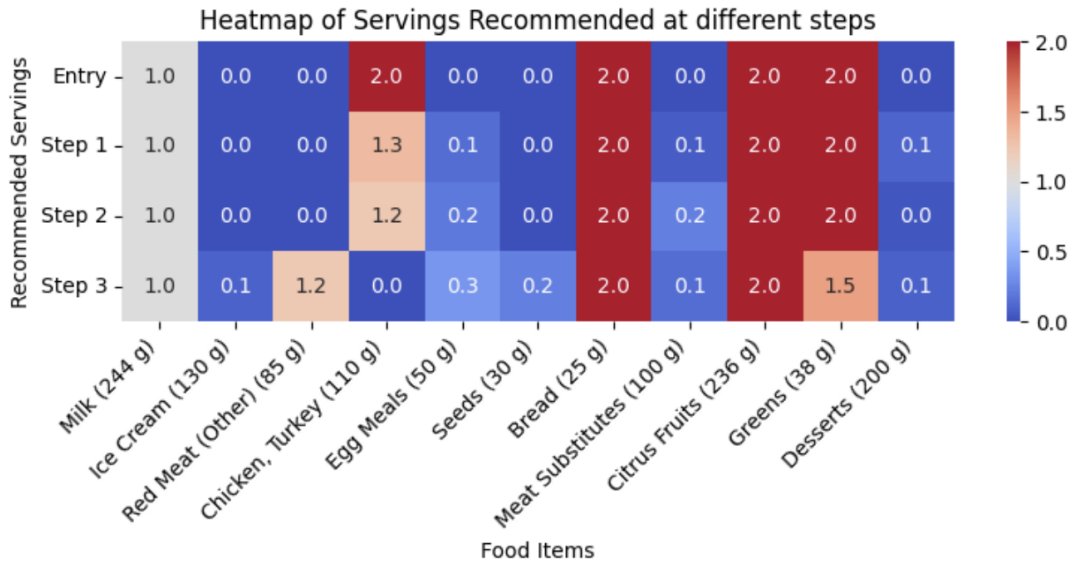


**Figure 16** Second snapshot of the interactive diet recommendation tool. The first row shows the user input while subsequent rows suggest nudges in the amounts and additions and removal of some food groups in order for the daily intake to adhere with the selected dietary regimen. Further steps aim to bind more bounds that the user has selected from the set of nutrients.

1081 We have also provided a preliminary web-based interactive dashboard for our case study of diet  
 1082 recommendations. This tool has two components, the first including data from the National Health  
 1083 and Nutrition Examination Survey data ([CDC 2020b](#)). This component is available publicly at  
 1084 <https://optimal-lab.com/optimal-diet> and includes all data and results presented in Section 5. Users  
 1085 can select different demographic groups, choose their own preferred constraints, and assume the role  
 1086 of the expert in identifying the number and type of binding constraints to investigate results and  
 1087 contrast them against each other.

1088 Figure 18 shows a screenshot of the interactive tool. The demographic group of choice can be  
 1089 selected from the dropdown menu marked as (a), for example, males between 31-50 years of age.  
 1090 The resulting diet recommendation for this group is then presented in part (b) with the binding  
 1091 lower- or upper-bound constraints displayed on the right, e.g., for this example sugar and iron. The  
 1092 historical observations are shown in boxplots with the average distance to observations shown on  
 1093 top left of the resulting figure. The diet recommendations are obtained by solving the MGIL models,  
 1094 and the user can explore binding different numbers of constraints by using the slider in part (c).  
 1095 This example illustrates the results for binding two constraints ( $r = 2$ ). The user can then define  
 1096 preferred constraints to bind from a set of DASH requirements as shown in part (d) and rerun the  
 1097 models with their new selection.

1098 The tool illustrates each learned diet with the average observed food intake. For each new model,  
 1099 a new set of figures are produced that showcase the details of the recommended diet with additional

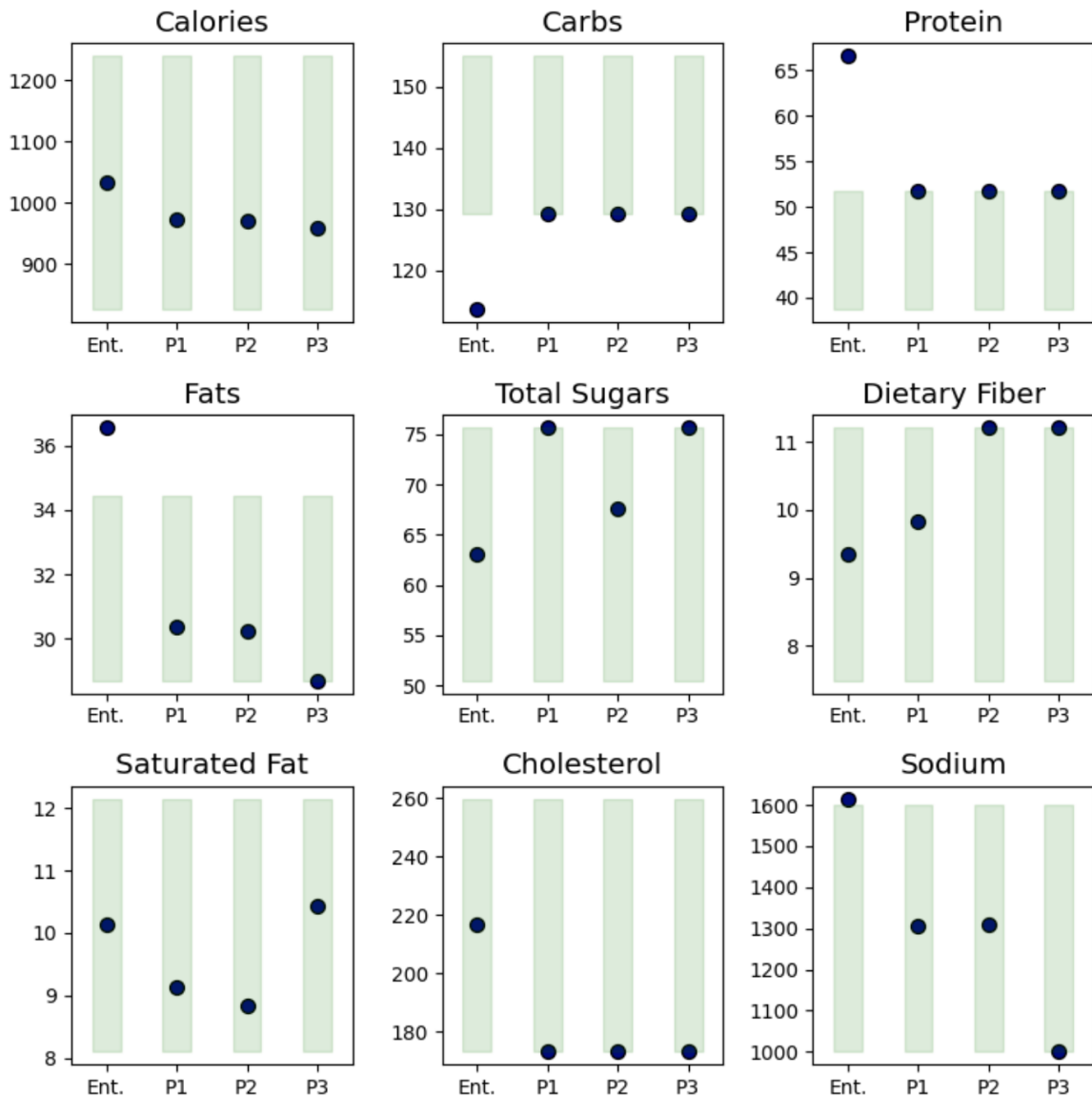


**Figure 17** Third snapshot of the interactive diet recommendation tool. Nutritional values of each step and the user entry are shown. As shown in the figure, step one maximizes protein with regards to preferences set by the user, step two maximizes dietary fiber on top of that and the final step reduces sodium to the minimum required amount.

information on its nutritional bounds. The nutritional bound graph consists of eleven sub-graphs, each representing one of the nutrients considered in the model. The y-axis on each sub-graph is scaled to the range of lower and upper bounds on the nutrient. The range limits are indicated by a dashed green line for the relevant constraints, a blue curve for the preferred constraints, and a yellow curve for other constraints. Should the user decide to run a second model with a different selection,

they can see their new results alongside the previous one for easier comparison. The results for the latest two selections can be navigated using *Current Results* and *Previous Results* sections.

## 6. Conclusions

This work introduces the inverse learning framework to recommend personalized diets for patients with chronic conditions like hypertension and pre-diabetes. The framework formulates the diet recommendation problem as an optimization model with unknown patient preference cost vectors and known nutritional constraints based on expert guidelines like the DASH diet. The key novelty of the inverse learning approach is concurrently learning the optimal diet solutions and underlying patient cost functions directly from observed food intake data. This enables better control and stability compared to traditional recover-then-optimize methods in inverse optimization. Additionally, the framework integrates constraint priority knowledge and provides a spectrum of

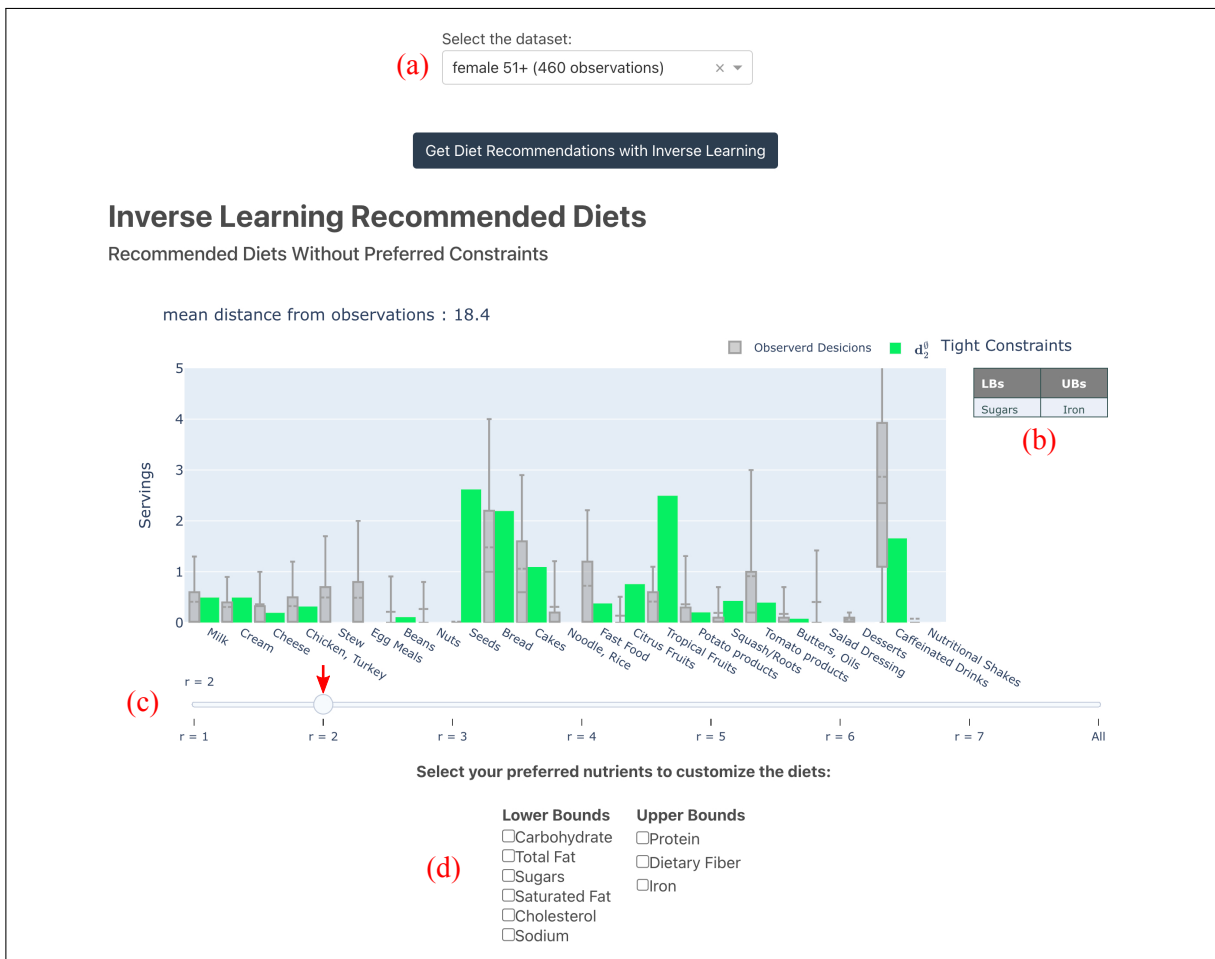


**Figure 18** A snapshot of the interactive decision-support tool that enables exploring a range of possible diets. Part (a) shows the dataset selection, (b) displays the binding relevant constraints, (c) enables exploring different numbers of binding constraints, and (d) provides a panel to choose preferred constraints.

1116 diet recommendations ranging from minimal adjustments to patients' existing behaviors to optimal  
1117 diets meeting all nutritional goals. The generalized goal-integrated inverse learning models can tailor  
1118 the optimal solutions based on the number and the type of active constraints at optimality and  
1119 prioritize binding those that are preferred by the user or based on the problem setting. Additional  
1120 models that sequentially bind more constraints are also shown to be superior in recovering correct  
1121 cost vectors when compared to benchmark inverse optimization models.

1122 Numerical experiments demonstrate the superior performance of inverse learning models in  
1123 accurately recovering cost vectors compared to benchmark inverse optimization methods, especially  
1124 with limited observations. The results exhibit increased control over the distance to the observations  
1125 and decreased sensitivity to potential outliers as perturbations of all observations are taken into  
1126 account in the objective of the inverse learning models. We apply the inverse learning framework  
1127 to derive diet recommendations based on historical dietary behaviors of hypertension patients as  
1128 well. The case study on a sample of around 2000 NHANES patients and further showcases the  
1129 practical merits in providing personalized and gradually improving diet plans to enhance likely  
1130 patient adherence. The models recommend a flexible set of diets based on observations and can tailor  
1131 to potential preferences of the users for nutritional goals or desirable food groups. The recommended  
1132 diets honor the healthy choices of the patients and replicate their favored dietary choices, when  
1133 nutritional constraints permit, and provide a range of options for improving the behavior based on  
1134 the user's priorities. Additionally, interactive decision support tools also allows dietitians to explore  
1135 suitable diet adjustments based on patient preferences and nutritional priorities.

1136 This research can be extended in several meaningful directions. The linear assumptions can be  
1137 relaxed to consider more complex diet-disease relationships and substitutions between food groups.  
1138 Robust optimization approaches would account for uncertainty in patient behaviors and guideline  
1139 effects. Finally, testing and validating the diet plans in clinical trials with actual patients can provide  
1140 insights into long-term diet adherence and health outcomes. Overall, the proposed methodology  
1141 offers a promising new application area for inverse optimization in precision nutrition and lifestyle  
1142 interventions. Additionally, the methods provided here are built on the assumption that the feasible  
1143 set of FO is known. If in addition to the unknown cost vector, part of the feasible region is also  
1144 unknown, new methods can be developed to recover both parameters.

## 1145 References

- 1146 Ahuja RK, Orlin JB (2001) Inverse optimization. *Operations Research* 49(5):771–783.
- 1147 Ajayi T, Lee T, Schaefer AJ (2022) Objective selection for cancer treatment: an inverse optimization  
1148 approach. *Operations Research* .
- 1149 Akhtar SA, Kolarijani AS, Esfahani PM (2021) Learning for control: An inverse optimization approach.  
1150 *IEEE Control Systems Letters* 1–1, URL <http://dx.doi.org/10.1109/LCSYS.2021.3050305>.

- 1151 Aswani A (2019) Statistics with set-valued functions: applications to inverse approximate optimization.  
1152     *Mathematical Programming* 174(1-2):225–251.
- 1153 Aswani A, Kaminsky P, Mintz Y, Flowers E, Fukuoka Y (2019) Behavioral modeling in weight loss  
1154     interventions. *European journal of operational research* 272(3):1058–1072.
- 1155 Aswani A, Shen ZJ, Siddiq A (2018) Inverse optimization with noisy data. *Operations Research* 66(3):870–  
1156     892.
- 1157 Babier A, Chan TC, Lee T, Mahmood R, Terekhov D (2021) An ensemble learning framework for model  
1158     fitting and evaluation in inverse linear optimization. *Informs Journal on Optimization* 3(2):119–138.
- 1159 Bärmann A, Martin A, Pokutta S, Schneider O (2018) An online-learning approach to inverse optimization.  
1160     *arXiv preprint arXiv:1810.12997* .
- 1161 Bas E (2014) A robust optimization approach to diet problem with overall glycemic load as objective function.  
1162     *Applied Mathematical Modelling* 38(19-20):4926–4940.
- 1163 Bassi L (1976) The diet problem revisited. *The American Economist* 20(2):35–39.
- 1164 Bazrafkan L, Choobineh MA, Shojaei M, Bozorgi A, Sharifi MH (2021) How do overweight people dropout  
1165     of a weight loss diet? a qualitative study. *BMC nutrition* 7(1):1–9.
- 1166 Beil DR, Wein LM (2003) An inverse-optimization-based auction mechanism to support a multiattribute rfq  
1167     process. *Management Science* 49(11):1529–1545.
- 1168 Bentley B, De Jong MJ, Moser DK, Peden AR (2005) Factors related to nonadherence to low sodium diet  
1169     recommendations in heart failure patients. *European Journal of Cardiovascular Nursing* 4(4):331–336.
- 1170 Bertsimas D, Gupta V, Paschalidis IC (2012) Inverse optimization: A new perspective on the black-litterman  
1171     model. *Operations research* 60(6):1389–1403.
- 1172 Besbes O, Fonseca Y, Lobel I (2023) Contextual inverse optimization: Offline and online learning. *Operations  
1173     Research* .
- 1174 Burton D, Toint PL (1992) On an instance of the inverse shortest paths problem. *Mathematical programming*  
1175     53(1-3):45–61.
- 1176 Campbell AP (2017) DASH Eating Plan: An Eating Pattern for Diabetes Management. *Diabetes Spectrum*  
1177     30(2):76–81, ISSN 1040-9165, URL <http://dx.doi.org/10.2337/ds16-0084>.
- 1178 CDC (2020a) Facts about hypertension. URL <https://www.cdc.gov/bloodpressure/facts.htm>.
- 1179 CDC (2020b) Nhanes dietary data. URL <https://wwwn.cdc.gov/nchs/nhanes/Search/DataPage.aspx?Component=Dietary>.
- 1180 Černý M, Hladík M (2016) Inverse optimization: towards the optimal parameter set of inverse lp with interval  
1181     coefficients. *Central European Journal of Operations Research* 24(3):747–762.
- 1182 Challa HJ, Ameer MA, Uppaluri KR (2021) Dash diet to stop hypertension. *StatPearls [Internet]* (StatPearls  
1183     Publishing).
- 1184 Chan TC, Craig T, Lee T, Sharpe MB (2014) Generalized inverse multiobjective optimization with  
1185     application to cancer therapy. *Operations Research* 62(3):680–695.
- 1186 Chan TC, Eberg M, Forster K, Holloway C, Ieraci L, Shalaby Y, Yousefi N (2022a) An inverse optimization  
1187     approach to measuring clinical pathway concordance. *Management Science* 68(3):1882–1903.

- 1189 Chan TC, Forster K, Habbous S, Holloway C, Ieraci L, Shalaby Y, Yousefi N (2022b) Inverse optimization  
1190 on hierarchical networks: an application to breast cancer clinical pathways. *Health Care Management  
1191 Science* 25(4):590–622.
- 1192 Chan TC, Kaw N (2020) Inverse optimization for the recovery of constraint parameters. *European Journal  
1193 of Operational Research* 282(2):415–427.
- 1194 Chan TC, Lee T (2018) Trade-off preservation in inverse multi-objective convex optimization. *European  
1195 Journal of Operational Research* 270(1):25–39.
- 1196 Chan TC, Lee T, Terekhov D (2019) Inverse optimization: Closed-form solutions, geometry, and goodness  
1197 of fit. *Management Science* 65(3):1115–1135.
- 1198 Chan TC, Mahmood R, Zhu IY (2021) Inverse optimization: Theory and applications. *arXiv preprint  
1199 arXiv:2109.03920*.
- 1200 Chow JY, Recker WW (2012) Inverse optimization with endogenous arrival time constraints to calibrate the  
1201 household activity pattern problem. *Transportation Research Part B: Methodological* 46(3):463–479.
- 1202 Civril A, Magdon-Ismail M (2009) On selecting a maximum volume sub-matrix of a matrix and related  
1203 problems. *Theoretical Computer Science* 410(47-49):4801–4811.
- 1204 Conforti M, Cornuéjols G, Zambelli G, et al. (2014) *Integer programming*, volume 271 (Springer).
- 1205 Corletto D, Iori M, Paiusco M, Brait L, Broggi S, Ceresoli G, Iotti C, Calandrino R, Fiorino C (2003)  
1206 Inverse and forward optimization of one-and two-dimensional intensity-modulated radiation therapy-  
1207 based treatment of concave-shaped planning target volumes: the case of prostate cancer. *Radiotherapy  
1208 and oncology* 66(2):185–195.
- 1209 Crönert T, Martin L, Minner S, Tang CS (2024) Inverse optimization of integer programming games for  
1210 parameter estimation arising from competitive retail location selection. *European Journal of Operational  
1211 Research* 312(3):938–953.
- 1212 Dantzig GB (1965) *Linear programming and extensions*, volume 48 (Princeton university press).
- 1213 DASH (2018) Dash eating plan. URL <https://www.nhlbi.nih.gov/health-topics/dash-eating-plan>.
- 1214 Dietvorst BJ, Simmons JP, Massey C (2015) Algorithm aversion: people erroneously avoid algorithms after  
1215 seeing them err. *J. Experiment. Psych. General* 144(1):114.
- 1216 Dietvorst BJ, Simmons JP, Massey C (2018) Overcoming algorithm aversion: People will use imperfect  
1217 algorithms if they can (even slightly) modify them. *Management Sci.* 64(3):1155–1170.
- 1218 Dong C, Chen Y, Zeng B (2018) Generalized inverse optimization through online learning. *Advances in  
1219 Neural Information Processing Systems*, 86–95.
- 1220 Downer MK, Gea A, Stampfer M, Sánchez-Tainta A, Corella D, Salas-Salvadó J, Ros E, Estruch R, Fitó M,  
1221 Gómez-Gracia E, et al. (2016) Predictors of short-and long-term adherence with a mediterranean-type  
1222 diet intervention: the predimed randomized trial. *International Journal of Behavioral Nutrition and  
1223 Physical Activity* 13(1):1–16.
- 1224 Esfahani PM, Shafeezadeh-Abadeh S, Hanusanto GA, Kuhn D (2018) Data-driven inverse optimization  
1225 with imperfect information. *Mathematical Programming* 167(1):191–234.
- 1226 Faragó A, Szentesi Á, Szviatoszki B (2003) Inverse optimization in high-speed networks. *Discrete Applied  
1227 Mathematics* 129(1):83–98.

- 1228 Ferguson EL, Darmon N, Fahmida U, Fitriyanti S, Harper TB, Premachandra IM (2006) Design of optimal  
1229 food-based complementary feeding recommendations and identification of key “problem nutrients” using  
1230 goal programming. *The Journal of nutrition* 136(9):2399–2404.
- 1231 Garille SG, Gass SI (2001) Stigler’s diet problem revisited. *Operations Research* 49(1):1–13.
- 1232 Gazan R, Brouzes CM, Vieux F, Maillot M, Lluch A, Darmon N (2018) Mathematical optimization to explore  
1233 tomorrow’s sustainable diets: a narrative review. *Advances in Nutrition* 9(5):602–616.
- 1234 Ghate A (2015) Inverse optimization in countably infinite linear programs. *Operations Research Letters*  
1235 43(3):231–235.
- 1236 Ghate A (2020) Inverse optimization in semi-infinite linear programs. *Operations Research Letters* 48(3):278–  
1237 285.
- 1238 Ghobadi K, Lee T, Mahmoudzadeh H, Terekhov D (2018) Robust inverse optimization. *Operations Research  
Letters* 46(3):339–344.
- 1239 Ghobadi K, Mahmoudzadeh H (2021) Inferring linear feasible regions using inverse optimization. *European  
Journal of Operational Research* 290(3):829–843.
- 1240 Gorissen BL, Den Hertog D, Hoffmann AL (2013) Mixed integer programming improves comprehensibility  
1241 and plan quality in inverse optimization of prostate hdr brachytherapy. *Physics in Medicine & Biology*  
1242 58(4):1041.
- 1243 Grand-Clément J, Pauphilet J (2022) The best decisions are not the best advice: Making adherence-aware  
1244 recommendations. *arXiv preprint arXiv:2209.01874* .
- 1245 Heuberger C (2004) Inverse combinatorial optimization: A survey on problems, methods, and results. *Journal  
of combinatorial optimization* 8(3):329–361.
- 1246 Hewitt M, Freijinger E (2020) Data-driven optimization model customization. *European Journal of  
Operational Research* 287(2):438–451.
- 1247 Inelmen EM, Toffanello ED, Enzi G, Gasparini G, Miotto F, Sergi G, Busetto L (2005) Predictors of drop-out  
1248 in overweight and obese outpatients. *International journal of obesity* 29(1):122–128.
- 1249 Iyengar G, Kang W (2005) Inverse conic programming with applications. *Operations Research Letters*  
1250 33(3):319–330.
- 1251 Keshavarz A, Wang Y, Boyd S (2011) Imputing a convex objective function. *2011 IEEE International  
Symposium on Intelligent Control*, 613–619 (IEEE).
- 1252 Konstantakopoulos IC, Ratliff LJ, Jin M, Sastry SS, Spanos CJ (2017) A robust utility learning framework  
1253 via inverse optimization. *IEEE Transactions on Control Systems Technology* 26(3):954–970.
- 1254 Lasserre JB (2013) Inverse polynomial optimization. *Mathematics of Operations Research* 38(3):418–436.
- 1255 Liese AD, Nichols M, Sun X, D’Agostino RB, Haffner SM (2009) Adherence to the dash diet is inversely  
1256 associated with incidence of type 2 diabetes: the insulin resistance atherosclerosis study. *Diabetes care*  
1257 32(8):1434–1436.
- 1258 Moghaddass M, Terekhov D (2021) Inverse integer optimization with multiple observations. *Optimization  
Letters* 15(4):1061–1079.
- 1259 Naghavi M, Foroughi AA, Zarepisheh M (2019) Inverse optimization for multi-objective linear programming.  
1260 *Optimization Letters* 13(2):281–294.

- 1267 Pibernik R, Zhang Y, Kerschbaum F, Schröpfer A (2011) Secure collaborative supply chain planning and  
1268 inverse optimization—the jels model. *European Journal of Operational Research* 208(1):75–85.
- 1269 Roland J, De Smet Y, Figueira JR (2013) Inverse multi-objective combinatorial optimization. *Discrete applied  
1270 mathematics* 161(16–17):2764–2771.
- 1271 Sacks FM, Svetkey LP, Vollmer WM, Appel LJ, Bray GA, Harsha D, Obarzanek E, Conlin PR, Miller ER,  
1272 Simons-Morton DG, et al. (2001) Effects on blood pressure of reduced dietary sodium and the dietary  
1273 approaches to stop hypertension (dash) diet. *New England journal of medicine* 344(1):3–10.
- 1274 Schaefer AJ (2009) Inverse integer programming. *Optimization Letters* 3(4):483–489.
- 1275 Schede EA, Kolb S, Teso S (2019) Learning linear programs from data. *ICTAI* 1019–1026.
- 1276 Shahmoradi Z, Lee T (2022a) Optimality-based clustering: An inverse optimization approach. *Operations  
1277 Research Letters* 50(2):205–212.
- 1278 Shahmoradi Z, Lee T (2022b) Quantile inverse optimization: Improving stability in inverse linear  
1279 programming. *Operations research* 70(4):2538–2562.
- 1280 Stigler GJ (1945) The cost of subsistence. *Journal of farm economics* 27(2):303–314.
- 1281 Tan Y, Delong A, Terekhov D (2019) Deep inverse optimization. *International Conference on Integration of  
1282 Constraint Programming, Artificial Intelligence, and Operations Research*, 540–556 (Springer).
- 1283 Tavashioğlu O, Lee T, Valeva S, Schaefer AJ (2018) On the structure of the inverse-feasible region of a linear  
1284 program. *Operations Research Letters* 46(1):147–152.
- 1285 USDA (2019) Fooddata central. URL [fdc.nal.usda.gov](https://fdc.nal.usda.gov).
- 1286 Wang L (2009) Cutting plane algorithms for the inverse mixed integer linear programming problem.  
1287 *Operations Research Letters* 37(2):114–116.
- 1288 Xu X, Rong H, Trovati M, Liptrott M, Bessis N (2018) Cs-psos: chaotic particle swarm optimization algorithm  
1289 for solving combinatorial optimization problems. *Soft Computing* 22(3):783–795.
- 1290 Yang C, Zhang J (1999) Two general methods for inverse optimization problems. *Applied Mathematics Letters  
1291* 12(2):69–72.
- 1292 Zhang J, Liu Z (1996) Calculating some inverse linear programming problems. *Journal of Computational  
1293 and Applied Mathematics* 72(2):261–273.
- 1294 Zhang J, Liu Z (1999) A further study on inverse linear programming problems. *Journal of Computational  
1295 and Applied Mathematics* 106(2):345–359.
- 1296 Zhang J, Ma Z (1999) Solution structure of some inverse combinatorial optimization problems. *Journal of  
1297 Combinatorial Optimization* 3(1):127–139.
- 1298 Zhang J, Xu C (2010) Inverse optimization for linearly constrained convex separable programming problems.  
1299 *European Journal of Operational Research* 200(3):671–679.

1300

## Electronic Companion

### EC.1. Proofs of Statements

1302 *Proof of Proposition 1.*  $\exists \hat{\mathbf{x}} \in \Omega$  for which the equality  $\mathbf{a}_j \hat{\mathbf{x}} = b_j$  holds (given the assumption that  
 1303 no relevant constraint is redundant). Defining  $\mathbf{c}_0 = \mathbf{a}'_j$ ,  $\mathbf{y}_0 = \mathbf{e}_j$ , and  $\mathbf{z}_0 = \hat{\mathbf{x}}$ , the solution  $(\mathbf{c}_0, \mathbf{y}_0, \mathbf{0}, \mathbf{z}_0)$   
 1304 is feasible for IL since (3b) and (3c) hold by the feasibility of  $\hat{\mathbf{x}}$ , (3d) holds by the assumption  
 1305  $\mathbf{a}_j \hat{\mathbf{x}} = b_j$  and the definition of  $\mathbf{c}_0$  and  $\mathbf{y}_0$ , and remaining constraints are also satisfied directly from  
 1306 the definition of the parameters.  $\square$

1307 *Proof of Proposition 2.* Assume to the contrary that for a feasible solution  $(\mathbf{c}, \mathbf{y}, \bar{\mathbf{y}}, \mathbf{z})$  for IL, we  
 1308 have  $\mathbf{c} = \mathbf{0}$  and therefore,  $\mathbf{y}' \mathbf{A} = \mathbf{0}$ . We have two cases:

- 1309 • **Case 1:**  $y_j = 0 \forall j \in \mathcal{J}$  which is a contradiction to the constraint (3g).
- 1310 • **Case 2:** There is a convex combination of the rows of the matrix  $\mathbf{A}$  such that  $\mathbf{y}' \mathbf{A} = \mathbf{0}$ . We  
 1311 show that this is a contradiction to the feasible set  $\Omega$  being full dimensional. Considering that  
 1312  $\Omega$  does not have redundant constraints, let  $\hat{\mathbf{y}}$  be the non-zero elements in  $\mathbf{y}$  and let  $\mathbf{D}$  be the  
 1313 index set of these elements. Note that  $2 \leq |\mathbf{D}| \leq n$ . Also, let  $\hat{\mathbf{A}}$  and  $\hat{\mathbf{b}}$  be sub-matrices of  $\mathbf{A}$   
 1314 and  $\mathbf{b}$  containing rows indexed by  $\mathbf{D}$  and let  $\mathbf{a}'_i$  be the  $i^{th}$  row of  $\hat{\mathbf{A}}$  and  $b_i$  be the  $i^{th}$  element  
 1315 of right-hand-side vector  $\hat{\mathbf{b}}$  for  $i \in \{1, \dots, |\mathbf{D}|\}$ . We have the following:

$$\hat{y}_1 \mathbf{a}'_1 + \dots + \hat{y}_{|\mathbf{D}|} \mathbf{a}'_{|\mathbf{D}|} = 0, \quad \hat{y}_i > 0 \quad \forall i \in \{1, \dots, |\mathbf{D}|\} \Rightarrow \hat{y}_1 \mathbf{a}'_1 + \dots + \hat{y}_{|\mathbf{D}|-1} \mathbf{a}'_{|\mathbf{D}|-1} = -\hat{y}_{|\mathbf{D}|} \mathbf{a}'_{|\mathbf{D}|}. \quad (\text{EC.1})$$

1316 Note that  $\forall \mathbf{x} \in \Omega$ , we have the following:

$$\left. \begin{array}{l} \mathbf{a}'_1 \mathbf{x} \geq b_1 \\ \vdots \\ \mathbf{a}'_{|\mathbf{D}|-1} \mathbf{x} \geq b_{|\mathbf{D}|-1} \end{array} \right\} \Rightarrow (\hat{y}_1 \mathbf{a}'_1 + \dots + \hat{y}_{|\mathbf{D}|-1} \mathbf{a}'_{|\mathbf{D}|-1}) \mathbf{x} \geq \hat{y}_1 b_1 + \dots + \hat{y}_{|\mathbf{D}|-1} b_{|\mathbf{D}|-1} \quad (\text{EC.2})$$

1317 Which yields the following using (EC.1):

$$-\hat{y}_{|\mathbf{D}|} \mathbf{a}'_{|\mathbf{D}|} \mathbf{x} \geq \sum_{i=1}^{|\mathbf{D}|-1} \hat{y}_i b_i. \quad (\text{EC.3})$$

1318 Additionally,  $\forall \mathbf{x} \in \Omega$ :

$$\mathbf{a}'_{|\mathbf{D}|} \mathbf{x} \geq b_{|\mathbf{D}|} \Rightarrow -\hat{y}_{|\mathbf{D}|} \mathbf{a}'_{|\mathbf{D}|} \mathbf{x} \leq -\hat{y}_{|\mathbf{D}|} b_{|\mathbf{D}|}. \quad (\text{EC.4})$$

1319 However, since strong duality conditions hold for solution  $\mathbf{z}$ , from the complementary slackness  
 1320 conditions, we have the following:

$$\left. \begin{array}{l} \mathbf{a}'_1 \mathbf{z} = b_1 \\ \vdots \\ \mathbf{a}'_{|\mathbf{D}|} \mathbf{z} = b_{|\mathbf{D}|} \end{array} \right\} \Rightarrow \left( \sum_{i=1}^{|\mathbf{D}|} \hat{y}_i \mathbf{a}'_i \right) \mathbf{z} = \sum_{i=1}^{|\mathbf{D}|} \hat{y}_i b_i. \quad (\text{EC.5})$$

1321 However, we know that  $\sum_{i=1}^{|D|} \hat{y}_i \mathbf{a}'_i = 0$ . Therefore,  $\sum_{i=1}^{|D|} \hat{y}_i b'_i = 0$  and we get the important  
 1322 equation  $\sum_{i=1}^{|D|-1} \hat{y}_i b_i = -\hat{y}_{|D|} b_{|D|}$ . Combining this equation with equality (EC.3) yields  
 1323  $-\hat{y}_{|D|} \mathbf{a}'_{|D|} \mathbf{x} \geq -\hat{y}_{|D|} b_{|D|}$ . Considering this inequality with inequality (EC.4) yields  $-\hat{y}_{|D|} \mathbf{a}'_{|D|} \mathbf{x} =$   
 1324  $-\hat{y}_{|D|} b_{|D|}$ , which considering that  $\hat{y}$  is non-zero, results in  $\mathbf{a}'_{|D|} \mathbf{x} = b_{|D|}$ . This means that  $\mathbf{a}'_{|D|} \mathbf{x} \geq$   
 1325  $b_{|D|}$  is an implicit inequality for  $\Omega$  which is a contradiction to  $\Omega$  being full dimensional (for  
 1326 more information on implicit equalities refer to Theorem 3.17 from Conforti et al. (2014)).  $\square$

1327 *Proof of Theorem 1.* Note that for any feasible solution  $(\hat{\mathbf{c}}, \hat{\mathbf{y}}, \hat{\mathbf{z}})$  for IL,  $\hat{\mathbf{z}}$  satisfies primal  
 1328 feasibility, dual feasibility, and strong duality conditions for  $\text{FO}(\hat{\mathbf{c}}, \Omega)$  and as such  $\hat{\mathbf{z}}$  is optimal for  
 1329  $\text{FO}(\hat{\mathbf{c}}, \Omega)$  and thus  $\hat{\mathbf{z}} \in \Omega^{opt}(\hat{\mathbf{c}})$ . Considering that  $\hat{\mathbf{z}}$  binds at least one relevant constraint (constraint  
 1330 (3g)), then  $\hat{\mathbf{z}} \in \Omega_{\mathcal{R}}^{opt}$ . The second part of the theorem can be shown by noting that  $\forall \hat{\mathbf{z}} \in \Omega_{\mathcal{R}}^{opt}$ , there  
 1331 exists a feasible solution  $(\mathbf{c}, \mathbf{y}, \bar{\mathbf{y}}, \mathbf{z})$  for IL such that  $\mathbf{z} = \hat{\mathbf{z}}$ .  $\square$

1332 *Proof of Theorem 2.* V1. Assume that all observations in  $\mathcal{X}$  are noised observations of  $\mathbf{x}^{opt}$  and  
 1333 note that  $\mathbf{x}^{opt} \in \Omega_{\mathcal{R}}^{opt}$  by assumption. By definition:

$$\mathbf{x}^{opt} = \mathbb{E}(\arg \min_{\mathbf{z} \in \mathbb{R}^n} \sum_{k \in \mathcal{K}} \|\mathbf{x}^k - \mathbf{z}\|_l) \quad (\text{EC.6})$$

1334 Therefore, the expectation of the sum of distances of the noised observations from  $\mathbf{x}^{opt}$  is smaller  
 1335 than any other point in  $\mathbb{R}^n$ . In other words:

$$\mathbb{E}(\sum_{k \in \mathcal{K}} \|\mathbf{x}^k - \mathbf{x}^{opt}\|_l) \leq \mathbb{E}(\sum_{k \in \mathcal{K}} \|\mathbf{x}^k - \mathbf{z}\|_l) \quad \forall \mathbf{z} \in \mathbb{R}^n \quad (\text{EC.7})$$

1336 On the other hand, let  $\mathbf{z}^* = \arg \min_{\mathbf{z} \in \Omega_{\mathcal{R}}^{opt}} \sum_{k \in \mathcal{K}} \|\mathbf{x}^k - \mathbf{z}\|_l$  and as such:

$$\mathbb{E}(\mathbf{z}^*) = \mathbb{E}(\arg \min_{\mathbf{z} \in \Omega_{\mathcal{R}}^{opt}} \sum_{k \in \mathcal{K}} \|\mathbf{x}^k - \mathbf{z}\|_l). \quad (\text{EC.8})$$

1337 If  $\mathbb{E}(\mathbf{z}^*) = \mathbf{x}^{opt}$ , we have the desired result. Assume to the contrary that  $\mathbb{E}(\mathbf{z}^*) = \mathbf{z}^{opt} \neq \mathbf{x}^{opt}$ . Noting  
 1338 EC.8, we have:

$$\mathbb{E}(\sum_{k \in \mathcal{K}} \|\mathbf{x}^k - \mathbf{z}^{opt}\|_l) \leq \mathbb{E}(\sum_{k \in \mathcal{K}} \|\mathbf{x}^k - \mathbf{z}\|_l) \quad \forall \mathbf{z} \in \Omega_{\mathcal{R}}^{opt} \quad (\text{EC.9})$$

1339 However, since  $\mathbf{x}^{opt} \in \Omega_{\mathcal{R}}^{opt}$ , we have:

$$\mathbb{E}(\sum_{k \in \mathcal{K}} \|\mathbf{x}^k - \mathbf{z}^{opt}\|_l) \leq \mathbb{E}(\sum_{k \in \mathcal{K}} \|\mathbf{x}^k - \mathbf{x}^{opt}\|_l) \quad (\text{EC.10})$$

1340 Combining EC.7 and EC.10, we get:

$$\mathbb{E}(\sum_{k \in \mathcal{K}} \|\mathbf{x}^k - \mathbf{z}^{opt}\|_l) = \mathbb{E}(\sum_{k \in \mathcal{K}} \|\mathbf{x}^k - \mathbf{x}^{opt}\|_l) \quad (\text{EC.11})$$

1341 Which is a contradiction if the sum minimizer of the  $l$ -norm is unique. Therefore, for such norms,  
 1342  $\mathbb{E}(\mathbf{z}^*) = \mathbf{z}^{opt} = \mathbf{x}^{opt}$  and for all other norms,  $\mathbf{z}^{opt}$  is as good as  $\mathbf{x}^{opt}$ .

1343 *Proof of Proposition 3.* Since the objective functions of formulations (4) and the IL model are  
 1344 the same, it suffices to show that  $(\mathbf{a}'_j, e_j, \mathbf{0}, \mathbf{z}^*)$  is optimal for IL. It can be readily seen that  $(\mathbf{a}'_j, e_j, \mathbf{0},$   
 1345  $\mathbf{z}^*)$  is indeed feasible for IL. Now assume to the contrary that there is a solution  $(\mathbf{c}, \mathbf{y}, \mathbf{0}, \mathbf{z})$  for IL  
 1346 such that the objective value of IL for this solution is strictly less than  $\mathcal{D}_{min}$ . However, from previous  
 1347 results, at least one relevant constraint is binding at  $\mathbf{z}$ . We denote this constraint as constraint  $j$ . As  
 1348 a result, we have  $\mathbf{a}_j \mathbf{z} = b_j$  which is exactly (4b). Therefore,  $\mathbf{z}$  is feasible for formulation (4) which is a  
 1349 contradiction with  $(\mathbf{a}'_{j_{min}}, e_{j_{min}}, \mathbf{0}, \mathbf{z}^*)$  being the solution with the minimum objective value among  
 1350 all solutions to different instances of formulations (4). Therefore,  $(\mathbf{a}'_{j_{min}}, e_{j_{min}}, \mathbf{0}, \mathbf{z}^*)$  is optimal for  
 1351 IL.  $\square$

1352 *Proof of Proposition 6* The constraints (6b)-(6e) in the CIL model ensure that the learned  
 1353 optimal solutions  $\mathbf{x}_{opt}^{k*}$  satisfy the KKT optimality conditions for the forward problem  
 1354 with the estimated unknown parameters  $\theta^*$ . Therefore,  $\mathbf{x}_{opt}^{k*}$  is an optimal solution to  
 1355  $\text{FO}(f(\mathbf{x}, \mathbf{u}^k, \theta^*), \Omega(\mathbf{u}^k, \theta^*))$  for each  $\mathbf{u}^k$ .  $\square$

1356 Here's the rewritten proof with formatting consistent with the paper's LaTeX style:

1357 *Proof of Theorem 3* We will prove this theorem in several steps:

1358 1) First, let's recall the CIL model's objective function:

$$\min_{\mathbf{x}_{opt}^k, \theta, \lambda_i^k} \sum_{k=1}^K \sum_{j \in J_k} \|\mathbf{x}^{k,j} - \mathbf{x}_{opt}^k\|_\ell \quad (\text{EC.12})$$

1359 2) By the theorem's assumptions, we have  $\mathbf{x}^{k,j} = \mathbf{x}_{true}^k + \epsilon^{k,j}$ , where  $\mathbf{x}_{true}^k$  is an optimal solution to  
 1360  $\text{FO}(f(\mathbf{x}, \mathbf{u}^k, \theta_0), \Omega(\mathbf{u}^k, \theta_0))$  and  $\epsilon^{k,j}$  are independent random noises with  $\mathbb{E}[\epsilon^{k,j}] = 0$  and  $\mathbb{E}[\|\epsilon^{k,j}\|_\ell^2] \leq$   
 1361  $\sigma^2$ .

1362 3) Let's consider the expected value of  $\|\mathbf{x}_{opt}^{k*} - \mathbf{x}_{true}^k\|_\ell$ :

$$\mathbb{E}[\|\mathbf{x}_{opt}^{k*} - \mathbf{x}_{true}^k\|_\ell] = \mathbb{E}[\|\mathbf{x}_{opt}^{k*} - \frac{1}{J_k} \sum_{j \in J_k} \mathbf{x}^{k,j} + \frac{1}{J_k} \sum_{j \in J_k} \mathbf{x}^{k,j} - \mathbf{x}_{true}^k\|_\ell] \quad (\text{EC.13})$$

1363 4) By the triangle inequality:

$$\mathbb{E}[\|\mathbf{x}_{opt}^{k*} - \mathbf{x}_{true}^k\|_\ell] \leq \mathbb{E}[\|\mathbf{x}_{opt}^{k*} - \frac{1}{J_k} \sum_{j \in J_k} \mathbf{x}^{k,j}\|_\ell] + \mathbb{E}[\|\frac{1}{J_k} \sum_{j \in J_k} \mathbf{x}^{k,j} - \mathbf{x}_{true}^k\|_\ell] \quad (\text{EC.14})$$

1364 5) For the first term, by optimality of  $\mathbf{x}_{opt}^{k*}$ :

$$\mathbb{E}[\|\mathbf{x}_{opt}^{k*} - \frac{1}{J_k} \sum_{j \in J_k} \mathbf{x}^{k,j}\|_\ell] \leq \mathbb{E}[\|\mathbf{x}_{true}^k - \frac{1}{J_k} \sum_{j \in J_k} \mathbf{x}^{k,j}\|_\ell] \quad (\text{EC.15})$$

1365 6) For the second term:

$$\mathbb{E}[\|\frac{1}{J_k} \sum_{j \in J_k} \mathbf{x}^{k,j} - \mathbf{x}_{true}^k\|_\ell] = \mathbb{E}[\|\frac{1}{J_k} \sum_{j \in J_k} (\mathbf{x}_{true}^k + \epsilon^{k,j}) - \mathbf{x}_{true}^k\|_\ell] = \mathbb{E}[\|\frac{1}{J_k} \sum_{j \in J_k} \epsilon^{k,j}\|_\ell] \quad (\text{EC.16})$$

1366 7) By Jensen's inequality and the concavity of the square root:

$$\mathbb{E}[||\frac{1}{J_k} \sum_{j \in J_k} \epsilon^{k,j}||_\ell] \leq \sqrt{\mathbb{E}[||\frac{1}{J_k} \sum_{j \in J_k} \epsilon^{k,j}||_\ell^2]} \quad (\text{EC.17})$$

1367 8) By linearity of expectation and independence of  $\epsilon^{k,j}$ :

$$\sqrt{\mathbb{E}[||\frac{1}{J_k} \sum_{j \in J_k} \epsilon^{k,j}||_\ell^2]} = \sqrt{\frac{1}{J_k^2} \sum_{j \in J_k} \mathbb{E}[||\epsilon^{k,j}||_\ell^2]} \leq \frac{\sigma}{\sqrt{J_k}} \quad (\text{EC.18})$$

1368 9) Combining steps 4-8:

$$\mathbb{E}[||\mathbf{x}_{opt}^{k*} - \mathbf{x}_{true}^k||_\ell] \leq 2\mathbb{E}[||\frac{1}{J_k} \sum_{j \in J_k} \epsilon^{k,j}||_\ell] \leq \frac{2\sigma}{\sqrt{J_k}} \quad (\text{EC.19})$$

1369  $\square$

1370 Here's the rewritten proof with formatting consistent with the paper's LaTeX style:

1371 *Proof of Theorem 4* We will prove this theorem in several steps:

1372 1) First, recall that the CIL model's objective function is:

$$\min_{\mathbf{x}_{opt}^k, \theta, \lambda_i^k} \sum_{k=1}^K \sum_{j \in J_k} ||\mathbf{x}^{k,j} - \mathbf{x}_{opt}^k||_\ell \quad (\text{EC.20})$$

1373 2) Let  $\theta^*$  be the estimated parameter from the CIL model and  $\theta_0$  be the true parameter. We aim  
1374 to show that  $\theta^* \xrightarrow{p} \theta_0$  as  $J_k \rightarrow \infty$  for all  $k$ .

1375 3) By the assumptions of the theorem, we have  $\mathbf{x}^{k,j} = \mathbf{x}_{true}^k(\theta_0) + \epsilon^{k,j}$ , where  $\mathbf{x}_{true}^k(\theta_0)$  is an  
1376 optimal solution to  $\text{FO}(f(\mathbf{x}, \mathbf{u}^k, \theta_0), \Omega(\mathbf{u}^k, \theta_0))$  and  $\epsilon^{k,j}$  are i.i.d. random noises with  $\mathbb{E}[\epsilon^{k,j}] = 0$  and  
1377  $\mathbb{E}[||\epsilon^{k,j}||_\ell^2] \leq \sigma^2$ .

1378 4) Let  $\mathbf{x}_{opt}^k(\theta)$  be an optimal solution to  $\text{FO}(f(\mathbf{x}, \mathbf{u}^k, \theta), \Omega(\mathbf{u}^k, \theta))$ . By the optimality of  $\theta^*$  in the  
1379 CIL model, we have:

$$\sum_{k=1}^K \sum_{j \in J_k} ||\mathbf{x}^{k,j} - \mathbf{x}_{opt}^k(\theta^*)||_\ell \leq \sum_{k=1}^K \sum_{j \in J_k} ||\mathbf{x}^{k,j} - \mathbf{x}_{opt}^k(\theta_0)||_\ell \quad (\text{EC.21})$$

1380 5) As  $J_k \rightarrow \infty$  for all  $k$ , by the law of large numbers:

$$\frac{1}{J_k} \sum_{j \in J_k} ||\mathbf{x}^{k,j} - \mathbf{x}_{opt}^k(\theta^*)||_\ell \xrightarrow{p} \mathbb{E}[||\mathbf{x}_{true}^k(\theta_0) + \epsilon^{k,j} - \mathbf{x}_{opt}^k(\theta^*)||_\ell] \quad (\text{EC.22})$$

$$\frac{1}{J_k} \sum_{j \in J_k} ||\mathbf{x}^{k,j} - \mathbf{x}_{opt}^k(\theta_0)||_\ell \xrightarrow{p} \mathbb{E}[||\mathbf{x}_{true}^k(\theta_0) + \epsilon^{k,j} - \mathbf{x}_{opt}^k(\theta_0)||_\ell] \quad (\text{EC.23})$$

1381 6) From step 4 and 5, we can conclude:

$$\mathbb{E}[||\mathbf{x}_{true}^k(\theta_0) + \epsilon^{k,j} - \mathbf{x}_{opt}^k(\theta^*)||_\ell] \leq \mathbb{E}[||\mathbf{x}_{true}^k(\theta_0) + \epsilon^{k,j} - \mathbf{x}_{opt}^k(\theta_0)||_\ell] \quad (\text{EC.24})$$

1382 7) Since  $\mathbb{E}[\epsilon^{k,j}] = 0$ , this implies:

$$\|\mathbf{x}_{true}^k(\theta_0) - \mathbf{x}_{opt}^k(\theta^*)\|_\ell \leq \|\mathbf{x}_{true}^k(\theta_0) - \mathbf{x}_{opt}^k(\theta_0)\|_\ell \quad (\text{EC.25})$$

1383 8) By the continuity of the feasible set mapping  $\Omega(\mathbf{u}, \theta)$  in  $\theta$  (assumption 2), we know that  $\mathbf{x}_{opt}^k(\theta)$   
 1384 is continuous in  $\theta$ . Therefore, the inequality in step 7 can only hold if:

$$\mathbf{x}_{opt}^k(\theta^*) = \mathbf{x}_{true}^k(\theta_0) \quad \text{for all } k \quad (\text{EC.26})$$

1385 9) Now, by the strict monotonicity of  $f(\mathbf{x}, \mathbf{u}, \theta)$  and  $g_i(\mathbf{x}, \mathbf{u}, \theta)$  in  $\theta$  (assumption 3), the only way  
 1386 for  $\mathbf{x}_{opt}^k(\theta^*) = \mathbf{x}_{true}^k(\theta_0)$  to hold for all  $k$  is if:

$$\theta^* = \theta_0 \quad (\text{EC.27})$$

1387 10) Therefore, as  $J_k \rightarrow \infty$  for all  $k$ , we have  $\theta^* \xrightarrow{p} \theta_0$ .  $\square$

1388 *Proof of Proposition 7* We have the following arguments for each part:

- 1389 (a) Let  $\mathbf{a}_j$  be the  $j^{\text{th}}$  row of  $\mathbf{A}$  and  $\mathbf{e}_j$  be the  $j^{\text{th}}$  unit vector (the set of relevant constraints is  
 1390 non-empty). There exists an FO feasible point  $\hat{\mathbf{x}}$  for which the equality  $\mathbf{a}_j \hat{\mathbf{x}} = b_j$  holds (given  
 1391 the assumption that no constraint is redundant). Defining  $\mathbf{v}_0 = \mathbf{e}_j$  and  $\mathbf{z}_0 = \hat{\mathbf{x}}$ , the solution  
 1392  $(\mathbf{v}_0, \mathbf{z}_0)$  is feasible for GIL( $\mathcal{X}, \Omega, r, \mathbf{P}$ ) with  $r = 1$  since (8b) and (8d) hold by the feasibility of  
 1393  $\hat{\mathbf{x}}$  and the assumption  $\mathbf{a}_j \hat{\mathbf{x}} = b_j$  and the definition of  $\mathbf{v}_0$ , and remaining constraints are also  
 1394 satisfied directly from the definition of the parameters.
- 1395 (b) Let  $\mathbf{x}^0$  be an extreme point of the feasible region of FO which binds exactly  $n$  relevant  
 1396 constraints. Let  $B \subseteq \mathcal{J}$  be the set of indices of relevant constraints that are binding at  $\mathbf{x}^0$ . For  
 1397  $r_0 \in \{1, \dots, n\}$ , let  $B_{r_0} \subseteq B$  be a set of indices of  $r_0$  binding constraints at  $\mathbf{x}^0$  and let  $\mathbf{v}_{r_0}$  be a  
 1398 vector such that  $v_j = 1 \forall j \in B_{r_0}$  and  $v_j = 0$  otherwise for  $j \in \mathcal{J}$ . Then,  $(\mathbf{v}_{r_0}, \mathbf{x}^0)$  is feasible for  
 1399 GIL with  $r = r_0$ .
- 1400 (c) Let  $\mathbf{z}_{r_1}^*$  and  $\mathbf{z}_{r_2}^*$  be the optimal solutions of GIL( $\mathcal{X}, \Omega, r_1, \mathbf{P}$ ) and GIL( $\mathcal{X}, \Omega, r_2, \mathbf{P}$ ) respectively.  
 1401 We show that  $\mathbf{z}_{r_2}^*$  is a feasible solution for GIL( $\mathcal{X}, \Omega, r_1, \mathbf{P}$ ). This can be easily seen by choosing  
 1402  $r_1$  number of binding relevant constraints of  $\mathbf{z}_{r_2}^*$ . Let  $B$  be a subset of indices of binding  
 1403 constraints at  $\mathbf{z}_{r_2}^*$  with  $|B| = r_1$  and let  $\mathbf{v}$  be a vector such that  $v_j = 1 \forall j \in B$  and  $v_j = 0$   
 1404 otherwise for  $j \in \mathcal{J}$ . It can be seen that  $(\mathbf{v}, \mathbf{z}_{r_2}^*)$  is feasible for GIL( $\mathcal{X}, \Omega, r_1, \mathbf{P}$ ). Therefore,  
 1405  $\mathcal{D}_{r_1}^* \leq \mathcal{D}_{r_2}^*$ .

- 1406 (d) If  $\Omega$  has at least one face  $\mathcal{F}$  with  $r_0$  binding relevant constraints, then  $\exists \mathbf{x}^0$  that binds  $r_0$  binding  
 1407 relevant constraints. The arguments that GIL is feasible for  $r \in \{1, \dots, r_0\}$  are similar to part 2.

1408 *Proof of Proposition 8.* Let  $(\mathbf{v}^*, \mathbf{z}^*)$  be an optimal solution to formulation 9. Then if we set  
 1409  $r_{max} = \sum_{j \in \mathcal{J}} v_j^*$ , it can be quickly verified that  $(\mathbf{v}^*, \mathbf{z}^*)$  satisfies all constraints of GIL( $\mathcal{X}, \Omega, r_{max}, \mathbf{P}$ ),  
 1410 as such  $(\mathbf{v}^*, \mathbf{z}^*)$  is feasible for GIL( $\mathcal{X}, \Omega, r_{max}, \mathbf{P}$ ). It follows readily that GIL( $\mathcal{X}, \Omega, r, \mathbf{P}$ ) is feasible  
 1411 for all  $1 \leq r \leq r_{max}$ .  $\square$

1412    *Proof of Theorem 5.* Let  $\mathbf{c} \in \text{cone}(\mathbf{a}_t : t \in \mathcal{J}_{z^*})$ . We have  $\mathbf{c} = \sum_{t \in \mathcal{J}_{z^*}} \lambda_t \mathbf{a}_t$  with  $\lambda_t \geq 0$ . It suffices  
 1413 to show that the dual feasibility and strong duality conditions hold for  $\mathbf{z}^*$  in  $\text{FO}(\mathbf{c}, \Omega)$ . We have  
 1414  $\mathbf{c}' \mathbf{z}^* = (\sum_{t \in \mathcal{J}_{z^*}} \lambda_t \mathbf{a}'_t) \mathbf{z}^* = \sum_{t \in \mathcal{J}_{z^*}} \lambda_t b_t$  with  $\lambda_t \geq 0 \ \forall t \in \mathcal{J}_{z^*}$ . Let  $\mathbf{y}$  be such that  $y_j = \lambda_t \ \forall t \in \mathcal{J}_{z^*}$  and  
 1415  $y_j = 0$  otherwise. We have  $\mathbf{A}' \mathbf{y} = \mathbf{c}$  and  $\mathbf{y} \geq 0$  and  $\mathbf{c}' \mathbf{z}^* = \mathbf{b}' \mathbf{y}$ .  $\square$

1416    *Proof of Theorem 6*  $\Rightarrow$ ) Let  $(\mathbf{c}_{IL}, \mathbf{y}_{IL}, \bar{\mathbf{y}}_{IL}, \mathbf{z}_{IL})$  optimal for IL. We construct a feasible solution  
 1417 for GIL based on the optimal solution of IL. For  $j \in \mathcal{J}$ , let  $v_j$  be the  $j$ th element of  $\mathbf{v}_{GIL}$  such that  
 1418  $v_j = 1$  if  $y_j > 0$  where  $y_j$  is the  $j$ th element of  $\mathbf{y}_{IL}$  and zero otherwise. Then, it is easy to verify  
 1419 that  $(\mathbf{v}_{GIL}, \mathbf{z}_{IL})$  is feasible for  $\text{GIL}(\mathcal{X}, \Omega, r = 1, \mathbf{P} = \emptyset)$ . If  $(\mathbf{v}_{GIL}, \mathbf{z}_{IL})$  is optimal for  $\text{GIL}(\mathcal{X}, \Omega, r =$   
 1420  $1, \mathbf{P} = \emptyset)$ , we are done. So assume to the contrary that there exists some solution  $(\hat{\mathbf{v}}, \hat{\mathbf{z}})$  optimal for  
 1421  $\text{GIL}(\mathcal{X}, \Omega, r = 1, \mathbf{P} = \emptyset)$  such that  $\mathcal{D}(\hat{\mathbf{z}}) < \mathcal{D}(\mathbf{z}_{IL})$ . However, by similar arguments, another feasible  
 1422 solution to IL can be constructed based on this optimal solution to  $\text{GIL}(\mathcal{X}, \Omega, r = 1, \mathbf{P} = \emptyset)$ . But  
 1423 this is a contradiction to  $(\mathbf{c}_{IL}, \mathbf{y}_{IL}, \bar{\mathbf{y}}_{IL}, \mathbf{z}_{IL})$  being optimal for IL.

1424     $\Leftarrow$ ) Showing that it is possible to construct feasible solutions from a solution of  $\text{GIL}(\mathcal{X}, \Omega, r =$   
 1425  $1, \mathbf{P} = \emptyset)$  to IL and vice versa in the previous part, this part can also be proven following similar  
 1426 arguments.  $\square$

1427    *Proof of Theorem 7.* For the sequence of solutions  $\mathbf{z}_1, \dots, \mathbf{z}_L$ , we have  $\mathcal{J}_{\mathbf{z}_1} \subseteq \dots \subseteq \mathcal{J}_{\mathbf{z}_L}$ . As such,  
 1428  $\forall i \in \{1, \dots, L\}$ ,  $\mathbf{z}_i$  binds the relevant constraints indexed by  $\mathcal{J}_{\mathbf{z}_1}$ . Therefore,  $\forall i \in \{1, \dots, L\}$ ,  $\mathbf{z}_i \in$   
 1429  $\mathcal{F} = \{\mathbf{z} \in \Omega \mid \mathbf{a}_j \mathbf{z} = b_j \ \forall j \in \mathcal{J}_{\mathbf{z}_1}\}$ . The results follow from Proposition 3. Note that for each  $\mathbf{z}_i$  where  
 1430  $i \in \{1, \dots, L\}$ ,  $\mathcal{J}_{\mathbf{z}_1} \subseteq \dots \subseteq \mathcal{J}_{\mathbf{z}_i}$  and therefore, due to Theorem 5, the results hold.  $\square$

1431    *Proof of Proposition 5* If the forward problem is feasible for all  $\mathbf{u}^k$  and  $\theta_0$ , then there exist  
 1432 optimal solutions  $\mathbf{x}_{opt}^k \in S(\mathbf{u}^k, \theta_0)$  that satisfy the constraints (6b)-(6f) with the true unknown  
 1433 parameters  $\theta_0$ . Thus, the CIL model is feasible.  $\square$

## 1434 EC.2. Diet Recommendation Problem Additional Data and Results

1435 This section includes additional information on the input data for the diet recommendation problem  
 1436 and figures indicating GIL solutions for all food types and nutrients. The intake data include more  
 1437 than 5,000 different food types. Given the large number of food types, we bundled them into 38  
 1438 broad food groups for ease of interpretation and to make the learned diets more tractable. This  
 1439 categorization is done based on the food codes from USDA. Table EC.1 shows the grouping developed  
 1440 for the dataset and the average serving size of each food item in grams. Table EC.2 illustrates the  
 1441 recommendations of the DASH diet in terms of the number of servings of each food group for different  
 1442 diets with distinct calorie targets. Since the DASH diet recommendations are in servings, Table EC.2  
 1443 provides additional details about a typical sample of each food group along with the corresponding  
 1444 amount in one serving size. We utilize the food samples from Table EC.2, the nutritional data  
 1445 from USDA, and the recommended amounts from the DASH eating plan to calculate the required

1446 bounds on nutrients. These bounds can serve as the right-hand side vector for constraints in linear  
1447 optimization settings. Figures EC.1 and EC.2 showcase results of applying GIL to all the data from  
1448 the same population groups, showing the results of implementing inverse learning models for all  
1449 food types and all nutrients. We also note that in this figure of nutrients, the lower bound of sugar is  
1450 binding for the  $r = 1$  of GIL and in increasing values of  $r$ , it becomes non-binding. This is due to the  
1451 fact that not only the binding constraints chosen by the binary variables are forced to remain binding  
1452 and any other constraint that becomes binding in addition to the ones chosen by the binary variables  
1453 might become non-binding in subsequent runs with higher  $r$  values. With the increasing applications  
1454 and importance of optimization and learning models, the ease of access to reliable, accurate, and  
1455 interpretable datasets has become paramount. We provided the details of a large-scale open-access  
1456 dataset on dietary behaviors and attributes of individuals in this section and have provided access to  
1457 the data at the following address <https://github.com/CSSEHealthcare/InverseLearning>. We hope  
1458 that the presence of such a dataset can help the researchers in different data-driven approaches to  
1459 evaluate proposed methods and get meaningful insights.

**Table EC.1** Food groups and their respective serving sizes in grams

Group Name	Description	Serving Size (g)
Milk	milk, soy milk, almond milk, chocolate milk, yogurt, baby food, infant formula	244
Cream	Cream, sour cream	32
Ice Cream	all types of ice cream	130
Cheese	all types of cheese	32
Beef	ground beef, steaks (cooked, boiled, grilled or raw)	65
Pork	chops of pork, cured pork, bacon (cooked, boiled, grilled or raw)	84
Red Meat (Other)	lamb, goat, veal, venison (cooked, boiled, grilled or raw)	85
Chicken, Turkey	all types of chicken, turkey, duck (cooked, boiled, grilled or raw)	110
Sausages	beef or red meat by-products, bologna, sausages, salami, ham (cooked, boiled, grilled or raw)	100
Fish	all types of fish,	85
Stew	stew meals containing meat (or substitutes), rice, vegetables	140
Frozen Meals	frozen meal (containing meat and vegetables)	312
Egg Meals	egg meals, egg omelets and substitutes	50
Beans	all types of beans (cooked, boiled, baked, raw)	130
Nuts	all types of nuts	28.35
Seeds	all types of seeds	30
Bread	all types of bread	25
Cakes, Biscuits, Pancakes	cakes, cookies, pies, pancakes, waffles	56
Noodle, Rice	macaroni, noodle, pasta, rice	176
Cereal	all types of cereals	55
Fast Foods	burrito, taco, enchilada, pizza, lasagna	198
Meat Substitutes	meat substitute that are cereal- or vegetable protein-based	100
Citrus Fruits	grapefruits, lemons, oranges	236
Dried Fruits	all types of dried fruit	28.3
Tropical Fruits	apples, apricots, avocados, bananas, cantaloupes, cherries, figs, grapes, mangoes, pears, pineapples	182
Fruit Juice	All types of fruit juice	249
Potato products	potatoes (fried, cooked)	117
Greens	beet greens, collards, cress, romaine, greens, spinach	38
Squash/Roots	carrots, pumpkins, squash, sweet potatoes	72
Tomato products	tomato, salsa containing tomatoes, tomato byproducts	123
Vegetables	raw vegetables	120
Puerto Rican Food	Puerto Rican style food	250
Smoothies	fruit and vegetable smoothies	233
Butter, Oils	butter, oils	14.2
Salad Dressing	all types of salad dressing	14
Desserts	sugars, desserts, toppings	200
Caffeinated Drinks	coffees, soda drinks, iced teas	240
Nutritional Shakes	Nutritional shakes, Energy Drinks, Protein Powders	166

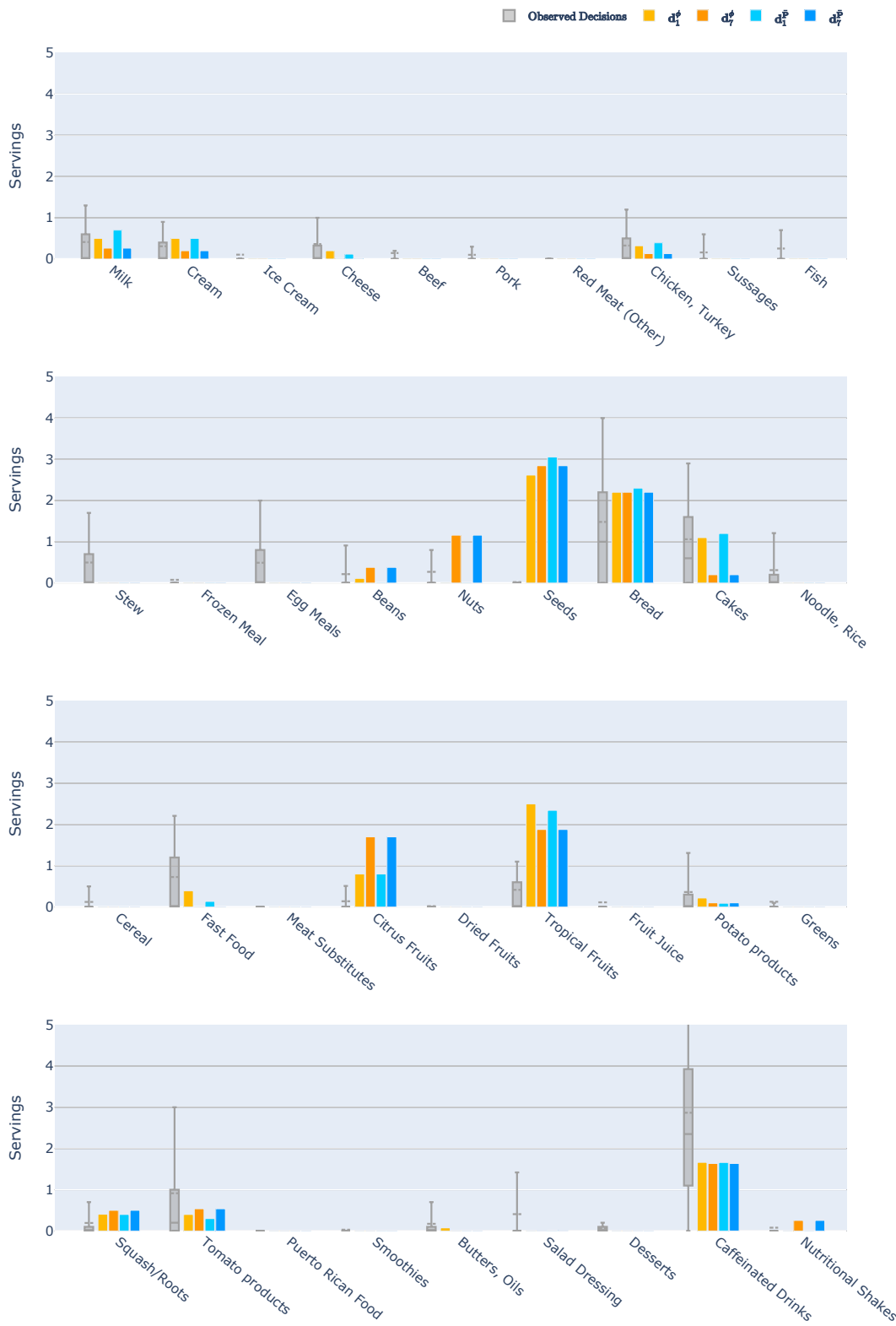


**Figure EC.1** Comparison of recommended diets by GIL with different values for  $r$  and a set of 460 observations for all food types.

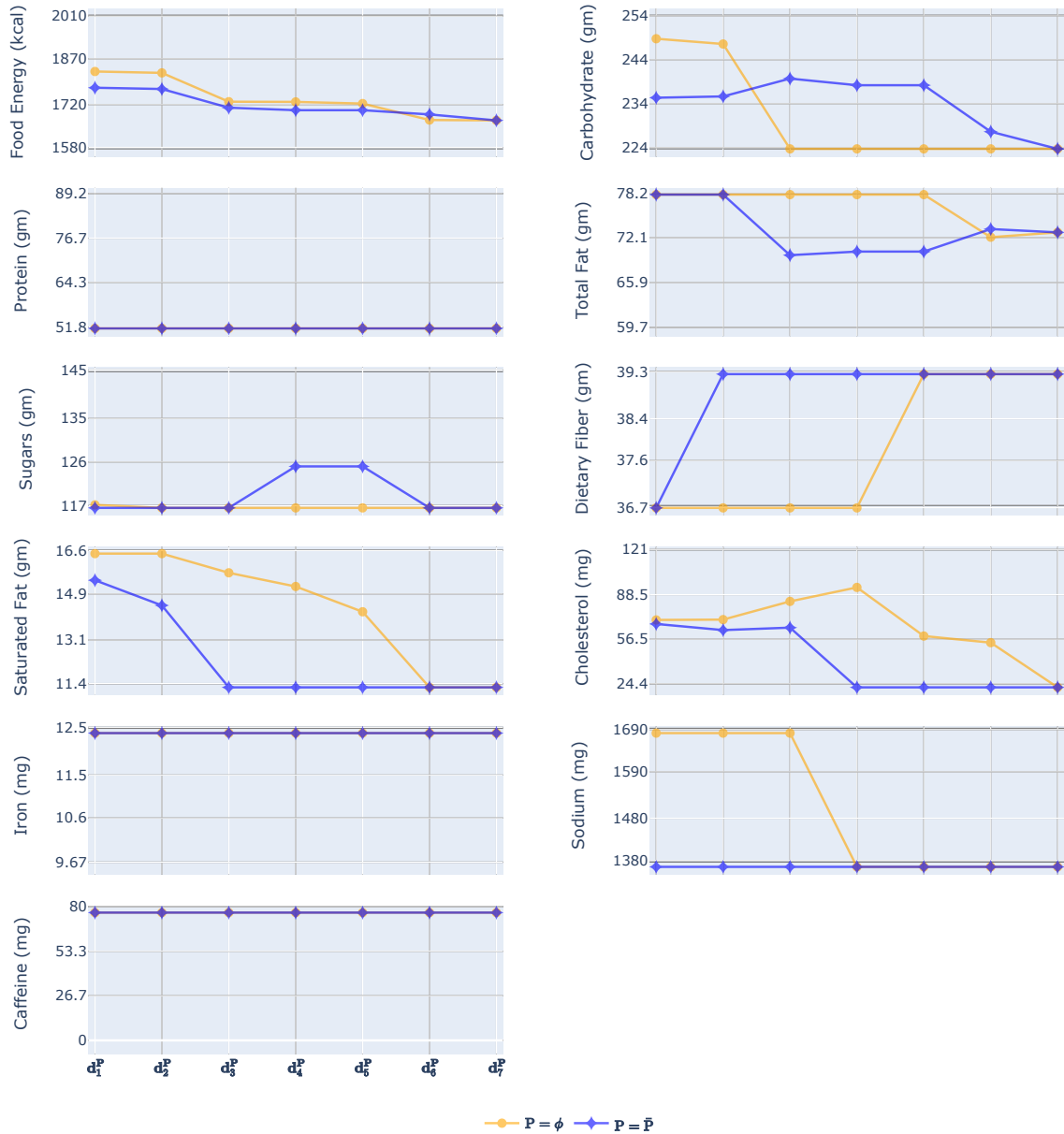


**Figure EC.2** Comparison of nutrients of recommended diets by  $IL^0$  and GIL for different values of  $r$  for all nutrients in the model. (Triv.: trivial constraint, Rel.: relevant constraint, Pref.: preferred constraint)

**Table EC.2** Food categories and their recommended number of servings for different targets based on the DASH diet (DASH 2018)

Food Category	Diet Target						
	1,200 Calories	1,400 Calories	1,600 Calories	1,800 Calories	2,000 Calories	2,600 Calories	3,100 Calories
Grains	4–5	5–6	6	6	6–8	10–11	12–13
Vegetables	3–4	3–4	3–4	4–5	4–5	5–6	6
Fruits	3–4	4	4	4–5	4–5	5–6	6
Fat-free or low-fat dairy products	2–3	2–3	2–3	2–3	2–3	3	3–4
Lean meats, poultry, and fish	≤ 3	≤ 3–4	≤ 3–4	≤ 6	≤ 6	≤ 6	6–9
Nuts, seeds, and legumes	3/week	3/week	3–4/week	4/week	4–5/week	1	1
Fats and oils	1	1	2	2–3	2–3	3	4
Sweets and added sugars	≤ 3/week	≤ 3/week	≤ 3/week	≤ 5/week	≤ 5/week	≤ 2	≤ 2
Maximum sodium limit(mg/day)	2,300	2,300	2,300	2,300	2,300	2,300	2,300

**Table EC.3** Food categories and their respective serving sizes in grams

Food Category	Serving Size (Example)
Grains	1 slice of whole-grain bread
Vegetables	1 cup (about 30 grams) of raw, leafy green vegetables like spinach or kale
Fruits	1 medium apple
Fat-free or low-fat dairy products	1 cup (240 ml) of low-fat milk
Lean meats, poultry, and fish	1 ounce (28 grams) of cooked meat, chicken or fish
Nuts, seeds, and legumes	1/3 cup (50 grams) of nuts
Fats and oils	1 teaspoon (5 ml) of vegetable oil
Sweets and added sugars	1 cup (240 ml) of lemonade